UC-25
LBL-6603 C1

THE DESIGN OF AN Fe-12Mn-0 . 2Ti ALLOY STEEL FOR LOW TEMPERATURE USE

Sun-Keun Hwang
(Ph. D. thesis)

June 1977

Prepared for the U. S. Energy Research and Development Administration under Contract W-7405-ENG-48

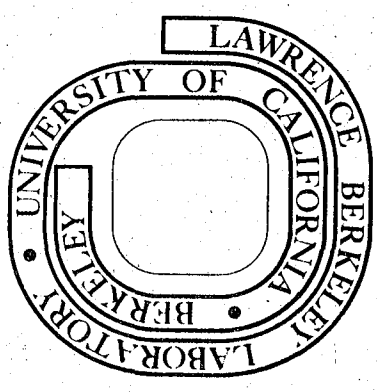

LBL-6603 C1

THE DESIGN OF AN Fe-12Mn-0 . 2Ti ALLOY STEEL FOR LOW TEMPERATURE USE

Sun- Keun Hwang

Lawrence Berkeley Laboratory
University of California
Berkeley, CA 94720

This work was done with support from the U. S. Energy Research and Development Administration

THE DESIGN OF AN Fe-12Mn-0.2Ti ALLOY STEEL FOR LOW TEMPERATURE USE

Doctor of Philosophy of Engineering | Sun-Keun Hwang | Physical Metallurgy

Chairman of Committee

ABSTRACT

An investigation has been made to improve the low temperature mechanical properties of Fe-8~12%Mn-0.2Ti alloy steels. A two-phase ($\alpha+\gamma$) tempering in combination with cold-working or hot-working has been identified as an effective treatment. In an Fe-12Mn-0.2Ti alloy a promising combination of fracture toughness and yield strength was obtained at -196°C. A potential application as a Ni-free cryogenic steel was thus shown for this alloy. These improvements of properties were mainly attributed to the ultra-fine grain size and to a uniform distribution of retained austenite. It was also shown that an Fe-8Mn steel could be grain-refined by a purely thermal treatment because of its dislocated martensitic structure and absence of ε phase. As a result, a significant reduction of the ductile-brittle transition temperature was obtained in this alloy.

The nature and origin of brittle fracture in Fe-Mn alloys were also investigated. Two embrittling regions were found in a cooling curve of an Fe-12Mn-0.2Ti steel which were shown to be responsible for intergranular fracture. A fast cooling through the martensite transformation temperatures results in a quench-crack type brittleness along prior γ grain boundaries. Auger electron spectroscopy identified no segregation during solution-annealing treatment. If held too long below the transformation

finish temperature, the 12Mn steel undergoes another form of embrittlement. This phenomenon was attributed to intergranular tempered martensite embrittlement. Avoiding the embrittling zones by controlled cooling led to a high cryogenic toughness in a solution-annealed condition.

THE DESIGN OF AN Fe-12Mn-0.2Ti ALLOY STEEL FOR LOW TEMPERATURE USE

Contents

I. INTRODUCTION

Recent advances in cryogenic devices for use in modern energy and transportation systems have created an increasing need for new alloys which retain good engineering properties at very low temperatures. Due to its excellent toughening effect in the Fe lattice, [1-5] Ni is widely used as a basic alloying element in most cryogenic steels. While the Ni steels show satisfactory mechanical properties, their applications are limited because of the high cost of Ni. The importance of developing a Ni-free cryogenic steel is obvious when the high cost of Ni is considered. Among various elements Mn has a potential to be developed for the replacement of Ni because of its similar characteristics as a substitutional alloying element with Fe.

A considerable amount of research has been conducted to identify the role of Mn in solid-state phase transformations in Fe. There is now general agreement [6-9] that the transformation products of Fe-Mn alloys of less than 10%* Mn are not far different from those of Fe-Ni alloys of less than 28%Ni. The only difference is when hcp ϵ forms as a metastable phase in an Fe-Mn alloy with more than 10%Mn. [10-15] Above 28%Mn concentration the binary alloy becomes austenitic and shows characteristics of an fcc structure.

Carbon has a strong influence on austenite stability in the Fe-Mn system. The presence of more than 1% of C in an Fe-13%Mn composition completely stabilizes the austenite, as is well known in Hadfield's alloy. [16] A moderately high yield strength can be obtained in a medium carbon, high manganese, ternary alloy system. However, these semi-austenitic steels encounter phase stability problems at cryogenic temperatures. Russian

*Weight percent unless specified otherwise

workers [17-18] have shown that the Fe-Mn-C alloys do not retain satisfactory impact resistance at cryogenic temperatures unless their phase stabilities are increased by adding Cr or Ni as alloying elements.

Because of the characteristics of their bcc structure, Fe-Mn alloys with less than 13%Mn show satisfactory yield strength at low temperatures. However, these steels have been considered inherently brittle for a long time and the origin of their brittleness has been given little investigation. Recently Bolton [19] reported a beneficial effect of tempering in suppression of the ductile-brittle transition temperature in 4~10%Mn alloys. Interestingly he reported no evidence of retained phase in his specimens in spite of the broad two-phase ($\alpha+\gamma$) region in the equilibrium Fe-Mn phase diagram. [11-20] Roberts [9] showed a moderate dependence of the transition temperature on the grain size in the martensitic alloys. However, to the author's knowledge, no serious attempt to refine the grain size of Fe-Mn alloys has been found in the literature except for preliminary work. [21] Therefore, there is a lack of information on the dependence of cryogenic mechanical properties on the two important metallurgical variables, retained austenite and grain size in Fe-Mn alloys.

The present ivestigation was designed to promote the understanding of the origin of the embrittlement and to improve the cryogenic mechanical properties of Fe-8~12%Mn steels by metallurgical processings. The approaches to obtain better mechanical properties were based on the control of microstructures and retained phases. A particular emphasis was made on the decomposition process in a two-phase region. To refine the size and distribution of the decomposition products, a prior deformation was employed in the form of either cold-working or hot-working. By this process a significantly improved cryogenic toughness was obtained in an Fe-12Mn-0.2Ti

alloy. To refine the grain size of Fe-8Mn and Fe-10Mn alloys a thermal cycling technique [22-24] was adopted. While ineffective in an Fe-12Mn alloy, this technique was extremely powerful in reducing the ductile-brittle transition temperature of an Fe-8Mn alloy.

The origin of intergranular fracture in an Fe-12Mn alloy was investigated by using an Auger electron spectrometer. Two discrete embrittling bands in a cooling curve of this alloy were found to be responsible for the brittle intergranular failure below the ductile-brittle transition temperature. It was then possible to avoid these embrittling regions by controlled cooling and thus obtain good low temperature toughness in an as-cooled condition of the Ni-free Fe-12Mn-0.2Ti steel.

II. EXPERIMENTAL PROCEDURE

A. MATERIAL PREPARATION AND INITIAL PROCESSING

Alloys of nominal compositions, Fe-8Mn, Fe-10Mn, and Fe-12Mn with minor additions of Ti (approximately 0.2%) were induction melted in an argon gas atmosphere. Several ingots were made for each composition. Each ingot was cast from a separate batch into a copper chill mold. The average weight of an ingot was 9kg. The ingots were homogenized under vacuum at 1200°C for 24 hours. Then they were upset cross-forged at 1100°C into plates of dimensions determined by specimen size (1.3cm thick by 10.2cm wide or 1.9cm thick by 6.4cm). The results of chemical analyses on randomly chosen ingots are shown in Table I.

B. MEASUREMENT OF TRANSFORMATION TEMPERATURES

A Theta Dilatronic IIR dilatometer was used to measure phase transformation temperatures. A drawing of a specimen used in this experiment is shown in Fig. 1. Each specimen was heated to 1100°C and held for 5 minutes before quenching to room temperature. Since the pressure of the specimen chamber was maintained below 10^{-5} torr, the specimen surfaces were well protected from oxidization. A programmed linear heating rate of 440°C/min was used and the quenching rate of approximately 70°C/sec was caused by a jet stream of He gas. Transformation temperatures were determined as first deviation points from linearity on dilation and temperature versus time charts. The experiment was repeated on the same specimen until consistent data were obtained.

C. MEASUREMENT OF PHASES

Specimens used for this experiment were either 2cm x 3cm x 0.5cm pieces cut from heat-treated blanks or optical microscopy specimens usually cut

from broken Charpy impact test specimens. In both cases x-ray diffraction measurements were made on sections transverse to the original rolling direction of the plate. When a specimen showed severe preferred orientation after cold rolling, another set of diffraction data were taken for two other vertical sections to check the extent. Specimen surfaces were carefully prepared to remove any strain-induced transformation products resulting from previous processes. For this purpose a grinding by emery paper of 600 grid grade was followed by chemical polishing in a solution of 100ml H_2O_2 + 3ml HF. A CuKα x-ray source was used and the beam was monochromatized by LiF. The volume percent of each phase present was caluculated by comparing integrated intensities of $(200)_\alpha$, $(200)_\gamma$, and $(10\cdot1)_\varepsilon$ peaks. When a specimen consisted of more than one phase, lattice parameter corrections were made under the assumption that each phase had an equilibrium concentration. The formulae used for this calculation are described elsewhere.[25]

D. MICROSCOPY

1. Optical Microscopy :

Specimens for optical microscopy were cut from tested Charpy bars. Transverse sections were examined. After emery paper grinding, a final polishing was carried out on an 1μm lapping wheel. Our best etching condition was found to be repetitive 10 second immersions in picral (1gm picric acid dissolved in 100ml ethyl alcohol - 5ml HCl).

2. Scanning Electron Microscopy (SEM):

Fracture surfaces of tested specimens were examined with an AMR 1000 scanning electron microscope operated at 20KV. When needed, energy dispersive analysis of x-rays (EDAX) was employed in combination with the SEM.

3. Transmission Electron Microscopy (TEM):

Specimens for transmission electron microscopy were cut from blanks

which received the desired treatment. Sheets of 0.2~0.3mm thickness were cut. The thickness was then chemically reduced to 0.05mm with a solution of 100ml H_2O_2 + 4ml HF. Final thinning was carried out by a jet-polishing technique with a chromic-acetic solution; 75g CrO_3 + 800ml CH_3COOH + 21ml H_2O. The optimum thinning condition was found at 20mA and 50V. The microscopes used were a Hitachi HU-125 and a Siemens Elmiscope 1A operated at 100KV.

E. AUGER ELECTRON SPECTROSCOPY (AES)

This technique was employed to probe fracture surface chemical compositions of specimens broken in a high vacuum chamber. The principles and applications of the AES technique are described elsewhere.[26-31] The machine used in this experiment was a PHI Model 545 scanning Auger electron spectrometer. A schematic diagram of the vacuum chamber equipped with an in-situ fracture device is shown in Fig. 2. The shape and dimensions of specimens used are illustrated in Fig. 3. Either single-notched or double-notched cylindrical rods were machined from heat-treated blanks. The temperature of fracture was controlled by liquid nitrogen flow through the fracture device. The temperature of a point close to our specimen was monitored by a thermocouple, so the actual temperature of the specimen might be a few degrees higher than our readings. The pressure of the chamber was maintained in the 10^{-10} torr range and never exceeded the middle 10^{-9} torr range.

The time needed to prepare the electronics for the first run after a fracture was normally less than 10 minutes. In most cases a primary electron beam voltage (Ep) of 3KeV with a 3eV modulation amplitude (Em) and a 1300V electron multiplier voltage (Vm) were used. Under medium focusing conditions, a primary electron beam current (Ip) of 2~3μm was sufficient to yield a reasonably strong signal. The beam

size under this operating condition corresponds to approximately 15μm in diameter. To obtain average data, at least three points on a fracture surface were examined. It took approximately 30 minutes to obtain the necessary data. After this time, a slow build-up of C and O intensities from background CO gas obscured valid data. Post-fracture surfaces were examined under a scanning electron microscope.

F. MECHANICAL TESTING

1. Tensile Testing:

Cylindrical tensile specimens of 12.7mm gage length and 3mm gage diameter, as shown in Fig. 4, were used. The loading direction was kept consistent with the rolling direction of the original plate. Tests were conducted at both room temperature and -196°C in an Instron machine. For low temperature testing, a cryostat was attached to the machine so that specimens were completely immersed in liquid nitrogen. A strain rate of 0.04/min. was employed. The engineering yield stress was determined as the 0.2% offset value. Elongation and reduction in area were measured by a travelling microscope with an accuracy of ±0.01mm. Uniform elongation was measured on the chart as the elongation obtained until the ultimate tensile strength was reached.

2. Charpy Impact Test:

V-notched Charpy specimens of ASTM standard size (1cm x 1cm x 5.5cm) were machined along the rolling direction of plate. Notches of 45° included angle were machined on the surfaces of the rolled plate. The impact test was carried out as described in ASTM E23-72. Various testing temperatures were obtained by a proper mixture of liquid nitrogen, isopentane, dry ice, and Corning 710 oil.

3. Fracture Toughness Test:

A compact tension specimen shown in Fig. 5 was machined from blanks

with its loading direction consitent with the rolling direction of plate. The fatigue pre-cracking and fracture toughness tests were conducted at room temperature and at -196^{o}C respectively in a 300K lb capacity MTS machine equipped with a cryostat. All data reported in this work were obtained according to ASTM E399-72. The thickness requirement for valid K_{IC} data was met for all except a reversion-cycled specimen.

III. EXPERIMENTAL RESULTS

A. HEAT AND MECHANICAL TREATMENTS OF Fe-12Mn-0.2Ti

1. Solution-Annealing Treatment, Initial Properties:

In Fe-12%Mn alloys, three different crystal structures have been found so far; [6, 8-15] fcc austenite (γ), bcc martensite (α'), and hcp martensite (ε). Depending on the mechanical and/or thermal treatment, each of the three structures may be present either separately or in combination with the others. The following designations will be used to define various transformation temperatures during continuous heating or cooling:

$M_s\alpha'$, $M_f\alpha'$: $\gamma \rightarrow \alpha'$ transformation temperatures during cooling ("s" for start and "f" for finish)

$M_s\varepsilon$, $M_f\varepsilon$: $\gamma \rightarrow \varepsilon$ during cooling

$A_s\alpha'$, $A_f\alpha'$: $\alpha' \rightarrow \gamma$ during heating

$A_s\varepsilon$, $A_f\varepsilon$: $\varepsilon \rightarrow \gamma$ during heating.

The transformation temperatures measured by dilatometry are shown in Table II. A typical dilation curve during heating and cooling an Fe-12Mn-0.2Ti alloy is shown in Fig. 6. $A_s\alpha'$, $A_f\alpha'$, $M_s\alpha'$, and $M_f\alpha'$ temperature were easily distinguishable. $A_s\varepsilon$ and $A_f\varepsilon$ could also be identified within $\pm 30^{\circ}C$. However, $M_s\varepsilon$ and $M_f\varepsilon$ temperatures were not detectable by the dilatometry.

Solution treatment was conducted at $900^{\circ}C$. Soaking for 2 hours at this temperature was sufficient to obtain recrystallized γ phase. The prior γ grain size ranged from 50 to 70μm as shown in Fig. 7a. A transformation substructure produced by subsequent water-quenching is shown in Fig. 7b. Two distinct morphologies of α' martensites were identified. One is the blocky martensite crystals which were often bound by thin ε

platellets. The other is lenticular martensite with an absence of the ε phase. In both cases the α' martensites were dislocated. No internal twinning was found. The association of α' and ε phases was delineated in detail by a TEM diffraction analysis as shown in Fig. 8.

Mechanical properties of a solution-annealed Fe-12Mn-0.2Ti alloy are shown in Table III. Tensile test behavior at -196°C is characterized by a moderately high yield strength and considerable work-hardening. A ductile-brittle transition occurred sharply at -50°C in the Charpy impact test as shown in Fig. 9. The transition was accompanied by a brittle intergranular fracture along prior γ grain boundaries. Two extremes of the fracture mode, a ductile dimple mode at room temperature and an intergranular mode at -196°C, are shown in Fig. 10.

2. Reversion-cycling Treatment and the Effect of the ε Phase:

The amount of ε phase in an Fe-12Mn-0.2Ti alloy is significantly influenced by thermal or mechanical treatment. During the course of present work a build-up of this metastable phase was found to occur through the $\alpha' \rightleftarrows \gamma$ reversion transformation. Hence, it was possible to closely observe the effect of the ε phase on the cryogenic mechanical properties of the 12Mn alloy with very little interference from other metallurgical factors.

Austenitizing treatments at different temperatures above Afα' resulted in differing amounts of ε phase increased with decreasing holding time at this temperature. Furthermore, a cycling heat-treatment between 680°C and room temperature rapidly increased the amount of ε phase. The accumulation of the hcp phase by the cycling heat-treatment is illustrated in Fig. 11b. The holding time at elevated temperature in each cycle was 5 minutes, and intermittent cooling was conducted in brine

water. The build-up of the ϵ phase was most pronounced in the first few cycles; no further change was observed after three cycles. A small amount of retained γ phase was detectable within the first 5 cycles, but was absent after subsequent cycles.

Mechanical properties were measured for the specimens reversion-cycled five times. Charpy impact energy was measured at various temperatures and is plotted in Fig. 12. For comparision purposes the same plot of the solution-annealed case is also presented. Apparently the ductile-brittle transition was suppressed to a lower temperature by the reversion-cycling treatment. An optical micrograph and a SEM fractograph of a reversion-cycled specimen are shown in Fig. 13a and b respectively. The fracture appearance at -196^{o}C shows a fibrous decohesion along prior γ grain boundaries in contrast to the flat facet appearance of the as-annealed specimen shown in Fig. 10b.

Although the reversion-cycled specimen showed an apparent increase of impact resistance, it revealed a drastic reduction of strength in tensile testing. The tensile properties measured at -196^{o}C are compared with those obtained in other treatments in Table III. The reversion-cycling treatment decreased the yield strength of the 12Mn alloy by more than 40ksi. Despite the reduced yield strength the ultimate tensile strength remained unaffected. A typical appearance of an engineering stress-strain curve of a reversion-cycled specimen is shown in Fig. 14. The premature yielding phenomenon is readily recognized in this curve.

3. Tempering and Retained Phases:

Tempering a martensitic Fe-Mn steel in the $\alpha + \gamma$ region of equilibrium phase diagram leads to a decomposition of the metastable martensite into equilibrium α and γ. The decomposition reaction and subsequent retention

of the transformation products may be complicated when the ε phase intrudes. The retained phases have a significant influence on cryogenic mechanical properties. In this section the results of an investigation on the characteristics of the two-phase decomposition, and the use of the retained phases in designing a cryogenic Fe-12Mn-0.2Ti alloy are described.

The changes of structure, hardness, and Charpy impact energy at -196°C on tempering the 12Mn alloy for 4 hours at various temperatures between 450°C and 700°C are shown in Fig. 15. The maxima of retained γ phase and retained ε phase concentrations were observed in specimens tempered at 500~550°C and 600°C, respectively. The hardness curve shows a broad plateau at 450°~550°C range. The maximum impact energy was observed after 500°C tempering, although a rather large scatter of data was observed. All the properties resumed the initial values found in the solution-annealed condition after annealing at 700°C (which is above Afα').

It is evident from the results shown in Fig. 15 that a 500°C treatment is most beneficial for the mechanical properties. Hence, an isothermal heat treatment was conducted at this temperature to assess the full capability of retained phases in enhancing cryogenic toughness. A variation of the retained phases and Charpy energy at -196°C on the isothermal treatment is shown in Fig. 16. The impact energy curve shows a gradual increase with holding time until 12 hours, after which an equilibrium is reached. The curve of the vol. % of the reverted γ phase closely follows the same trend. On the other hand, the amount of reverted ε does not show a major increase during an initial period of up to 4 hours.

Microstructural characterisitics of a two-phase tempered specimen are shown in Fig. 17 and Fig. 18. The most distinctive feature in these micrographs is the straight directionality of the original α' lath

boundaries. For a comparison purpose an optical micrograph of an identically heat-treated Fe-8Mn steel is shown in Fig. 19. The lath boundaries in the 8Mn alloy are rather undulated. The reason for the pronounced straightness in the 12Mn alloy is due to the presence of ε phase in the initial structure, which will be discussed later. The particular microstructural features remain even after an extended heat treatment (120 hours at 500°C) as shown in Fig. 18.

For the particular heat treatment of 500°C/8hrs/ice brine quenching, a set of low temperature mechanical properties was measured. Tensile properties and K_{IC} values are presented in Table III. All the properties measured were better than those of the solution-annealed specimens. Especially pronounced were the increases of yield strength, uniform elongation and K_{IC} values. The ductile-brittle transition temperature measured in Charpy tests was significantly suppressed (as shown in Fig. 20) with a concomittant transition of fracture mode; at -196°C the fraction of the brittle intergranular fracture mode was decreased by one half (as shown in Fig. 25b).

4. Effect of Cold-working on Tempering:

The improvement of cryogenic mechanical properties by two-phase tempering as described in the former section can be considerably enhanced by plastic deformation. This is achieved through structural refinement of the decomposed product by destroying preferential nucleation and growth sites. This present section describes how prior deformation affects the subsequent decomposition reaction and thus increases the potential of an Fe-12Mn-0.2Ti alloy as a Ni-free cryogenic steel.

A fixed amount of deformation was given to the blanks of 12Mn steel by rolling at room temperature. After a 50% reduction in thickness no trace of ε phase was detected by x-ray analysis, which indicates

the occurrence of a stress-assisted transformation of $\epsilon \rightarrow \alpha'$ during the deformation. After annealing the cold-rolled specimens for 4 hours at various temperatures, changes of structures and properties occurred and the results are summarized in Fig. 21. Several different aspects of the results are noted for comparison with those obtained by two-phase tempering alone (Fig. 15).

The amount of the retained γ phase was considerably increased by adding cold-working to the two-phase tempering treatment, whereas ϵ phase concentration was substantially reduced. It must be noted that the measurement of each phase by x-ray diffraction methods was obscured by the development of a preferred orientation during the rolling process. The shape of the curve, however, was essentially unaffected when the data averaged over three different sections were plotted, as shown in Fig. 22. The curve of Charpy energy at -196^{o}C, Fig. 21c, is in excellent correlation with the concentration of retained γ phase. The plateau of the hardness curve was raised to a much higher level by the combination of deformation and tempering, than by tempering alone.

An as-deformed structure is characterized by distorted martensite laths with a high dislocation density. A TEM micrograph of such a structure is shown in Fig. 23a. The blocky martensite morphology, typical of solution-annealed structures (see Fig. 7b), was no longer visible. After annealing at 600^{o}C the structure became a mixture of phase:fine-scale equilibrium γ, equilibrium α and untransformed α' (as shown in Fig. 23b). The distribution of each phase was not only fine (approximately 0.5μm) but also uniform. The directional growth of the γ phase characteristic of a two-phase tempered structure, was completely absent.

Low temperature mechanical properties were evaluated for specimens annealed 4 hours at 600°C, and the results are shown in Table III and Fig. 24. An extremely high yield strength was obtained. Also noted in Table III are the remarkably enhanced elongation and the fracture toughness at -196°C. The enhanced toughness is also evident in the Charpy test results shown in Fig. 24. The fracture mode at -196°C, shown in Fig. 25a, is predominantly a ductile tearing type. Therefore, it is demonstrated in the above results that an Fe-12Mn-0.2Ti alloy can be suitably processed into being a strong and tough steel at cryogenic temperatures.

5. Hot-working and Tempering:

The cold-rolling process in the previous section could be replaced by hot-working, but the extent of mechanical property improvement is reduced. From a practical point of view the hot-rolling is more easily accomplished than is cold-rolling. In principle, the decomposition of metastable α' martensite on tempering takes place more effectively in a perturbed structure. A perturbed structure can be retained by quenching a hot-rolled plate. In this section a set of experimental data obtained in hot-rolled and tempered Fe-12Mn-0.2Ti steel is described.

The hot-rolling was conducted at several different temperatures in the austenitic range. An 1"-thick plate received a 50% thickness reduction in one pass. The rolled blanks were immediatly water-quenched. A part of the blank underwent a further treatment, tempering at 500°C for 4 hours. The hardness and low temperature Charpy impact test data are shown in Table IV. Optical micrographs and SEM fractographs taken from the broken Charpy bars are shown in Fig. 26.

The impact toughness was improved by hot-rolling alone. However, the gain by additional tempering was marginal. It must be taken into account

that the particular ingot used in this experiment happened to show poor tempering response in its solution-annealed state. Therefore, the impact energy values listed in Table IV should be taken only for comparison purposes. The hardness was increased by hot-rolling, but was independent of the rolling temperature. Low temperature fracture appearances shown in Fig. 26 are consistent with the Charpy data. Unlike the mixed intergranular fracture mode in a solution-annealed and tempered specimen, the thermomechanically processed specimens revealed mostly a ductile tearing type fracture mode.

B. THE SOURCES AND THE PREVENTION OF INTERGRANULAR BRITTLENESS IN Fe-12Mn-0.2Ti

Below the ductile-brittle transition temperature an Fe-12Mn-0.2Ti steel suffers intergranular cracking along prior γ grain boundaries. Information on the source of this phenomenon is of vital importance for obtaining a desired toughness at cryogenic temperature. In the previous sections, various processing techniques to prevent this diastrous failure were described. In this section the results of an investigation on the origins and the minimization of the phenomenon in the as-cooled condition is described.

1. Intergranular fracture in As-quenched Condition:

Not all the martensitic Fe-Mn alloys show predominantly intergranular fracture below their ductile-brittle transition temperatures. The dominance of the intergranular failure mode over the quasi-cleavage mode increases with Mn content within 8~12% as shown in the fractographs of Fig. 27. While exhibiting mostly transgranular cleavage, the fracture appearance of Fe-8Mn alloys show some indications of decohesion along martensite packet boundaries.

An attempt to identify a precipitate formed along prior γ grain boundaries in Fe-12Mn-0.2Ti alloy by TEM techniques was not successful. As shown in Fig. 28, the prior γ grain boundaries were apparently free of precipitation in the as-quenched condition.

To confirm the TEM results on a different basis, a further investigation was carried out by employing an AES technique. This technique is extremely surface-sensitive; thus a segregation within a few atomic layers of the surface should be easily detectable. For this experiment a larger grain size of approximately 200μm was obtained by solution annealing at a higher temperature, 1100°C.

The AES spectra obtained from in-situ fracture surfaces of a solution-annealed and water-quenched Fe-12Mn alloy are shown in Fig. 29. The spectrum in Fig. 29a was obtained from a ductile fracture surface produced at room temperature; thus it represents the chemistry of bulk. The spectrum in Fig. 29b was obtained from an intergranular fracture surface produced at approximately -140°C and thus indicates the chemistry of the prior γ grain boundaries.

No significant differences between the two spectra are recognized except an S peak. A rather higher intensity of the S peak was frequently observed on the ductile fracture surface. Examination of a post-fracture surface by SEM-EDAX showed that the regions of ductile fracture were often associated with inclusion particles and that these particles mainly consisted of Mn and S as shown in Fig. 30. The absence of segregation was also confirmed in the specimens austenized below 1100°C; thus segregation was independent of austenitization temperature.

2. Martensite Embrittlement:

The upper limit for observing intergranular fracture in an Fe-12Mn is

extended to a higher temperature when the alloy is heat-treated at 350°C. The aggravated embrittlement by this particular heat-treatment is illustrated in the ductile-brittle transition curves shown in Fig. 31. The embrittling treatment resulted in an approximately 150°C increase of the transition temperature. This phenomenon was also observed in an Fe-8Mn alloy. In this alloy the Charpy impact energy at -196°C had deteriorated from 2~3 ft-lb to 0.6 ft-lb by the same treatment.

The characteristeics of brittle fracture modes in both alloys were not affected much by the embrittling treatment. However, some significant change of the chemistry of prior γ grain boundaries was detected by the AES technique.

Typical AES spectra obtained from the embrittled Fe-12Mn and Fe-8Mn specimens are shown in Fig. 32 and Fig. 34, respectively. The most pronounced change of the prior γ grain boundary chemistry in 12Mn steel during the treatment was a build-up of Mn concentration. A rough estimate [32] gave approximately 24%Mn. Significantly, the Mn concentration on the embrittled fracture surface of the 8Mn steel was also high, approximately 12%, in spite of the predominantly cleavage type fracture mode. Besides the high Mn peak in both alloys, an N peak was also observed on the embrittled surface, although the intensity was not significantly high. Other than the features just described the AES data for embrittled specimens were not too much different from those obtained from the as-quenched specimens.

3. Embrittling Sources in the Fe-12Mn-0.2Ti Alloy:

From the AES data described so far, it is apparent that the intergranular cracking in an Fe-12Mn-0.2Ti alloy involved more than one source. The observation of the phenomenon in both as-quenched and embrittled conditions

led to an experiment to locate the embrittling zones in a field with coordinates of temperature and time. This was successfully achieved in a furnace-cooling/interrupted fast cooling experiment, whose results are described below.

Blanks of Fe-12Mn-0.2Ti steel received a solution treatment at 1100°C for 2 hours followed by a furnace-cooling for a specific period which gave a specific final temperature. Then they were taken out of the furnace and subjected to air-cooling to room temperature. Charpy specimens were machined from the blanks and tested at -196°C. An intriguing set of data was obtained and illustrated in Fig. 35 with the corresponding cooling curve. The specimens interrupted from the continuous furnace-cooling either too early or too late showed not only low impact energy but also intergranular fracture (as shown in Fig. 36). However, the specimens transferred to room temperature after 11-12 hours of furnace-cooling did not experience this intergranular cracking and showed high impact absorption energy. The temperature of the furnace at the moment of interruption was in the range of 120~100°C. Comparatively high impact energy was also observed in a specimen air-cooled after 9 hours of furnace-cooling. The increment of the impact energy in this case, however, was comparatively small.

The AES spectra obtained from the specimens subjected to three different modes of cooling are shown in Fig. 37. The Fe-12Mn-0.2Ti alloy directly quenched from the austenitization treatment shows essentially the same characteristics of Auger peaks (Fig. 37a) as those of an identically treated Fe-12Mn alloy (Fig. 29b). The specimen air-cooled after 12 hours of furnace-cooling could not be fractured intergranularly, even at a very low temperature. Therefore, Fig. 37b was obtained from a ductile fracture surface and shows essentially the same characteristics of bulk Fe-12Mn as

shown in Fig. 29a. Fig. 37c was obtained from an intergranular surface of a completely furnace-cooled specimen. In this spectrum an Auger peak is observed at an energy level closely corresponding to N.

To summarize, it is clear from the above experiments that there are two separate sources of intergranular brittleness in an Fe-12Mn-0.2Ti alloy. One is due to fast cooling from above 120°C. The other is due to a prolonged exposition below 100°C. No indication of segregation was found in the former case while in the latter a minor N concentration was found along prior γ grain boundaries.

C. GRAIN REFINEMENT OF Fe-8Mn AND Fe-10Mn ALLOYS

Various processing techniques to improve the cryogenic toughness of an Fe-12Mn-0.2Ti alloy steel were described in section A. In this steel an attempt to obtain a uniform, ultra-fine grain size by a thermal cycling technique developed for Fe-12Ni-0.25Ti alloy was not successful. The ineffectiveness of this technique in the 12Mn alloy steel appeared to be due to the intrusion of the ε phase, which will be discussed later. However, the thermal cycling grain refinement technique was found to be effective in an Fe-8Mn alloy. The results of its application in the 8Mn and 10Mn alloys are described below.

1. Fe-8Mn:

Details of the thermal cycling grain refinement technique are described elsewhere.[22-24] A schematic diagram of the heat treatment is shown in Fig. 38. It essentially consists of alternate heat-treatments between γ and α+γ regions in the equilibrium phase diagram. The temperatures for each heat-treatment was determined from the previously obtained transformation temperatures shown in Table II. Specimens were water-quenched after each heat treatment.

A series of micrographs in Fig. 39 shows successive grain refinement by each treatment. The initial grain size, designated as AS (As Solution-annealed, 900°C/2h), was 70μm. In the first step, 1A, the grain size was reduced by a recrystallization of γ at a relatively low temperature above Afα'. The next refinement, 1B, was obtained by exposing the 1A structure at 650°C, which is inside the two-phase region. By repeating 1A and 1B two times, 2B, a substantial reduction of grain size was achieved. A repetition of all these steps one more time, 4B, destroyed all traces of long martensite laths of the 2B structure. Average grain size after the 2B treatment was approximately 1 μm.

In order to obtain retained γ phase a further heat-treatment at 600°C was given to the grain-refined specimen. While the structure after grain refinement was 100% bcc α or α' it contained 10 vol.% each of γ and ε phases as a result of the additional heat-treatment.

The Fe-8Mn alloy has little ductility at -196°C in its solution-annealed condition, as shown in Table V and Fig. 40. After the grain refinement, however, reduction in area was enhanced from 6% to 70% and total elongation was increased from 4% to 26%. Initial yield strength and ultimate tensile strength were maintained during the grain refining. A further increase of the elongation was observed after the additional retained γ treatment. However, this was accompanied by slight decreases in yield strength and reduction in area.

The improvement in impact toughness was also pronounced. As shown in Fig. 41 the transition temperature was suppressed by 130°C after the grain refinement. The retained γ treatment suppressed it an additional 50°C; thus a toughness transition was not observed above -150°C in the final structure. Fractographs taken from both Charpy specimens and tensile

specimens tested at -196°C are shown in Fig. 43. The fracture surfaces of grain refined specimens show evidently higher plasticity than solution-annealed ones.

2. Fe-10Mn:

The principles of thermal cycling grain refinement might well be applied to an Fe-10Mn alloys as it is to Fe-8Mn alloys. As an intermediate composition the 10Mn alloy has less ε phase than the 12Mn alloy and a lower initial ductile-brittle transition temperature than that of the 8Mn alloy. Therefore, a moderate suppression of the transition temperature was expected by the thermal treatment. However, the results described below showed that the extent of the suppression was not as large as was expected.

The schedule of heat-treatment was determined in the same way as in the Fe-8Mn steel. In Fig. 44, microstructures of a solution-annealed and a grain refined Fe-10Mn alloy are shown. Apparently, the effectiveness of grain size reduction was not less than that which was observed in the Fe-8Mn alloy. However, a much smaller suppression of the ductile-brittle transition temperature was observed in the grain refined Fe-10Mn steel, as shown in Fig. 45. In spite of the relatively small decrease of transition temperature, the shelf energy values were increased with resulting improvements in ductility, as shown in Fig. 46.

In summary, the data obtained on Fe-8Mn and Fe-10Mn alloys clearly indicate that the thermal-cycling grain-refinement technique is effective only in on ε-free dislocated martensite structure.

IV. DISCUSSION

A. STRUCTURE AND PROPERTIES OF Fe-12Mn-0.2Ti ALLOY

Phase transformation studies in Fe-Mn [10] or Fe-Mn-C [33] systems began even before the 1930's. Most of the equilibrium transformation products were determined by Troiano's [11] work. Transformation studies using continuous cooling have been completed more recently. [6,8,9]

Except for the fact that Mn is a stronger stabilizer of γ iron than Ni, the aspects of transformations on continuous cooling of Fe-Mn alloys with less than 10% Mn are quite similar to those of the Fe-Ni system with less than 29% Ni. [7,34] At modest cooling rate an equilibrium ferrite, massive ferrite and dislocated martensite structures are obtained for 0~2%, 3~5%, and 6~10% Mn steels, respectively. The presence of 10~28%Mn in an Fe lattice produces some hcp ε phase, which is not observed in the Fe-Ni system. The relative amount of ε phase increases with Mn concentration, then decreases as the high temperature γ phase is retained by more than 28% addition of Mn. The structure of Fe-12Mn-0.2Ti alloy is basically dislocated martensite with approximately 15 vol.% of ε phase in the solution-annealed condition.

The solid-solution hardening effect of Mn in Fe-4~10%Mn alloys is minimal. [9,13,21] Most strengthening in these compositions is originated by dislocation substructures in the continuous transformation products. A minor addition, up to 3%, of Mn does not affect the ductility of Fe. [1-2,35] However, increasing Mn from 4% to 8% increases the ductile-brittle transition temperature of the bcc structure through a substructural hardening effect. With more than 12% Mn, the alloys become less susceptible to a sharp transition because the soft phases such as ε or γ become predominant. The gain of low temperature toughness in these alloys, of course, is accompanied by

a deterioration of strength. In our present investigation, Fe-12Mn was chosen as the main composition of interest because the lowest transition temperature is obtained in this composition concomitant with the highest martensitic strength. Ti was added to scavenge interstitial impurities.

1. Effect of the ε Phase on Mechanical Properties:

The observation of the presence of hcp ε phase has been made in numerous systems; pure Fe under high pressure,[36] Fe-Ru,[37] Fe-Mn,[10-11, 14-15, 38] and Fe-Ni-Cr.[38-44] In Fe-Ni-Cr alloys it has been well established that ε is a discrete phase with a hcp structure and not merely an aggregate of random faults in γ.[41-42] Often the hexagonal phase is observed in association with α' martensite. This raised a question of controversy concerning the mechanism of the transformation decomposition of the γ phase.

Venables[41] and Schumann[14-15] suggested a sequential transformation mechanism of $\gamma \rightarrow \varepsilon \rightarrow \alpha'$. On the other hand, Dash[40] and Stone[44] insisted on independent transformation routes of $\gamma \rightarrow \varepsilon$ and $\gamma \rightarrow \alpha'$. Despite the controversies, it is generally accepted that the phase is metastable. An exceptional observation was made, however, of an Fe-18Cr-8Ni stainless steel in which the ε phase was detected by TEM after a prolonged holding at a subzero temperature.[43]

In Fe-Mn binary alloys, the ε phase has been observed for concentrations of 10~28%Mn.[10-11, 14-15, 38] The metastability of this phase against plastic deformation has been well documented in the literature.[11, 22, 38] However, it is less obvious whether the transitional behavior of the ε phase has any beneficial or detrimental influence[21] on cryogenic mechanical properties. This is an important point to be clarified in initially martensitic Fe-Mn alloys since this phase may intrude frequently during a specific heat treatment.

In a solution-annealed Fe-12Mn-0.2Ti alloy, there are two distinct morphologies of α' as shown in Fig. 7b. The TEM observations of the ε phase in this specimen were possible only in the regions of block-like α' martensite morphology. However, not all such regions were associated with ε. Holden et al, [8] did not observe the ε phase in an Fe-12.5%Mn alloy, and attributed its absence to the ε → α' transformation during his electro-thinning process. However, in view of the specimen dimensions it is unlikely that the stress-assisted transformation occurred locally during the preparation in the present investigation. Therefore, present data support the proposition by Breedis [42] that the peculiar block-like morphology of α' crystals is not a sufficient condition for the presence of the ε phase.

A typical appearance of the ε phase is shown in Fig. 8 in TEM dark-field contrast of an $\left[\bar{1}2\bar{1}C\right]_{\varepsilon}$ zone. A streaking due to the thinness of the ε platelets was observed in the diffraction pattern, but the micrograph shows that the thin ε phase plates do not cover α' lath boundaries in any continuous fashion. [44] It may be a consequence of an ε → α' transformation by a locallized strain which accompanies α' crystal formation. Although a complete analysis is not available, this result favors the sequential γ → ε → α' transformation. [14-15, 41]

The amount of ε phase in Fe-12Mn-0.2Ti steel is dependent on the soaking temperature in the austenitization process. Although the variation is not significant, the dependence of the amount of ε phase on the previous austenitization temperature is shown in Fig. 11a. A similar observation was made earlier by Parr [12] in a low carbon, Fe-18.5%Mn alloy. He reported the occurrence of a maximum ε concentration after a 1250°C treatment. Present data show a rather smooth plateau at around 950~1050°C.

Since the highest temperature employed in this work was 1050°C, the data cannot confirm Parr's observation.

The accumulation of the ε phase by a heat-cycling to a temperature just above Afα', as shown in Fig. 11b, is an interesting phenomenon. A similar example is found in a maraging steel [46-47] where an accumulation of reverted γ phase was observed by essentially the same treatment. A local adjustment of composition occurs during heating through the two-phase region. Once the temperature exceeds Afα', homogenization takes place. However, the removal of compositional fluctuation is difficult because of the slow rate of diffusion of solute atoms in the fcc γ structure and the insufficient time allowed for the diffusion.

In Fe-12Mn-0.2Ti, the local perturbation of composition may be favorable for the formation of some metastable ε phase. Therefore, the accumulation of ε phase occurs by repeating the brief austenitization process.

The reversion-cycled structure is a useful matrix in which to determine the effect of ε phase on cryogenic mechanical properties of martensitic Fe-Mn steels, since the structure is relatively unaffected by other metallurgical factors such as grain size and retained austenite. From the results obtained in this experiment (Fig. 12-14 and Table III) it can be concluded that the ε phase is beneficial for impact toughness, but only through some sacrifice in yield strength. The serious loss of strength is mainly due to the stress-assisted transformation of ε to α'. Therefore, an attempt to use ε phase to obtain toughness by a TRIP [45, 48-49] (Transformation Induced Plasticity) mechanism must be preceeded by a treatment to maintain the strength of the original matrix.

2. Tempering and Retained Phases:

As described earlier, the structure of a solution-annealed Fe-12Mn-0.2Ti

alloy is essentially dislocated martensite with a small mixture of ε phase. When this structure is heated to a temperature within the two-phase ($\alpha+\gamma$) region of the equilibrium phase diagram, equilibrium γ phase nucleates. The new γ phase has a higher solute concentration, and thus a lower transformation temperatures than the previous matrix. The retained austenite may be stable against a transformation to α' at -196°C.

The nature of the two-phase decomposition and the retention of the γ phase is essentially the same as in Fe-Ni alloys. The effect of the retained γ phase on low-temperature mechanical properties of Fe-Ni steels has been studied extensively. [24, 50-57] Many workers have observed improved impact toughness with a small amount of retained γ phase. [2, 52-55, 57] However, it is not clear yet whether the toughness comes from the retained γ per se, or from an interaction between the fcc phase and interstitial impurities in the matrix. Stability of the retained γ phase against mechanical deformation is another subject of question. [50]

In Fe-Mn alloys, data on the effect of two-phase decomposition products on mechanical properties are scarce. Bolton [19] reported some beneficial effect of tempering on low temperature impact properties of martensitic Fe-Mn steels with less than 10% Mn. No retained phase was found in this work. The results obtained in this present investigation on Fe-12Mn-0.2Ti alloy are quite different.

As shown in Fig. 15, the amount of each constituent in a two-phase tempered structure is strongly dependent on the tempering temperature. This must be a consequence of the diffusional characteristics of the $\alpha' \rightarrow \alpha + \gamma$ transformation. The occurence of maximum concentration of the retained γ phase is determined by a kinetic constraint at low temperatures and an lower equilibrium solute concentration at high temperatures. At high temperatures the rapid increase of ε with decreasing γ concentration is a

result of the low stability of the γ formed at this temperature.

The two-phase decomposition in Fe-12Mn-0.2Ti alloy results in a unique microstructure, as shown in Fig. 17 and Fig. 18. The preferential nucleation and growth of the equilibrium γ phase along prior γ or α' martensite lath boundaries has been observed in many alloys.[24, 50, 54, 58] In the 12Mn steel, this reaction is particularly accelerated because of the pre-existing ε phase in the solution-annealed specimens. In the previous section it was noted that the location of discontinuous ε sheets was always along the blocky martensite boundaries. A diffusionless reversion transformation of ε → γ occurs at 240~350°C (see Table II) during heating. Therefore this process precedes the diffusional two-phase decomposition. In the latter reaction the easiest path for the growth of the reverted γ phase is along the pre-existing lath boundaries. This results in a much more straightly aligned microstructure than an identically heat-treated ε-free Fe-8Mn martensite structure as shown in Fig. 19.

The low temperature impact toughness of a two-phase tempered Fe-12Mn-0.2Ti alloy can be correlated with the amount of retained γ phase.

The proportional increase of the two values is most evident in the isothermal heat-treatment at 500°C, whose results are shown in Fig. 16. The effect of some retained ε phase must be insignificant. This is shown by the lack of correlation between the retained ε and the impact energy curves, particularly in the initial period (up to 4 hours). This is in agreement with the former result that the ε phase is only beneficial for the toughness through some sacrifice in yield strength.

The significance of two-phase tempering from the mechanical property point of view is that it increases strength and toughness simultaneously, as shown in Table III. This increase is mainly due to the grain refining

effect which accompanies the $\alpha' \rightarrow \alpha + \gamma$ decomposition reaction. Impingement of the newly formed phases of two different structures imposes a constriction on grain coarsening. [57] The resulting fine grain size is sufficient to compensate the softening effect of recovery in the initial martensite structure and increase the retention of γ or ε phases. The unaffected yield strength with the presence of retained γ has been also observed in many other Fe-Ni based systems. [24, 46, 50, 59]

From the present data it is difficult to isolate the contribution of reduced grain size to the impact energy from that of the retained γ phase. However, the latter must be more significant than the former, at least in the initial period of tempering. Supporting this view is an observation made by Hwang [50] et al. in an Fe-12Ni-0.25Ti alloy of ultra-fine grain size. An enhanced impact energy in this alloy was observed by introducing retained γ without any apparent change of grain size.

3. Effects of Working on Tempered Structure:

The extremely directional characteristics of the new phase growth in the two-phase tempered Fe-12Mn-0.2Ti alloy can be substantially changed by adding plastic deformation to the tempering treatment. Miller [57] reported similar results in some martensitic Fe-Ni alloys and Fe-Mn alloys of low Mn concentration. The effect is more dramatic in the 12Mn steel because of the ε phase which is an origin for the γ phase directionality in the microstructure.

The deformation provides the alloy with a large driving force for the nucleation of the new phase in the $\alpha' \rightarrow \alpha + \gamma$ decomposition process. In addition to increasing the stored energy, the deformation transforms ε to α' by a stress-assisted mechanism and thus removes the origin of deleterious $\varepsilon \rightarrow \gamma$ reversion during subsequent heating.

During the two-phase tempering, new γ grains appears to nucleate randomly on severely deformed boundaries as well as on dislocation cell walls. The nucleation and growth in the deformed structure proceed at much higher rates than in solution-annealed structures. This is evident by the comparison of the amount of transformation products in each case (Fig. 21 and Fig. 15). The coarsening of the new phases is restricted, however, by the two-phase impingement. This leads to a structure which consists of uniformly distributed ultra-fine grains, as shown in Fig. 23.

The effect of cold-working on the subsequent two-phase decomposition is most pronounced in the phase analysis of the final structure, as shown in Fig. 21. The substantial increase of retained γ is a consequence of two factors: 1) high decomposition rate and 2) the increased stability of γ due to the ultra-fine grain size. The effect of the fine grain size in reducing the $\gamma \rightarrow \alpha'$ transformation temperature was demonstrated by Leslie [56] in an Fe-Ni alloy. The significantly reduced ε phase concentration is also a consequence of the increased stability of the γ phase.

The improvement of mechanical properties by the cold-working and tempering treatment is phenomenal. The enhanced properties may be attributed to the fine grain size and the high stability of retained austenite. The relationship between the increase in the cryogenic impact absorption energy and the amount of retained austenite is shown in Fig. 21.

From the results shown in Table III and Fig. 21 it is confirmed that the yield strength of a two-phase decomposed structure is not affected by the presence of retained γ phase. [24, 50, 59] The unusually high

yield strength, 170ksi at -196°C, was obtained from a specimen which contained more than 70 vol.% of γ phase. However, this may be an overestimate if the preferred orientation effect shown in Fig. 22 is taken into account. The average grain size observed in Fig. 23 is approximately 0.3μm.

The replacement of a cold-working process by a hot-working one may be advantageous from the financial point of view. In this case the structural refinement is governed by recrystallization of the γ phase. Since the deformation is conducted at a high temperature well above Afα', a dynamic recovery may take place. Therefore, to maintain a perturbed structure for the subsequent tempering, a hot-rolled specimen must be rapidly cooled before full recrystallization and grain growth of the γ phase occur. This appeared to be achieved by water-quenching, as the hardness in Table IV indicates.

However, a relatively small gain in the impact energy by this additional treatment was observed. This suggests that the stored energy provided by hot-working is not so large as to keep the decomposition reaction proceeding at a high rate, as it was in the cold-worked case. Nevertheless, the moderately improved Charpy impact energy and the ductile appearance of the fracture surface in the as-rolled condition (shown in Fig. 26) indicate that hot-rolling may have potential usefulness.

B. SOURCES AND PREVENTION OF INTERGRANULAR FRACTURE IN AN Fe-12Mn-0.2Ti ALLOY

A solution-annealed Fe-12Mn-0.2Ti alloy fails intergranularly below its ductile-brittle transition temperature. The brittle fracture occurs along prior austenite grain boundaries and the denuded grain boundary facets reveal little plasticity. The intergranular fracture mode is

uniquely observed for this composition. Other martensitic Fe-Mn alloys are prone to transgranular cleavage type fracture with decreasing Mn concentration. This is illustrated in Fig. 27. It was confirmed that the addition of 0.2%Ti did not influence the nature of the fracture mode.

Bolton et al. [19] reported the intergranular fracture as a common mode of brittle failure in Fe-Mn alloys with less than 13%Mn, which is in disagreement with the present observations. On the other hand, Roberts [9] reported a cleavage fracture in Fe-9%Mn alloy. This was supported by other observations [21, 60] including the present one. However, it must be noted that intergranular embrittlement in some tempered low carbon steels is accelerated by the addition of a few percent of Mn. [61-65]

The information on the source of intergranular embrittlement in Fe-Mn binary alloys is of critical importance when designing a cryogenic steel based on this system. Unfortunately, little data are found in the literature which deal with the disastrous failure mechanism for this particular system. The results of the present investigation do not provide a full explanation of this phenomenon, but they do provide some new insights into the problem.

1. Intergranular Fracture in the Solution-annealed Condition:

An extensive amount of research work has been done on intergranular fracture which occurs in iron-based alloys ranging from relatively pure Fe to stainless steels. The observed phenomena are diverse, but they may be divided into two broad categories. The first category includes all the instances where the particular mode of brittle fracture is observed after a specific heat-treatment at a relatively low temperature. Examples of such a heat-treatment are annealing of pure Fe, tempering of Ni-Cr steel, [76-85] etc. To the second category belong the occurence of inter-

granular fracture in specimens solution-annealed at relatively high temperatures in the γ region. Quench-cracking [86-91] and phosphorous embrittlement [61] are specific examples. The problem in Fe-12Mn alloys belongs to both categories. This alloy shows intergranular fracture in the as-quenched condition as well as after a heat-treatment at a specific temperature.

Except for quench-cracking, the grain boundary failures cited above mostly involve a segregation of harmful impurities or alloying elements along prior γ grain boundaries. The chemical segregation is presumed to decrease the cohesive energy of these boundaries. In fact, Bolton et al.[19] attributed the brittleness of dislocated martensitic Fe-Mn alloys to the same cause. However, the present experimental data on Fe-12Mn alloys show that the hypothesis of segregation is not always true.

In detecting chemical species the problem involves both spatial and spectroscopic resolution. High resolution TEM e.g. lattice imaging [92] and optical microdiffraction is capable of detecting minor second phases and solid solution effects (through changes in lattice parameter) at high spatial resolution (~10Å). On the other hand spectroscopic resolution such as by Auger, whilst distinguishing elements of adjacent atomic number, suffers from relatively poor area spatial resolution but good depth resolution. The Auger technique, [29-30, 65, 93-95] because of the short escape depth of the secondary electrons, can be powerful for detecting a segregation of few atomic layers if the region can be denuded by fracture.

In a solution-annealed specimen no significant segregation was observed by TEM (Fig. 28) within the resolution limit available in the present investigation. It was neither detected by AES, as shown in Fig. 29. The only difference between bulk and grain boundaries of a solution-annealed

specimen was the erratically high S peak in the former. This turned out to be a result of the higher population of MnS particles on the ductile fracture surface as shown in Fig. 30. Therefore, from present data the intergranular fracture in the solution-annealed 12Mn alloy does not appear to be a consequence of chemical segregation. Of course this does not preclude the possibility of having segregation in the austenitizing treatment if the alloy is doped by a specific element such as P. [61]

2. Martensite Embrittlement:

Many martensitic steels [9, 83, 96-97] show a deterioration of toughness when they are subjected to a tempering in the relatively low temperature range of 260°C-360°C. The phenonmenon is often called "martensite embrittlement" of "350°C embrittlement." The embrittling sites have been delineated to be either transgranular or intergranular. In the former case Thomas [102] attributed the phenomenon to the thermal instability of interlath retained austenite. For the latter case McMahon [64, 83] proposed a model which assumed segregation of impurities in the austenitizing treatment. In his model, carbon diffuse onto the prior austenite grain boundaries during the tempering and thereby forms a brittle interface between the carbides and matrix. However, no experimental evidence is yet available to prove this hypothetical segregation in the austenitizing treatment.

The martensite embrittlement in martensitic Fe-Mn alloys was reported by Bolton et al. [19] In this work the embrittlement was evidenced by a measurement of impact absorption energy at room temperature. The embrittlement is confirmed by the present observations in Fe-12Mn and Fe-8Mn alloys. The decreased toughness of the Fe-12Mn alloy by 350°C heat treatment was revealed by the rising of the ductile-brittle transition temperature, as shown in Fig. 31. In the Fe-8Mn alloy this property was measured by a drop of Charpy impact energy at -196°C.

The AES data obtained from low temperature fracture surfaces of embrittled specimens differ from these obtained from bulk surfaces in their Mn peaks. Therefore, it is evident that Mn diffusion occurred during the heat treatment. Since the treatment is conducted essentially within the two-phase region of the equilibrium phase diagram, it is not surprising to observe higher Mn concentrations on high angle boundaries. In fact, the higher concentration of Mn on the embrittled surface of Fe-8Mn alloy strongly indicate that the cleavage path in this alloy may be along martensite packet boundaries.

It is not entirely obvious whether the segregation of Mn in these alloys is directly responsible for the observed embrittlement. However, a hypothesis for an extreme case may be made such that a brittle interface forms between two thin layers of Mn-depleted and Mn-enriched regions. This is feasible since the diffusion of the substitutional Mn atoms must be limited to short distances at a low temperature of 350^{o}C. In addition to the Mn segregation, a small amount of N was often detected on the embrittled surface. This may further weaken the brittle interface.

3. Embrittling Sources During a Slow Cooling:

From the results discussed in the previous sections it was deducted that the intergranular fracture in an Fe-12Mn steel may not be of single source but of multiple ones. The idea was that either a diffusionless or a sub-micro scale diffusional process could result in the same fracture appearnce in SEM. This is evidenced by the experimental results shown in Fig. 35 and Fig. 36.

There are two extremes of cooling rate which cause intergranular weakness. Quenching from the austenitization temperature is one extreme and a complete furnace-cooling is the other. Surprisingly, a stepwise

cooling almost entirely prevents the intergranular fracture and thus increases the low temperature impact toughness. The stepwise cooling essentially consists of a furnace-cooling to approximately 120°C followed by an air-cooling from this temperature to room temperature. The critical temperature turned out to be very close to Mfα', as shown in Table II.

The nature of intergranular fracture in the quenched condition appears to be a sort of quench-cracking. When the alloy is cooled rapidly through the Mfα' temperature it encounters a violent impingement of α' martensite plates on its prior γ grain boundaries. The damage to the prior γ grain boundaries will be amplified in the presence of the ε phase via the $\gamma \rightarrow \varepsilon \rightarrow \alpha'$ transformation route. Since the ε phase is the densest phase in the Fe-Mn alloys, neighboring γ grains undergo a sudden contraction and expansion over a short time and temperature interval. The grain boundaries will fail to find time to accomodate the local strains in the adjacent grains and thus become micro-cracked. This explains why the cracking along prior γ grain boundaries is far more dominant in an Fe-12Mn alloy with approximately 15 vol.% of ε phase than in an Fe-8Mn alloy with virtually no ε phase.

Another source of the intergranular weakness in an Fe-12Mn-0.2Ti alloy sets in after the alloy is completely transformed to α' martensite with an admixture of some ε phase. The fact that this source can be suppressed by a fast cooling suggests that the origin of embrittlement in this case is related to diffusional characteristics. The embrittlement is pronounced in a specimen held below the Mfα' temperature for more than 2 hours. Therefore, the diffusional process must be active at a temperature as low as 100°C.

This observation is strongly suggestive that the source of the second embrittling phenomenon has a common nature with the martensite embrittlement discussed in the previous section. The reasons are: 1) the embrittling occurs only in the martensitic structure 2) it shows the diffusional characteristics. However, it is not clear at this moment what kind of species is responsible for the embrittlement. The AES data (Fig. 32) for the quenched and embrittled (at 350°C) specimen showed a significant concentration of Mn on the grain boundaries. On the other hand, the Mn concentration on the grain boundaries of the furnace-cooled specimen was not higher than the bulk. In both specimens some intensities of an N peak were observed, but the concentration was too small and the data scatter was too large to draw a conclusion. Therfore, further investigation is needed to identify the element which is commonly responsible for the embrittlement in both cases.

C. THERMAL CYCLING GRAIN REFINEMENT IN Fe-8Mn and Fe-10Mn STEELS

Jin et al. [22-23] showed that an Fe-12Ni-0.25Ti steel can be grain-refined through a thermal cycling technique. This technique essentially consists of an alternating heat-treatment in the γ and $\alpha + \gamma$ regions, as shown in Fig. 38. It was demonstrated that an ultra-fine grain size was obtained by this technique, and the fracture toughness of this alloy was significantly enhanced as a consequence. Similar grain-refining techniques have been reported in other alloy systems. [24, 55, 98-100]

The application of the thermal-cycling technique for refining the grain size of a Fe-12Mn-0.2Ti alloy was not successful. The reason appears to be the intrusion of the ε phase in this alloy. As discussed earlier, the diffusionless $\varepsilon \rightarrow \gamma$ reversion induces an extremely directional growth of equilibrium γ during the subsequent two-phase heat treatment.

This must not be a problem in an ε-free dislocated martensite structure, such as in an Fe-8Mn-0.2Ti steel. In fact, the structural development shown in Fig. 39 demonstrates that the thermal cycling technique can be successfully applied to this type of structure.

The reduction of grain size from 70μm to approximately 1μm resulted in a suppression of the ductile-brittle transition temperature (Tc) by 130°C. According to Stroh's [101] relationship this gives a slope of 31°C/ℓn(μm) in a plot of Tc vs. ℓn d, as shown in Fig. 42. This value is slightly less than what Roberts [9] observed in an Fe-9Mn alloy, but higher than Bolton's [19] data for an Fe-8Mn alloy.

The introduction of retained austenite in the grain-refined structure results in an additional suppression of Tc by 50°C. However, this accompanies a slight degradation of yield strength, as shown in Fig. 40. This appears to be an indication that the retained austenite produced in the fine structure has low stability against mechanical deformation. Therefore, as reported by Hwang et al. [50] for an Fe-Ni alloy, the K_{IC} value might have not been increased by the supplementary heat-treatment.

The application of the thermal cycling technique to an Fe-10Mn steel was not as effective as it had been expected. The reason appears to be the presence of an unexpectedly higher amount of ε phase in the initial structure. X-ray analysis identified approximately 12 vol.% ε in this alloy, as compared to 15 vol.% ε in an Fe-12Mn alloy. Accordingly, the suppression of Tc was not as significant as it was in an Fe-8Mn alloy, in spite of the apparently fine structue, as shown in Fig. 44. Therefore, this result confirms again that the thermal-cycling grain-refinement is effective only in an ε-free dislocated martensite structure.

V. CONCLUSIONS

The following conclusions may be drawn from the present investigation:

1. A tempering treatment within the two-phase ($\alpha + \gamma$) region is beneficial for the low temperature mechanical properties of Fe-12Mn-0.2Ti steel. The property improvement is obtained mainly by retained austenite and grain size reduction. However, a martensite embrittlement is induced by the treatment at a particular temperature around 350°C.

2. Cold-working enhances the improvement in the cryogenic mechanical properties produced by the two-phase tempering. This is achieved chiefly through an increase of the decomposition rate and the removal of preferential sites for the new phase. Combining the two processes results in a simulataneous improvement of toughness and yield strength in the 12Mn steel.

3. Hot-working can replace cold-working to a certain extent. However, the increase in toughness by additional tempering is not as significant.

4. The presence of ϵ phase suppresses the ductile-brittle transition temperature of 12Mn steel, but only at the expense of yield strength.

5. The source of brittle intergranular fracture in an Fe-12Mn-0.2Ti alloy is two-fold. The first one is connected with the continuous transformations during a fast cooling from an austenitization treatment. The second one can be delineated by either a quench and tempering or a complete furnace-cooling. This source has diffusional characteristics, but the identity of the responsible species needs further investigation.

6. The embrittling sources can be avoided by a step-wise cooling with respect to the critical temperature (around 120°C) with resulting in an increased cryogenic toughness.

7. An Fe-8Mn alloy can be toughened by a thermal cycling grain-refinement

technique. This technique is ineffective in Fe-12Mn and Fe-10Mn alloys due to the presence of ε phase in the initial structure.

ACKNOWLEDGEMENTS

The author would like to express his deepest gratitude to Professor J. W. Morris, Jr. for his guidance and support throughout this investigation. He would like to appreciate personal encouragements of Drs. Sungho Jin and Cholkyl Syn.

The technical assistance procided by the support staff of the Materials and Molecular Research Division, Lawrence Berkeley Laboratory, Brian Pope (ingot melting), Ed Edwards, Julian Patenaude, Duane Newhart, and Herb Riebe (machining), Lee Johnson (metallography), Richard Lindberg (scanning electron microscopy), John Holthius (alloy preparation), Don Krieger (mechanical testing), Jim Severns (electronics), Sandy Stewart (purchasing), Gloria Pelatowski (line drawings) and Marilyn Stefonetti (typing) is acknowledged.

Special thanks are extended to Professor G. Somorjai, Drs. Yipwha Chung and Wigbert Siekhaus for their helpful advices in using Auger electron spectrometer. A special thanks is also extended to Mr. Brent Fultz for his help in manuscript arrangement.

The author wishes to thank his family, especially his mother and his wife Jung-Hoon, for their invaluable encouragement and assistance.

This work was supported by National Aeronautics and Space Administration through the Materials and Molecular Research Division of the Lawrence Berkeley Laboratory.

REFERENCES

1. W. C. Leslie, R. J. Sober, S. G. Babcock, and S. J. Green: Trans. ASM, 1969, V. 62, p. 690.
2. W. Jolley: J. Iron Steel Inst., Feb., 1968, V. 206, p. 170.
3. M. Gensamer: Trans. AIME, 1959, V. 215, p. 2.
4. B. E. Hopkins and H. R. Tipler: J. Iron Steel Inst., Mar., 1958, v. 188, p. 218.
5. G. R. Brophy and A. J. Miller: Trans. ASM, 1949, v. 41, p. 1185.
6. D. W. Gomersall and J. Gordon Parr: J. Iron Steel Inst., Mar., 1965, v. 203, p. 275.
7. W. S. Owen, E. A. Wilson, and T. Bell: High Strength Materials ed., (V.F. Zackay, John Willey and Sons, 1965, p. 167.)
8. A. Holden, J. D. Bolton, and E. R. Petty: J. Iron Steel Inst., Sept., 1971, v. 209, p. 721.
9. M. J. Roberts: Met. Trans., 1970, v. 2, p. 3287.
10. F. M. Walters, Jr. and C. Wells: Trans. ASM., 1935, v. 23, p. 727.
11. A. R. Troiano and F. T. McGuire: Trans. ASM, 1943, v. 31, p. 340.
12. J. G. Parr: J. Iron Steel Inst., June, 1952, v. 171, p. 137.
13. H. Schumann: Arch. Eisenhuttenwesen, 1967, v.38, p. 743.
14. H. Schumann: Z. Metallk., 1967, v. 58, p. 207.
15. H. Schumann: Arch. Eisenhuttenwesen, 1967, v. 8, p. 647.
16. C. H. White and R. W. K. Honeycombe: J. Iron Steel Inst., June, 1962, v. 200, p. 457.
17. V. I. Grigorkin: Metal Sci. and Heat Treat., 1969, No. 7, p. 568.
18. M. M. Belenkova, I. I. Kodlubik, K. A. Malyshev, M. N. Mikheyel, and V. D. Sadovski: Phys. Met. Metallo, 1960, v. 10, No. 1, p. 111.
19. J. D. Bolton, E. R. Petty, and G. B. Allen: Met. Trans., 1971, v. 2, p. 2915.

20. ASM Metal Handbook, 1973, v. 8, p. 303.

21. M. J. Schanfein, M. J. Yokota, V. F. Zackay, E. R. Parker, and J. W. Morris, Jr.,: ASTM STP 579, 1975, p. 361.

22. S. Jin, J. W. Morris, Jr., and V. F. Zackay: Met. Trans. A, 1975, v. 6A, p. 141.

23. S. Jin, S. K. Hwang, and J. W. Morris, Jr., : Met. Trans. A, 1975, v. 6A, p. 1569.

24. S. Jin, S. K. Hwang and J. W. Morris, Jr.: Met. Trans. A., 1975, v. 6A, p. 1721.

25. B. D. Cullity: Elements of X-ray Diffraction, (Addison-Wesley, 1967, p. 391).

26. L. A. Harris: J. Appl. Phys., 1968, v. 39, p. 1419.

27. C. C. Chang: Characterization of Solid Surfaces, ed, Kane and Larrabee, Plenum, 1974, p. 509

28. G. A. Somorjai and F. J. Szalkowski: Advances in High Temperature Chemistry (Academic Press, 1971, v. 4, p. 137).

29. P. W. Palmberg: Electron Spectroscopy, ed. D. A. Shirley, (Asilomar Conference, 1972, p. 385).

30. R. L. Park: Physics Today, 1975, April, p. 52.

31. H. L. Marcus: J. Metals, 1977, v. 29, No. 2, p. 20.

32. Handbook of Auger Electronic Spectroscopy, ed. L. E. Davis, Physical Electronics Ind. Inc., p. 5.

33. E. C. Bain, E. S. Davenport, and W. S. N. Waring: Trans. AIME, 1932, v. 100, p. 228.

34. G. R. Speich and P. R. Swann: J. Iron Steel Inst., May, 1965, v. 203, p. 480.

35. W. P. Rees, B. E. Hopkins, and H. R. Tipler: J. Iron Steel Inst., Oct. 1951, v. 169, p. 157.

36. F. P. Bundy: J. Appl. Phys., 1965, v. 36, p. 616.

37. L. D. Blackburn, L. Kaufmann, and M. Cohen: Acta Met., 1965, v. 13, p. 533.

38. B. Cina: Acta Met., 1958, v. 6, p. 748.

39. J. F. Breedis and W. D. Robertson: Acta Met., 1962, v. 10, p. 1077.

40. J. Dash and H. M. Otte: Acta Met., 1963, v. 11, p. 1169.

41. J. A. Venables: Phil. Mag., 1962, v. 7, p. 35.

42. J. F. Breedis and L. Kaufman: Met. Trans, 1971, v. 2, p. 2359.

43. P. L. Manganon, Jr. and G. Thomas: Met. Trans., 1970, v. 1, p. 1577.

44. G. A. Stone and G. Thomas: Met. Trans., 1974, v. 5, p. 2095.

45. V. F. Zackay, E. R. Parker, D. Fahr, and R. Bush: Trans. ASM, 1967, v. 60, p. 252.

46. A. Goldberg: Trans. ASM, 1968, v. 61, p. 26.

47. S. D. Antolovich, A. Saxena, and G. R. Chanani: Met. Trans., 1974, v. 5, p. 623.

48. D. Bhandarkar, V. F. Zackay, and E. R. Parker: Met. Trans., 1972, v. 3, p. 2619.

49. D. Fahr: Met. Trans., 1971, v. 2, p. 1883.

50. S. K. Hwang, S. Jin, and J. W. Morris, Jr.: Met. Trans., 1975, v. 6, p. 2015.

51. C. W. Marschall, R. F. Heheman, and A. R. Troiano: Trans., ASM, 1962, v. 55, p. 135.

52. S. Nagashima, T. Ooka, S. Sekino, H. Mimura, T. Fujishima, S. Yano, H. Sakurai: Trans. Iron Steel Inst., Japan, 1971, v. 11, p. 402.

53. S. Yano, H. Sakurai, H. Mimura, N. Wakita, T. Ozawa, and K. Aoki: Trans. Iron Steel Inst., Japan, 1973, v. 13, p. 133.

54. H. Haga: Trans., Iron Steel Inst., Japan, 1973, v. 13, p. 141.

55. C. K. Syn, S. Jin, and J. W. Morris, Jr.,: Met. Trans. A, 1976, v. 7A, p. 1827.

56. W. C. Leslie and R. L. Miller: Trans. ASM, 1964, v. 57, p. 972.

57. R. L. Miller: Met. Trans., 1972, v. 3, p. 905.

58. D. T. Peters and C. R. Cupp: Trans. AIME, 1966, v. 236, p. 1420.

59. C. A. Pampillo and H. W. Paxton: Met. Trans., 1972, v. 3, p. 2895.

60. G. A. Charushnikova, Y. E. Goldshtein, and Y. G. Razumov: Metal Sci. Heat Treat., 1969, No. 7, p. 539.

61. B. J. Schulz and C. J. McMahon, Jr.: ASTM STP 499, 1972, p. 104.

62. J. M. Capus: ASTM STP 407, 1968, p. 3.

63. G. C. Gould: ibid, p. 59.

64. C. J. McMahon, Jr.: ibid, p. 127.

65. A. Joshi, P. W. Palmberg, and D. F. Stein: Met. Trans. A, 1975, v. 6A, p. 2160.

66. C. J. McMahon, Jr.: Grain Boundaries in Engineering Metals, (Proc., 4th Bolton Landing Conf., 1974, ed. J. L. Walter et al, Claitors Pub. 525).

67. J. R. Low, Jr. and R. G. Feustel: Acta Met., 1953, v. 1, p. 185.

68. D. S. Tomalin and D. F. Stein: Trans. AIME, 1965, v. 233, p. 2056.

69. C. J. McMahon: Acta Met., 1966, v. 14, p. 839.

70. R. Honda and H. Taga: Metal Sci. J., 1968, v. 2, p. 172.

71. J. R. Rellick and C. J. McMahon, Jr.: Met. Trans., 1970, v. 1, p. 929.

72. P. Jolly: Met. Trans., 1971, v. 2, p. 341.

73. J. R. Rellick, C. J. McMahon, Jr., and H. L. Marcus: Met. Trans., 1971, v. 2, p. 342.

74. H. J. Rack: Met. Trans., 1972, v. 3, p. 1667.

75. B. D. Powell, H. J. Westwook, D. M. R. Taplin, and H. Mykura: Met. Trans., 1973, v. 4, p. 2357.

76. A. Joshi and D. F. Stein: ASTM STP 499, 1972, p. 59.

77. H. L. Marcus, I. H. Hackett, Jr., and P. W. Palmberg: ibid, p. 90.

78. T. Inoue: Grain Boundaries in Engineering Metals (Proc. 4th Bolton Landing Conf., 1974, ed. J. L. Walter et al., Claitors Pub., p. 525).

79. L. Delage, A. Galibois, and M. R. Krishnadev: ibid, p. 561.

80. B. J. Schultz and C. J. McMahon, Jr.: Met. Trans., 1973, v. 4, p. 2485.

81. R. A. Mulford, C. J. McMahon, Jr., D. P. Pope, and H. C. Feng: Met. Trans. A, 1976, v. 7A, 1183.

82. R. Viswanathan: Met. Trans., 1971, v. 2, p. 809.

83. C. J. McMahon, Jr., J. R. Rellick, and B. J. Schultz: Fracture, ed. P. L. Pratt, 1969 (Chapmann and Hall, p. 278).

84. H. Ohtani and C. J. McMahon, Jr., : Acta Met., 1975, v. 23, p. 377.

85. H. Ohtani, H. C. Feng, and C. J. McMahon, Jr., : Met. Trans. A, 1976, v. 7A, p. 1123.

86. A. R. Marder and A. O. Benscoter: Met. Trans., 1970, v. 1, p. 3234.

87. R. G. Davies and C. L. Magee: Met. Trans., 1972, v. 3, p. 307.

88. M. G. Mendiratta, J. Sasser, and G. Krauss: Met. Trans., 1972, v. 3, p. 351.

89. L. Jena and P. Heich: Met. Trans., 1972, v. 3, p. 588.

90. M. G. Mendiratta and G. Krauss: Met. Trans., 1972, v. 3, p. 1755.

91. B. V. N. Rao and G. Thomas: Mat. Sci. Eng., 1975, v. 20, p. 195.

92. G. Thomas: J. Metals, 1977, v. 29, No. 2, p. 31.

93. A. Joshi and D. F. Stein: J. Testing Eval., 1973, v. 1, p. 202.

94. D. F. Stein, A. Joshi, and R. P. Laforce: Trans. ASM, 1969, v. 62, p. 776.

95. P. W. Palmberg and H. L. Marcus: Trans. ASM, 1969, v. 62, p. 1016.

96. G. Delislie and A. Galibois: J. Iron Steel Inst. Dec., 1969, v. 207, p. 1628.

97. T. M. F. Ronald: Met. Trans., 1970, v. 1, p. 2583.

98. J. W. Morris, Jr., S. Jin, and C. K. Syn: Proc., 1st Int. Sym. New Aspects of Martensitic Transformation, Kobe, Japan, 1976, p. 393.

99. S. P. Gupta: Mat. Sci. Eng., 1975, v. 21, p. 211.

100. B. Karlson: Mat. Sci. Eng., 1973, p. 185.

101. A. N. Stroh: Advan. Phs., 1957, v. 6, p. 418.

102. G. Thomas: Submitted to Met. Trans. A.

Table I. Chemical Composition of Alloys

Composition (wt. pct)	Alloy Designation Fe-8Mn	Fe-10Mn	Fe-12Mn-0.2Ti
Fe	Bal.	Bal.	Bal.
Mn	7.8	10.5	11.9
Ti	0.04	-	0.16
C	0.002	0.043	0.001
O	0.050	-	0.028
S	0.006	-	0.007
P	0.007	-	0.007
Al	-	0.38	-
Mo	-	-	0.010
Ni	-	-	0.050
Cr	-	-	0.002
V	-	-	0.010
Nb	-	-	0.005

- : Not Analyzed

Table II. Transformation Temperatures (^{o}C) of Fe-Mn Alloys

Nominal Composition	Asε	Afε	Asα'	Afα'	Msα'	Mfα'
Fe-8Mn	-	-	660	700	460	310
Fe010Mn	-	-	600	670	310	160
Fe-12Mn-0.2Ti	240	350	570	670	260	120

Asε, Afε - Start and finish temperature for $\varepsilon \rightarrow \gamma$ transformation on heating.

Asα', Afα' - $\alpha' \rightarrow \gamma$ on heating.

Msα', Mfα' - $\gamma \rightarrow \alpha'$ on cooling.

Table III. Mechanical Properties of Fe-12Mn-0.2Ti Steel

Treatment	Test Temperature	Yield Strength(ksi)	Ultimate Tensile Strength(ksi)	Uniform Elongation(%)	Total Elongation(%)	Reduction in Area	K_{IC} (ksi $\sqrt{in}$)
Solution-Annealed*	25°C	87	134	6	25	78	-
Solution-Annealed	-196°C	129	196	11	25	54	57
Reversion-Cycled	-196°C	86	202	19	33	61	72**
Two-Phase Tempered	-196°C	138	197	18	33	62	64
Cold-Work and Tempered	-196°C	171	218	26	38	66	91

Solution-Annealed - 900°C/2h/IBQ.
Reversion-Cycled - Solution-Annealing plus 680°C/5m/IBQ, 5 cyc.
Cold-Worked and Tempered - 30% reduction at room temperature plus 600°C/4h/IBQ.

* This row of data was obtained from Fe-12Mn-0.2Ti-1Mo alloy.
** K_Q value. ASTM thickness requirement for K_{IC} was not met.

Conversion factors: 1 ksi = 6.90 MPa, 1 ksi $\sqrt{in}$ = 1.10 MPa $\sqrt{m}$

Table IV. Properties of Hot-rolled and Tempered Fe-12Mn-0.2Ti Steel

Treatment	Charpy Impact Energy at -196°C (ft-lb)	Hardness (R_C)
Solution-Annealed	6	27
Above + Tempering	10	30
As-Rolled (900°C, 50%)	20	29
" " (1000°C, 50%)	18	30
" " (1100°C, 50%)	20	30
900°C Roll. + Tempering	22	31
1000°C " "	19	32
1100°C " "	18	31

All Tempering was conducted at 500°C for 4 hrs followed by water-quenching.

Table V. Tensile Properties of Fe-8Mn Steel

Treatment	Yield Strength (ksi)	Ultimate Tensile Strength (ksi)	Uniform Elongation (%)	Total Elongation (%)	Reduction in Area (%)
Solution-Annealed	140	151	4	4	6
Grain-Refined	140	153	26	7	70
Grain-Refined and Retained γ	123	157	32	18	64

Conversion factor: 1 ksi = 6.90 MPa.

FIGURE CAPTIONS

Fig. 1. Dilatometry specimen for measuring phase transformation temperature.

Fig. 2. Schematic diagram of the ultra high vacuum chamber with in-situ fracture device used for Auger electron spectroscopy (AES)

Fig. 3. Single notched specimen for Auger electron spectoscopy.

Fig. 4. Subsize tensile test specimen.

Fig. 5. Fracture toughness test specimen for K_{IC} measurement.

Fig. 6. Dilation curve during continuous heating and cooling of an Fe-12Mn-0.2Ti specimen.

Fig. 7. Fe-12Mn-0.2Ti. Microstructures after solution-treatment ($900^{o}C/2h/IBQ$).

(a) Optical micrograph showing recrystallized γ structure.

(b) TEM micrograph showing transformation substructures.

Fig. 8. Fe-12Mn-0.2Ti. After solution-treatment ($900^{o}C/2h/IBQ$). Localized region of blocky martensites showing the association of α' and ε phase.

(a) Selected area diffraction pattern.

(b) Analysis of (a).

(c) Bright field image.

(d) Dark field image taken from an $(10\bar{1}0)_{\varepsilon}$ reflection.

Fig. 9. Fe-12Mn-0.2Ti. Ductile-brittle transition in solution-annealed ($900^{o}C/2h/IBQ$) specimens.

Fig. 10 Fe-12Mn-0.2Ti. SEM fractographs taken from Charpy specimens tested (a) at room temperature and (b) at $-196^{o}C$.

Fig. 11. Fe-12Mn-0.2Ti. Variation of ε phase on the (a) austenitization at different temperatures and on the (b) reversion-cyclings between 680°C and room temperature. Holding time at 680°C; 5 minutes. AS: As solution-annealed. A_f:Afα' temperature.

Fig. 12. Fe-12Mn-0.2Ti. Ductile-brittle transition behaviours after the reversion-cycling treatment (680°C/5m/IBQ, 5 cyles).

Fig. 13. Fe-12Mn-0.2Ti. Reversion-cycled (680°C/5m/IBQ, 5 cycles) specimen. (a) Optical micrograph. (b) SEM fractograph of a Charpy specimen tested at -196°C. Same magnifications.

Fig. 14. Fe-12Mn-0.2Ti. Engineering stress-strain curves obtained in the tensile tests at -196°C on differently heat-treated specimens. Solution-annealing: 900°C/2h/IBQ. Reversion-cycling: 680°C/5m/IBQ, 5 cycles. Two-phase tempering: 500°C/8h/IBQ.

Fig. 15. Fe-12Mn-0.2Ti. Changes of structures and properties on tempering. (a) Vol. % of retained phases. (b) Hardness at room temperature. (c) Charpy impact energy at -196°C. AS: As-solution-annealed (900°C/2h/IBQ).

Fig. 16. Fe-12Mn-0.2Ti. Structure and property changes during the isothermal treatment at 500°C. (a) Retained phases. (b) Charpy impact energy at -196°C.

Fig. 17. Fe-12Mn-0.2Ti. Structures after a heat treatment in the two-phase (500°C/8h/IBQ). Note the severe directionality. (a) Optical micrograph. (b) TEM micrograph.

Fig. 18. Fe-12Mn-0.2Ti. TEM micrograph of a specimen heat-treated for an extended time in the two-phase (500°C/120h/IBQ). (a) Bright-field image. (b) Dark-field contrast of retained phases (mostly retained austenite).

Fig. 19. Fe-8Mn. Optical micrograph taken from a specimen tempered in the two-phase region (500°C/8h/IBQ).

Fig. 20. Fe-12Mn-0.2Ti. Improvements of ductile-brittle transition behaviour by the two-phase heat treatment (550°C/8h/IBQ).

Fig. 21. Fe-12Mn-0.2Ti. Changes of structures and properties on cold-working followed by tempering. (a) Retained phases. (b) Room temperature hardness (c) Charpy impact energy at -196°C. AS: As-solution-annealed. CW: Cold-worked (50% reduction) at room temperature.

Fig. 22. Fe-12Mn-0.2Ti. Cold-worked (50%) and annealed at different temperatures. Variation of amount of retained phases measured on different sections. T: Transverse section. L: Longitudinal section. V: Vertical section.

Fig. 23. Fe-12Mn-0.2Ti. TEM micrographs of (a) cold-worked (50% reduction) and (b) annealed (500°C/8h/IBQ) specimens.

Fig. 24. Fe-12Mn-0.2Ti. Improvement of impact resistance by a combination of cold-working and annealing (600°C/4h/IBQ) in the two-phase region.

Fig. 25. Fe-12Mn-0.2Ti. SEM fractographs taken from fracture surfaces of Charpy specimens tested at -196°C. (a) Cold-worked (50%) and annealed (600°C/4h/IBQ). (b) Two-phase tempered (500°C/8h/IBQ).

Fig. 26. Fe-12Mn-0.2Ti. Optical micrographs (b,d) and SEM fractographs (a,c,e) from Charpy bars tested at -196°C. (a) Solution annealing plus two-phase tempering (500°C/8h/IBQ). (b) Hot-rolled (50%) at 900°C. (c) Same as (b). (d) Hot-rolled (50%) at 900°C and tempered (500°C/4h/IBQ). (e) Same as (d). All in the same magnifications.

Fig. 27. SEM fractographs taken from Charpy specimens tested at -196°C. (a) Fe-8Mn. (b) Fe-10Mn. (c) Fe-12Mn-0.2Ti. All solution-annealed condition (900°C/2h/IBQ).

Fig. 28. Fe-12Mn-0.2Ti. As solution-annealed (900°C/2h/IBQ). TEM micrographs showing prior γ-grain boundaries.

Fig. 29. Fe-12Mn. AES spectra obtained from two different fracture surfaces produced at different temperatures.

Fig. 30. Fe-12Mn. SEM-EDAX analysis of particles in a region of dimpled structure of a fracture surface. Heat treatment: 1100°C/2h/IBQ.

Fig. 31. Fe-12Mn. Shift of ductile-brittle transition temperature by the martensite embrittlement.

Fig. 32. Fe-12Mn. AES spectrum obtained from an intergranular fracture surface of a martensite embrittled specimen.

Fig. 33. Fe-8Mn. AES spectrum obtained from a ductile fracture surface produced at room temperature.

Fig. 34. Fe-8Mn. AES spectra and SEM fractographs obtained from brittle fracture surfaces of (a) the solution-treated and (b) the martensite embrittled specimens, respectively.

Fig. 35. Fe-12Mn-0.2Ti. Furnace-cooling curve and the Charpy impact energy measured at -196°C. Specimens were soaked at 1100° for 2 hours followed by the furnace-cooling. They were then taken out from the furnace at the specified time and temperature and air-cooled.

Fig. 36. Fe-12Mn-0.2Ti. SEM fractographs of Charpy specimens tested at -196°C. (a) Furnace-cooled 6 hours/air-cooled. (b) Furnace-cooled 11 hours/air-cooled. (c) Furnace-cooled 15 hours/air cooled.

Fig. 37. Fe-12Mn-0.2Ti. AES spectra obtained from the specimens heat treated: (a) 1100°C/2h/WQ. (b) 1100°C/2h/FC 12 h/AC. (c) 1100°C/2h/FC.

Fig. 38. Schematic diagram illustrating the schedule of thermal-cycling grain refinement. AS: As solution-annealed (900°C/2h/IBQ).

Fig. 39. Fe-8Mn. Optical micrographs showing the development of grain size reduction by the thermal cycling treatment. Refer to Fig. 38 for the designation of each step.

Fig. 40. Fe-8Mn. Changes of low temperature (-196°C) mechanical properties by grain size reduction and the retained austenite. AS: as-solution-annealed (900°C/2h/WQ). Retained austenite treatment: 600°C/4h/WQ.

Fig. 41. Fe-8Mn. Suppression of the ductile-brittle transition temperature by the grain-refining and the retained austenite treatment.

Fig. 42. Fe-8Mn. Dependence of the ductile-brittle transition temperature on the prior austenite grain size, d.

Fig. 43. Fe-8Mn. Fracture modes at -196°C, SEM. (a) As-solution-annealed, Charpy specimen. (b) The same as (a), tensile specimen. (c) Grain-refined, Charpy specimen. (d) The same as (c), tensile specimen.

Fig. 44. Fe-10Mn. Optical micrographs of (a) a solution-annealed specimen (900°C/2h/WQ) and (b) a grain-refined specimen by the thermal-cyclings (730°C/2h/WQ + 650°C/2h/WQ, 2 cycles).

Fig. 45. Fe-10Mn. Ductile-brittle transition behaviours of the thermal-cycled specimens.

Fig. 46. Fe-10Mn. SEM fractographs of Charpy specimens tested at -196°C. (a) Solution-annealed (900°C/2h/WQ). (b) Grain-refined by the thermal-cyclings.

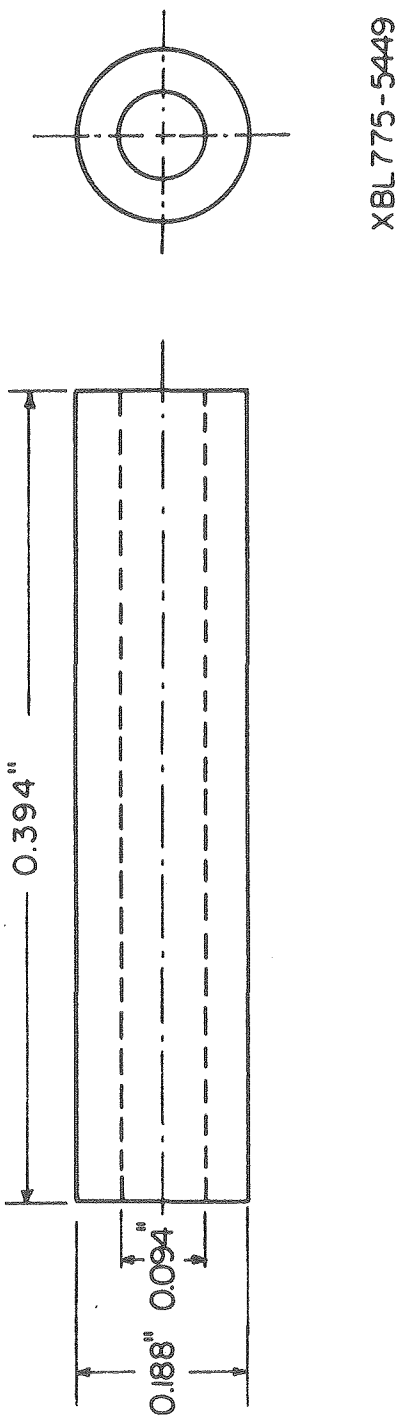

XBL 775-5449

Fig. 1.

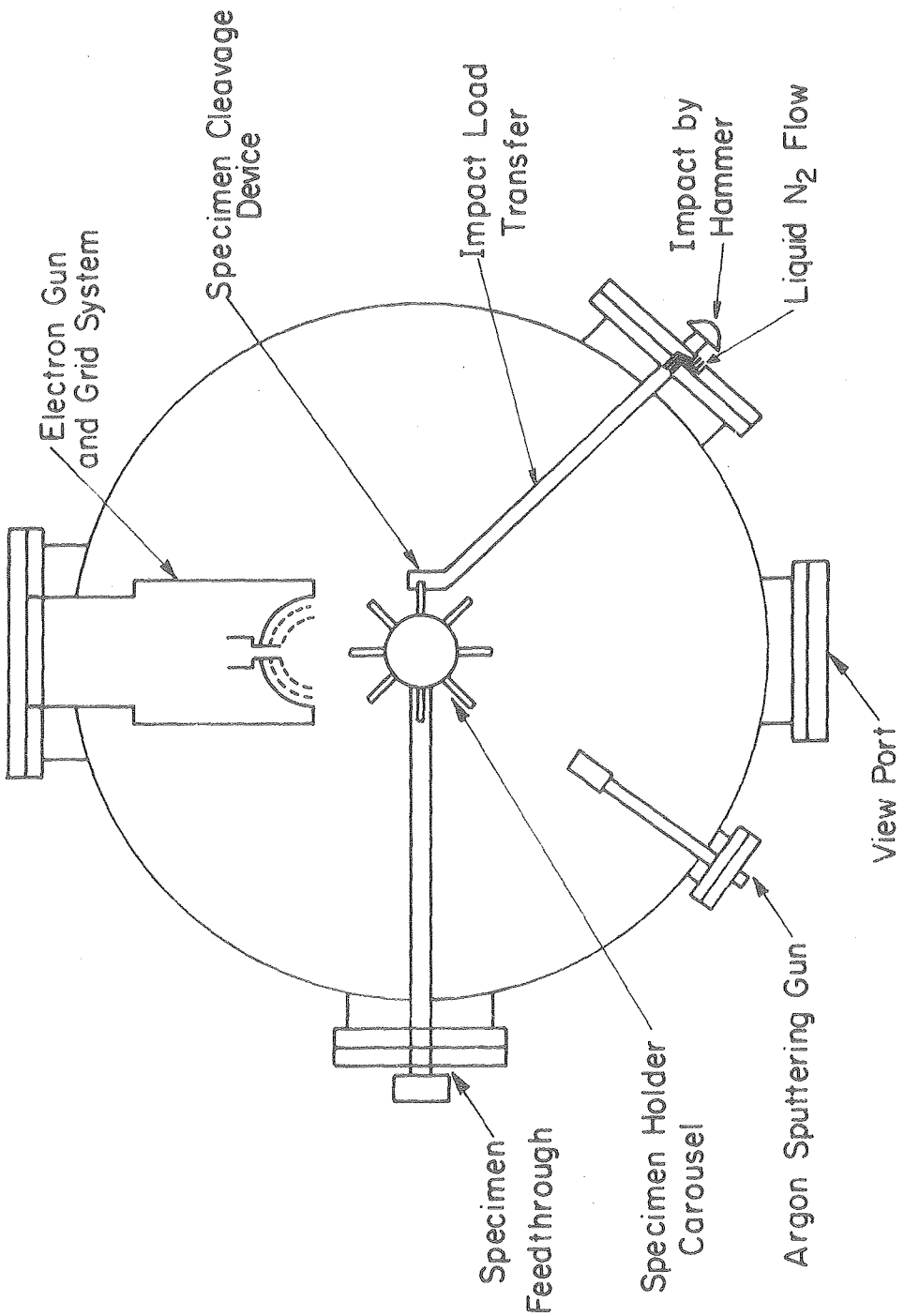
Electron Gun and Grid System
Specimen Cleavage Device
Impact Load Transfer
Impact by Hammer
Liquid N_2 Flow
View Port
Argon Sputtering Gun
Specimen Holder Carousel
Specimen Feedthrough
XBL 775-5402

Fig. 2.

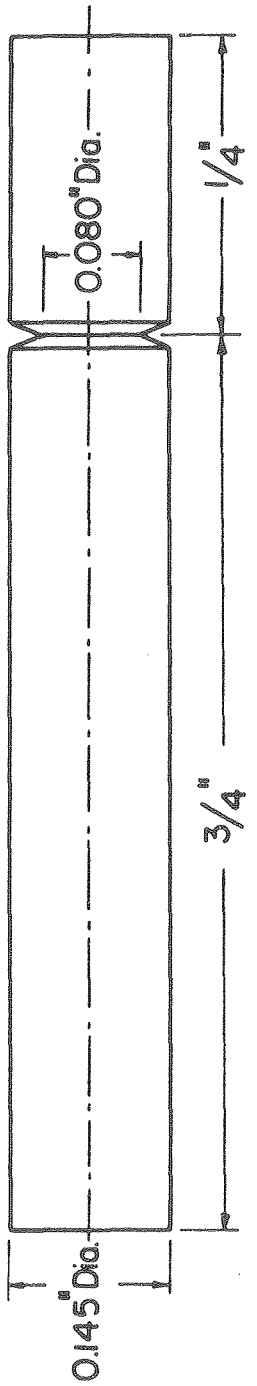

XBL 774-5353

Fig. 3.

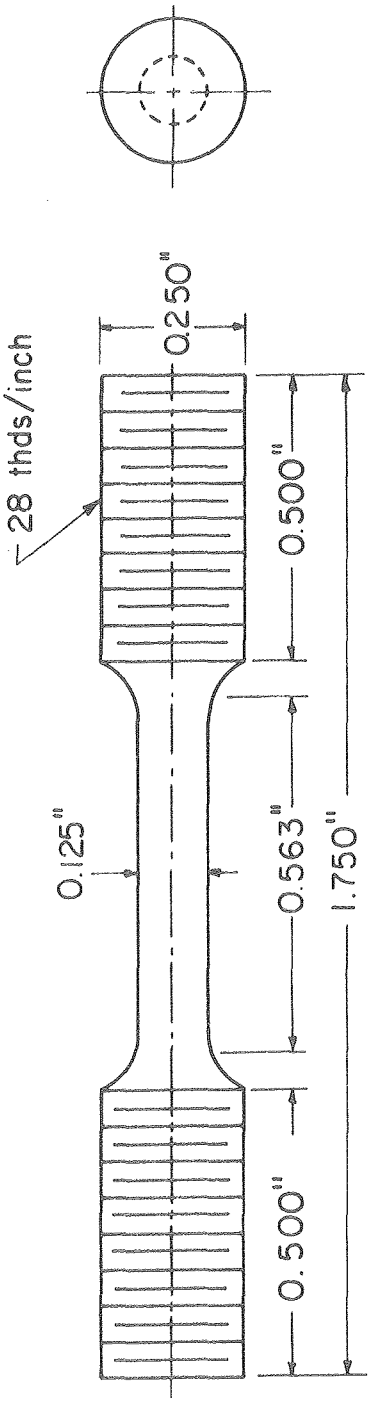

XBL 774-5354

Fig. 4.

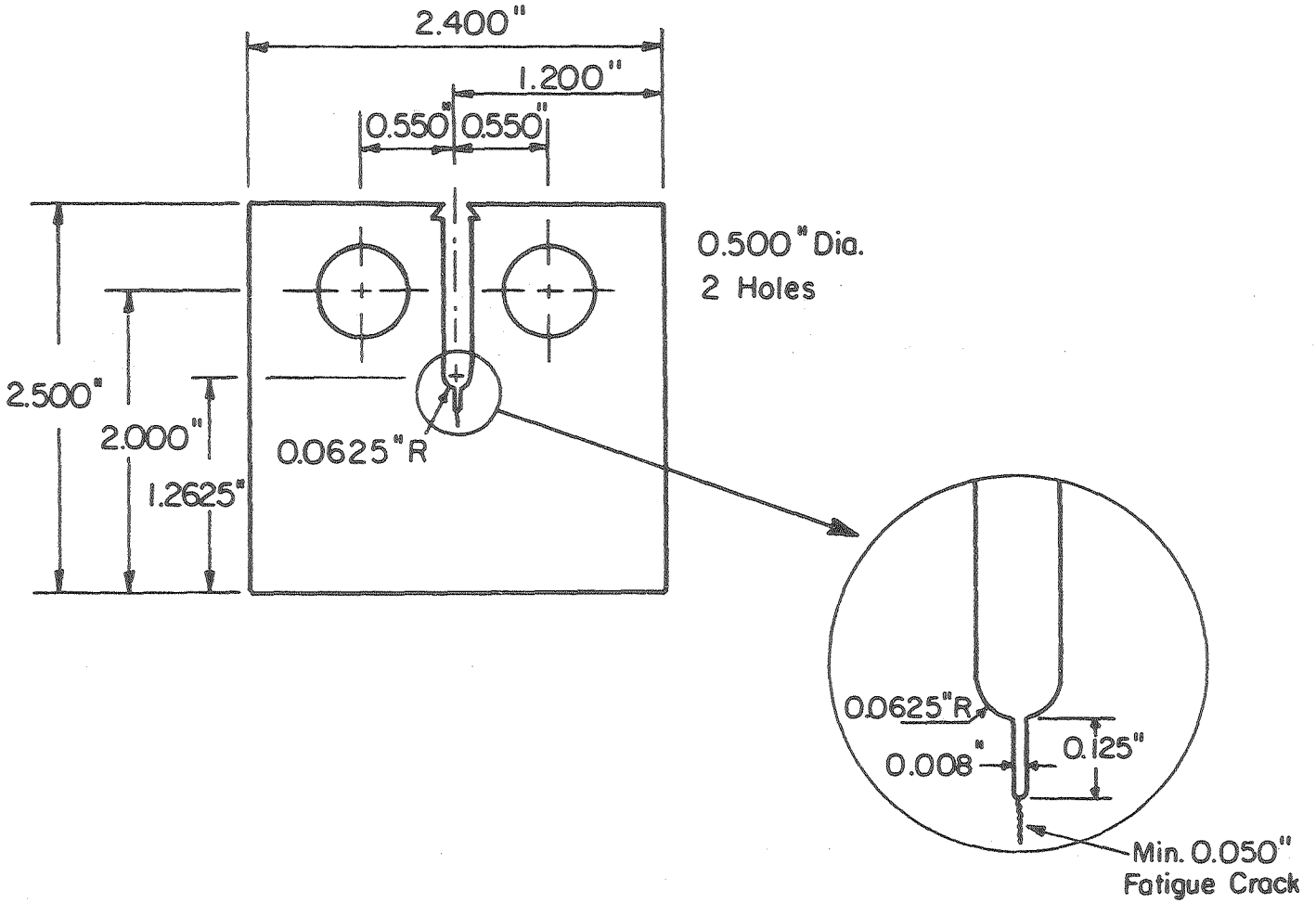
2.400"
1.200"
0.550"
0.550"
0.500" Dia.
2 Holes
2.500"
2.000"
1.2625"
0.0625"R
0.0625"R
0.008"
0.125"
Min. 0.050"
Fatigue Crack
XBL 775-5403

Fig. 5.

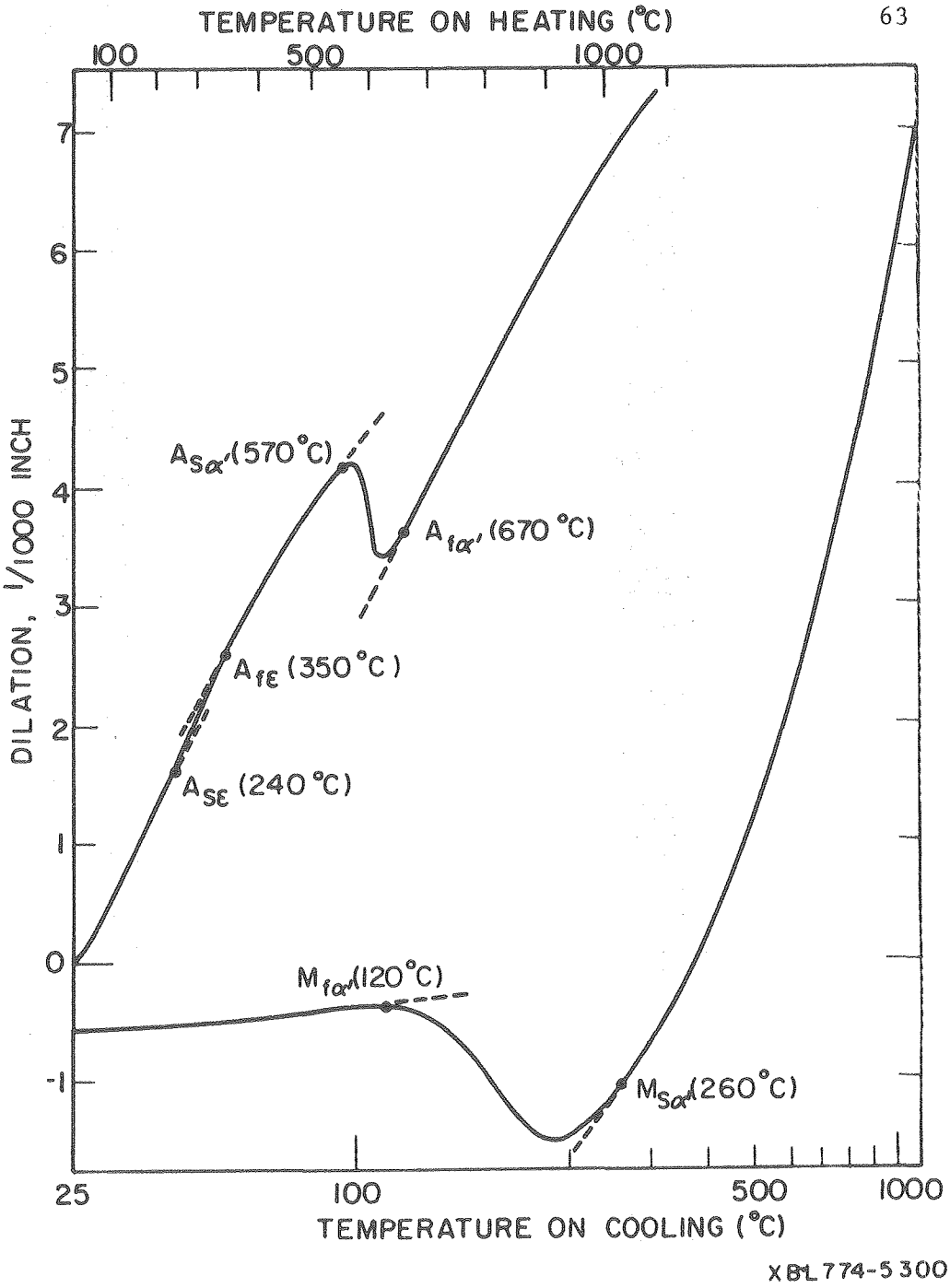

Fig. 6.

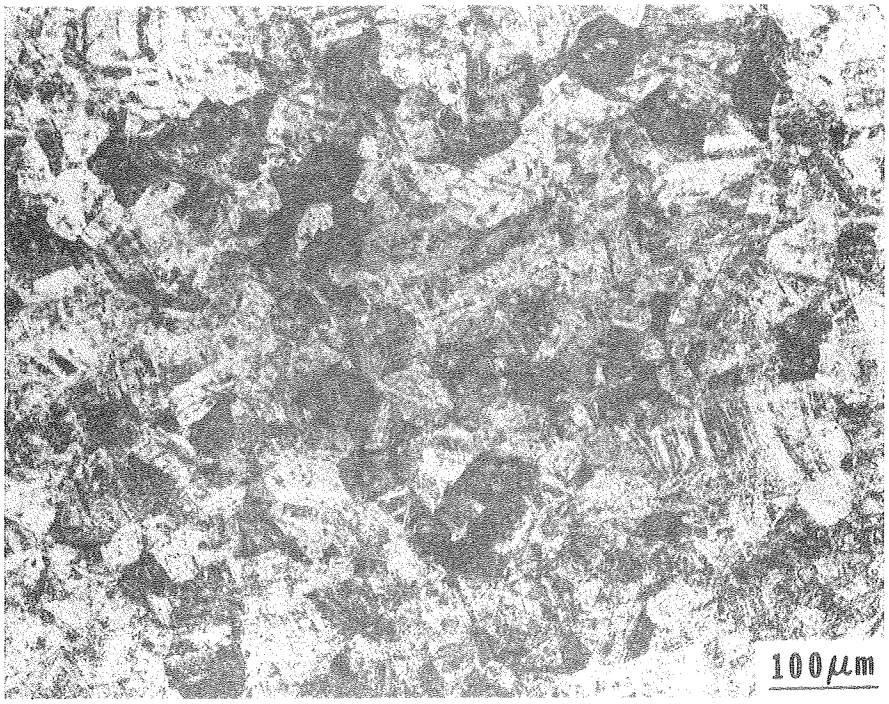

(a)

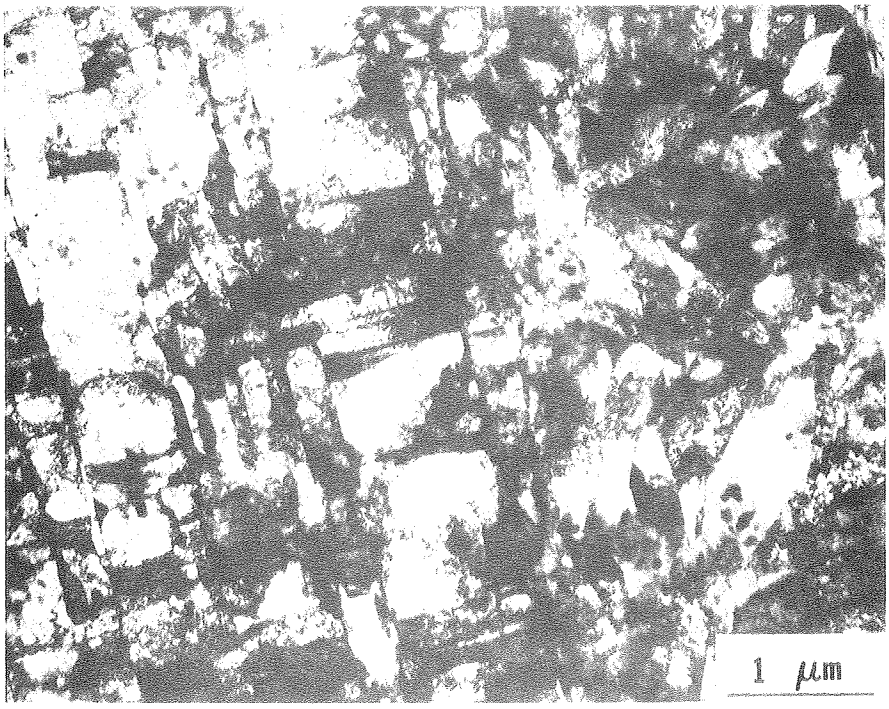

(b)

Fig. 7.

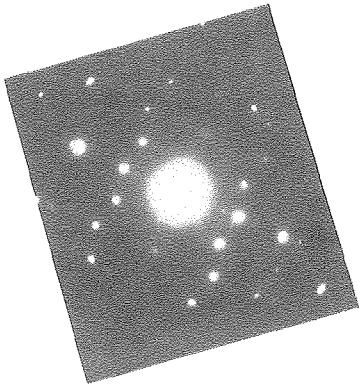

(a)

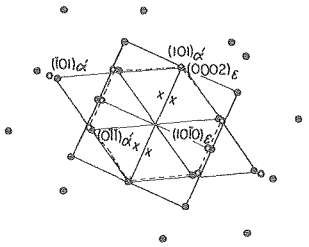

(b)

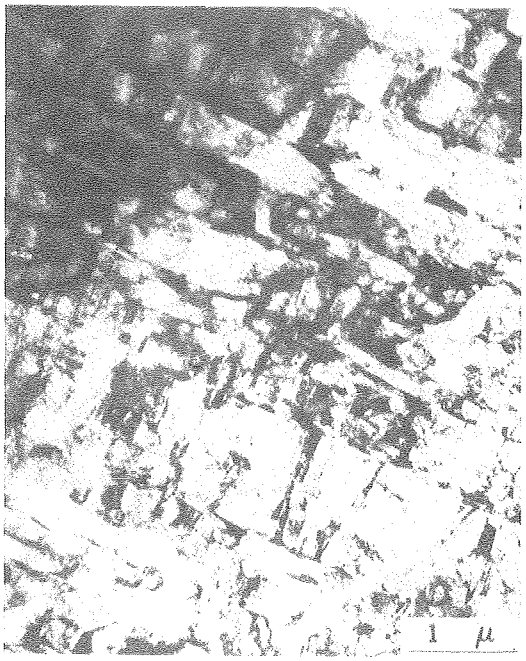

(c)

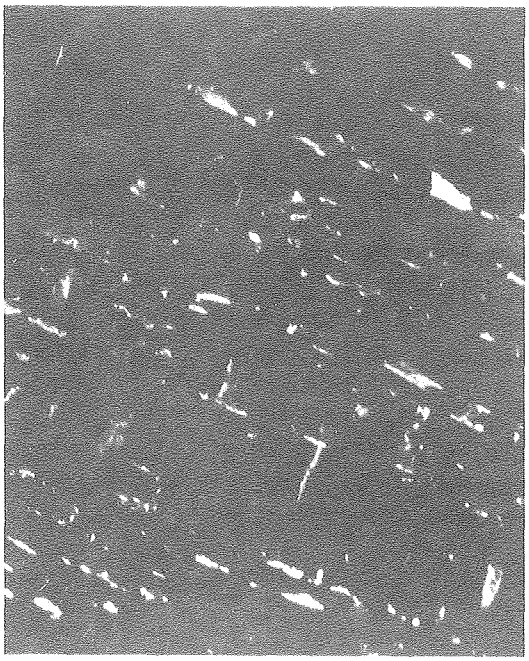

(d)

Fig. 8.

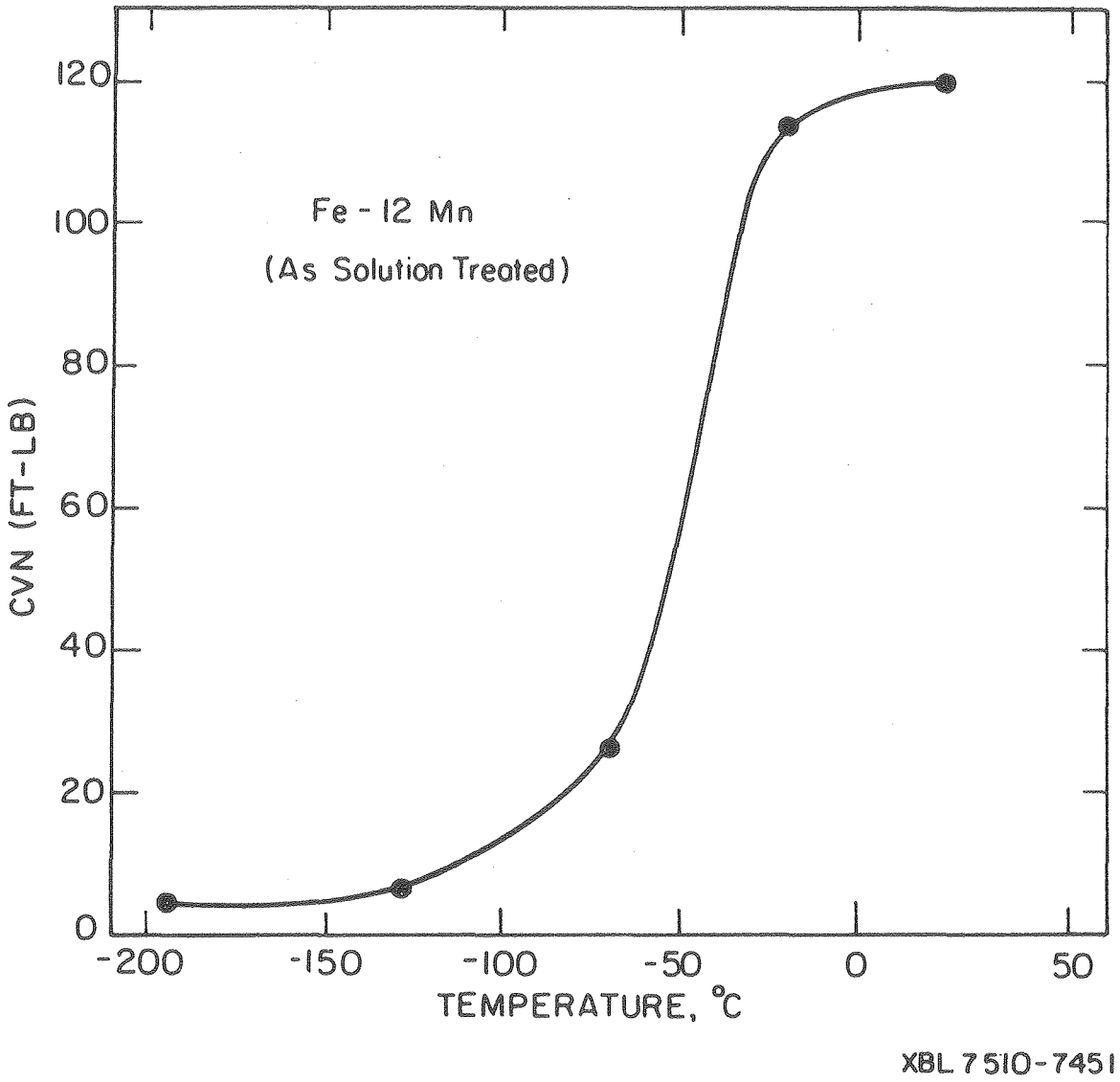
Fe - 12 Mn
(As Solution Treated)
CVN (FT-LB)
120
100
80
60
40
20
0
-200
-150
-100
-50
0
50
TEMPERATURE, °C
XBL 7510-7451

Fig. 9

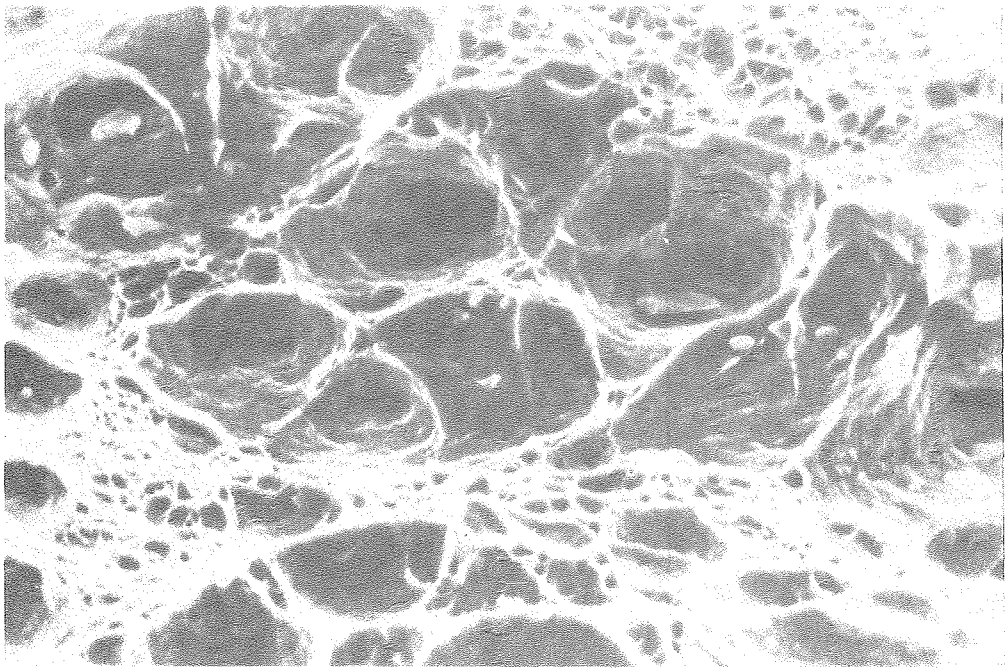

a

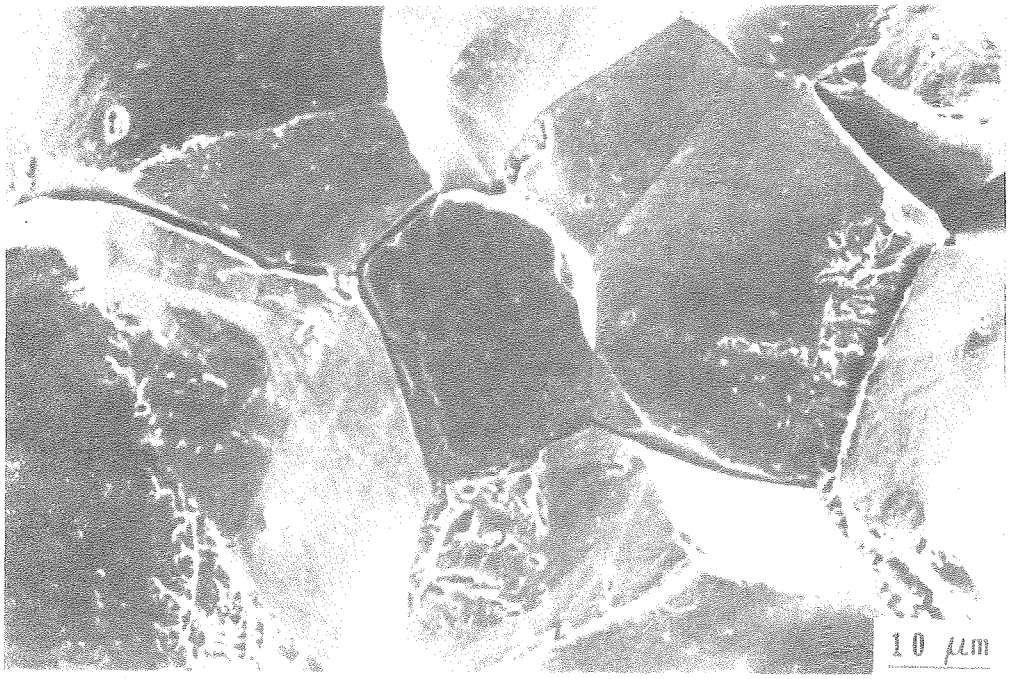

b

Fig. 10.

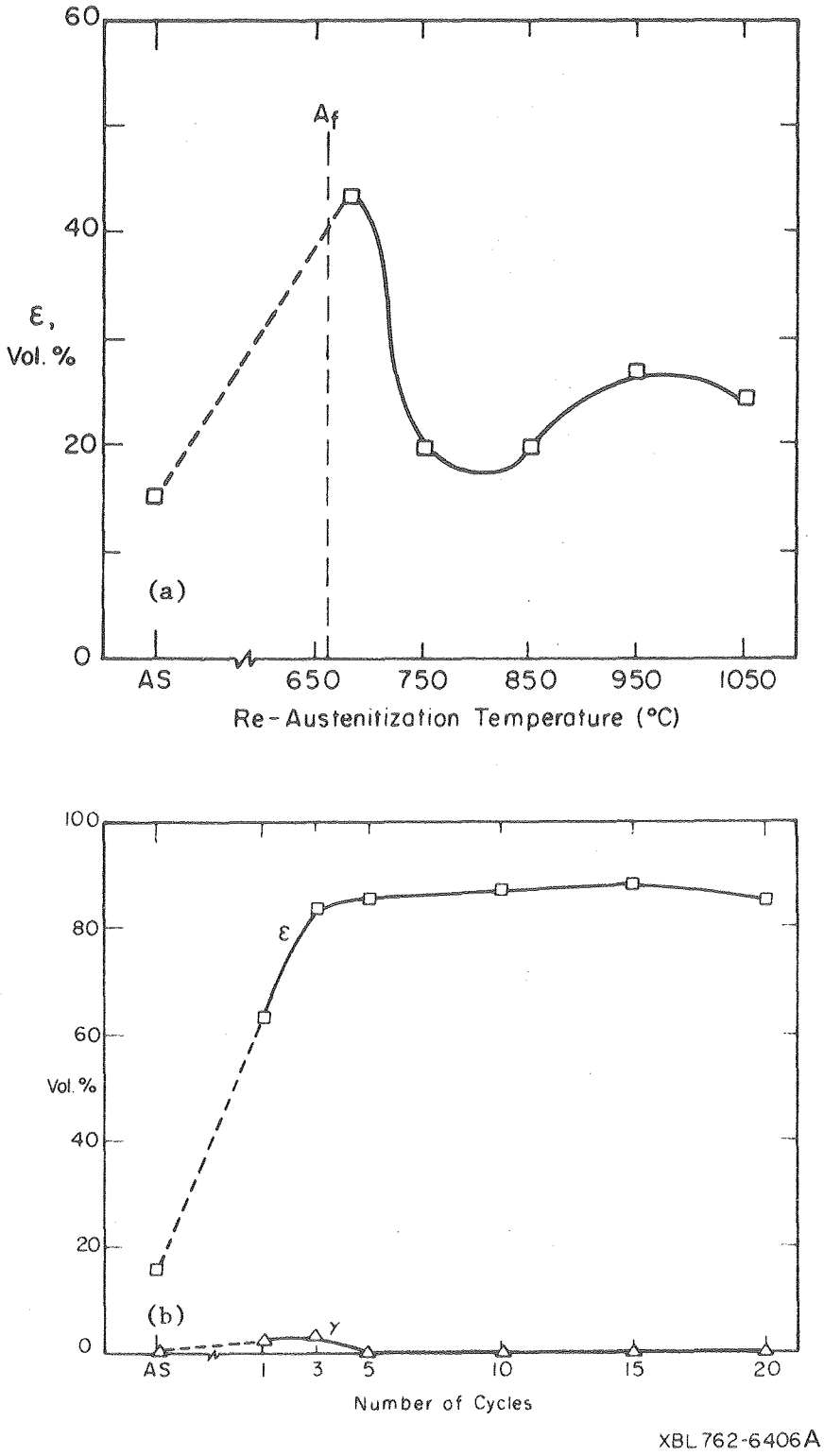
60
40
20
0
ε,
Vol. %
A_f
(a)
AS
650
750
850
950
1050
Re-Austenitization Temperature (°C)
100
80
60
40
20
0
Vol. %
ε
γ
(b)
AS
1
3
5
10
15
20
Number of Cycles
XBL 762-6406A

Fig. 11.

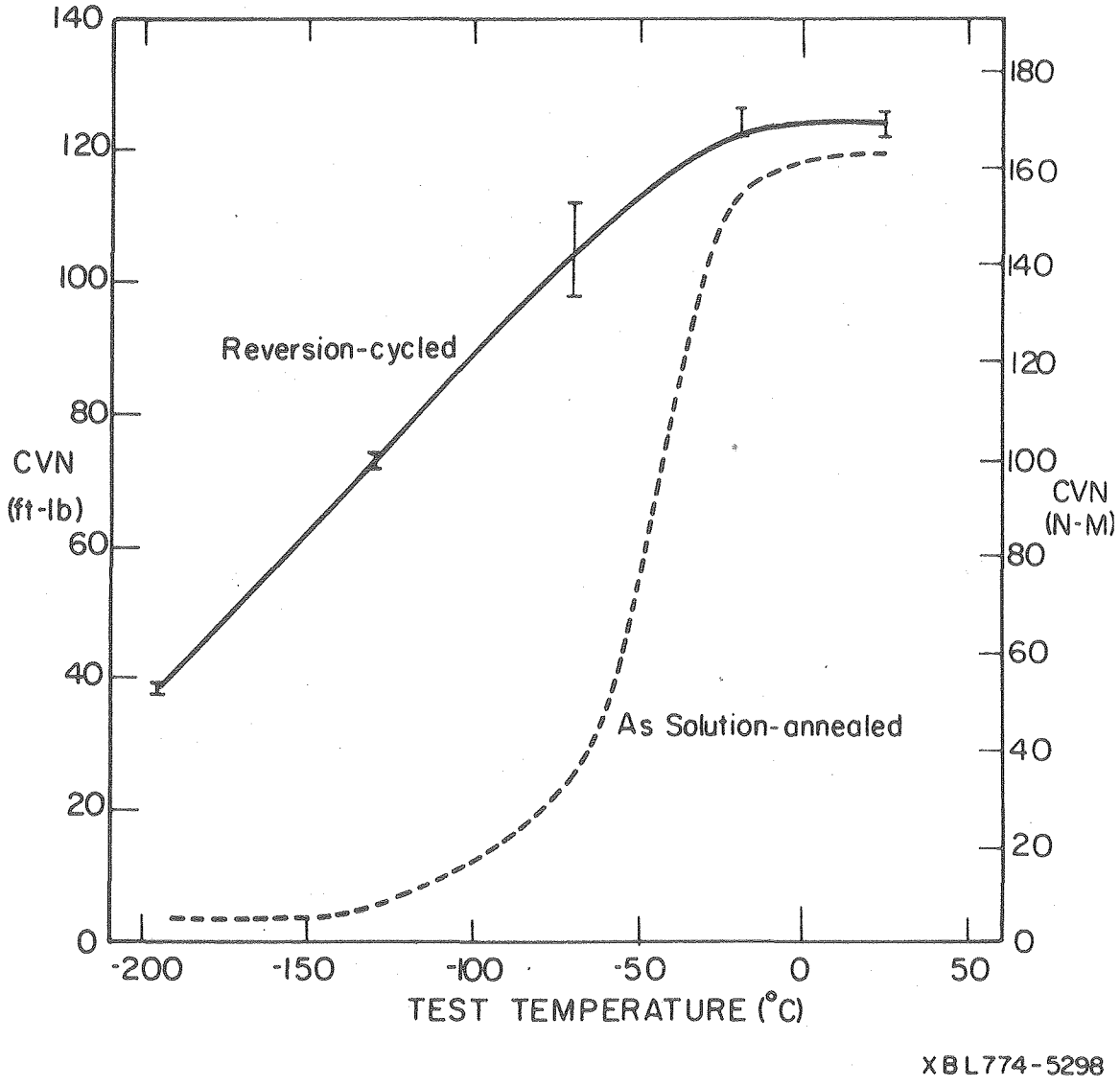

Fig. 12.

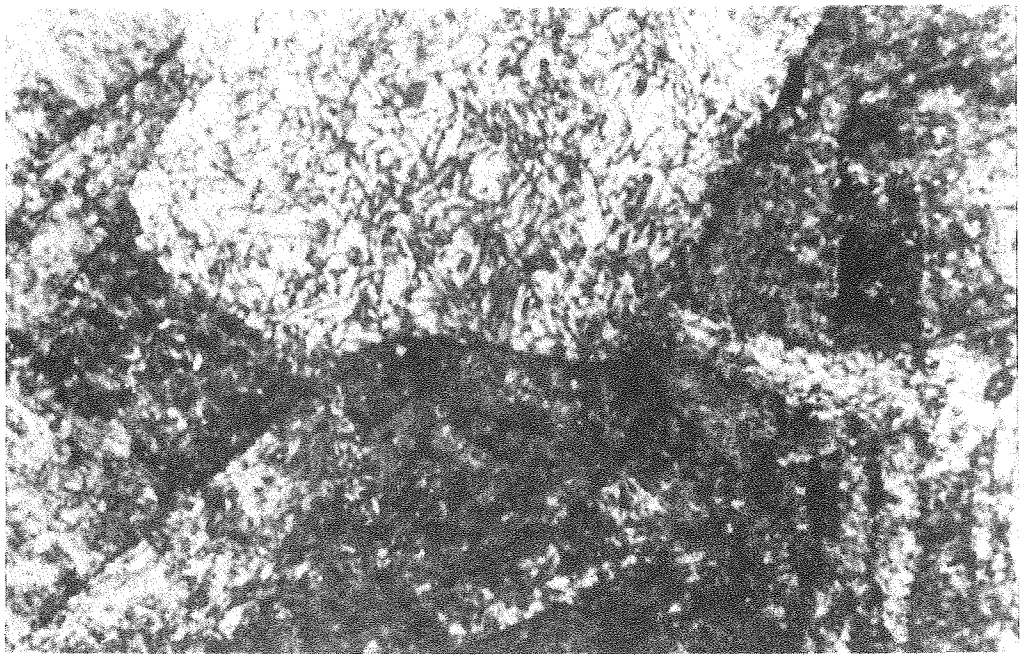

a

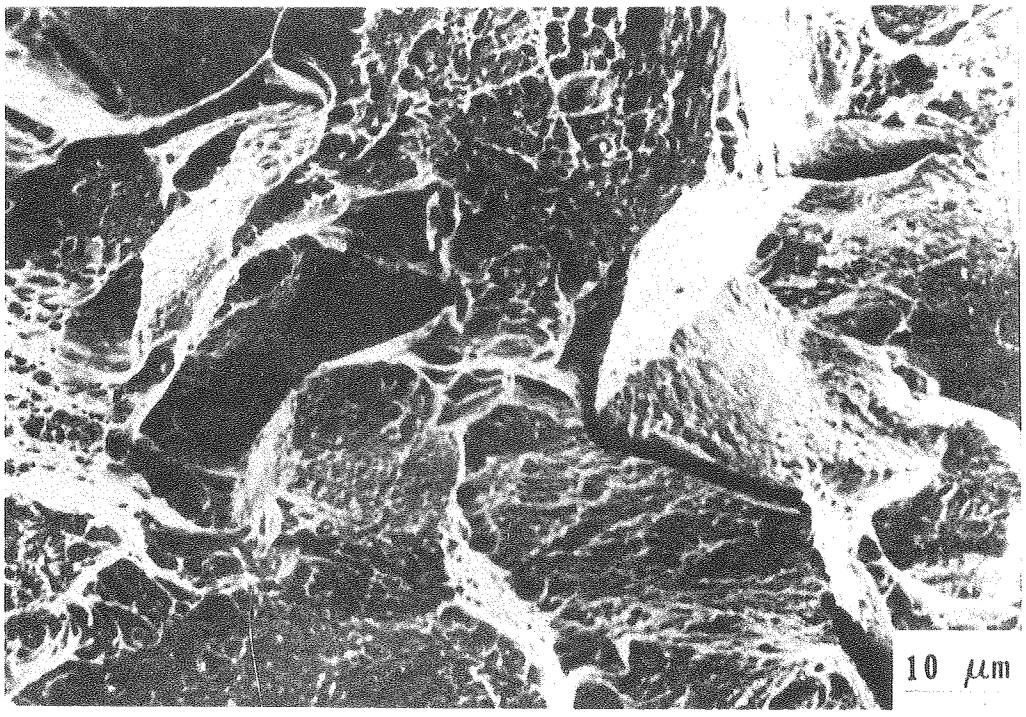

b

Fig. 13.

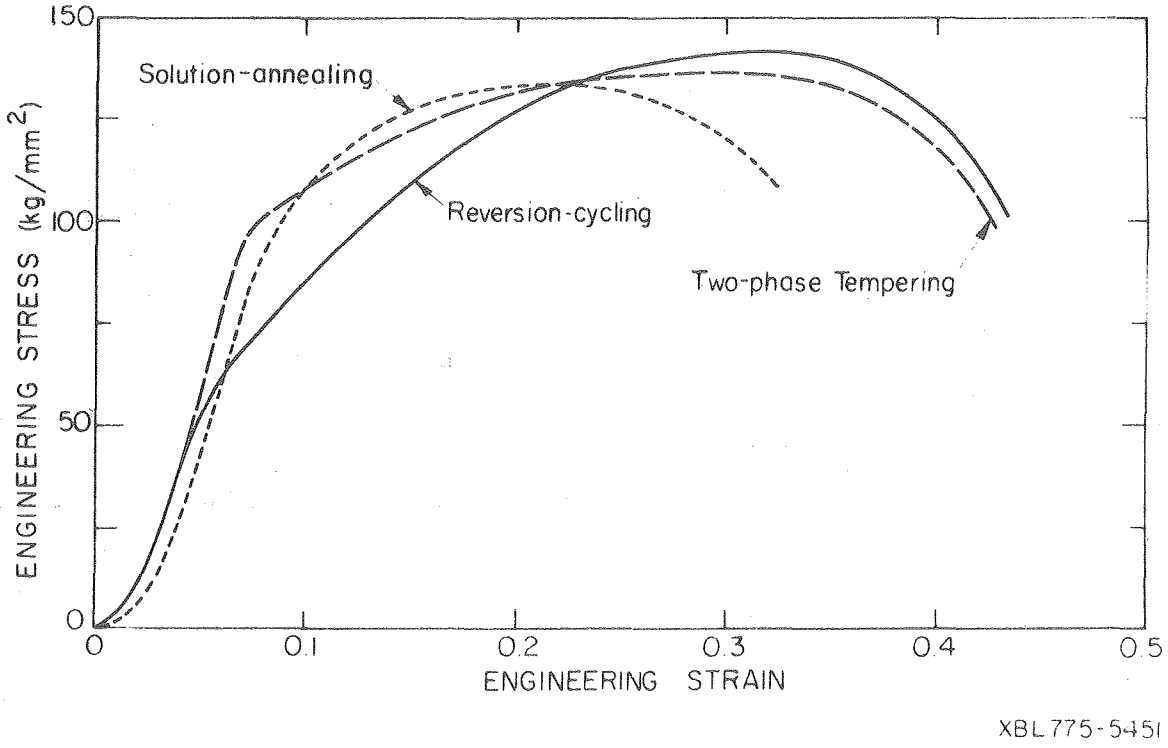

Fig. 14.

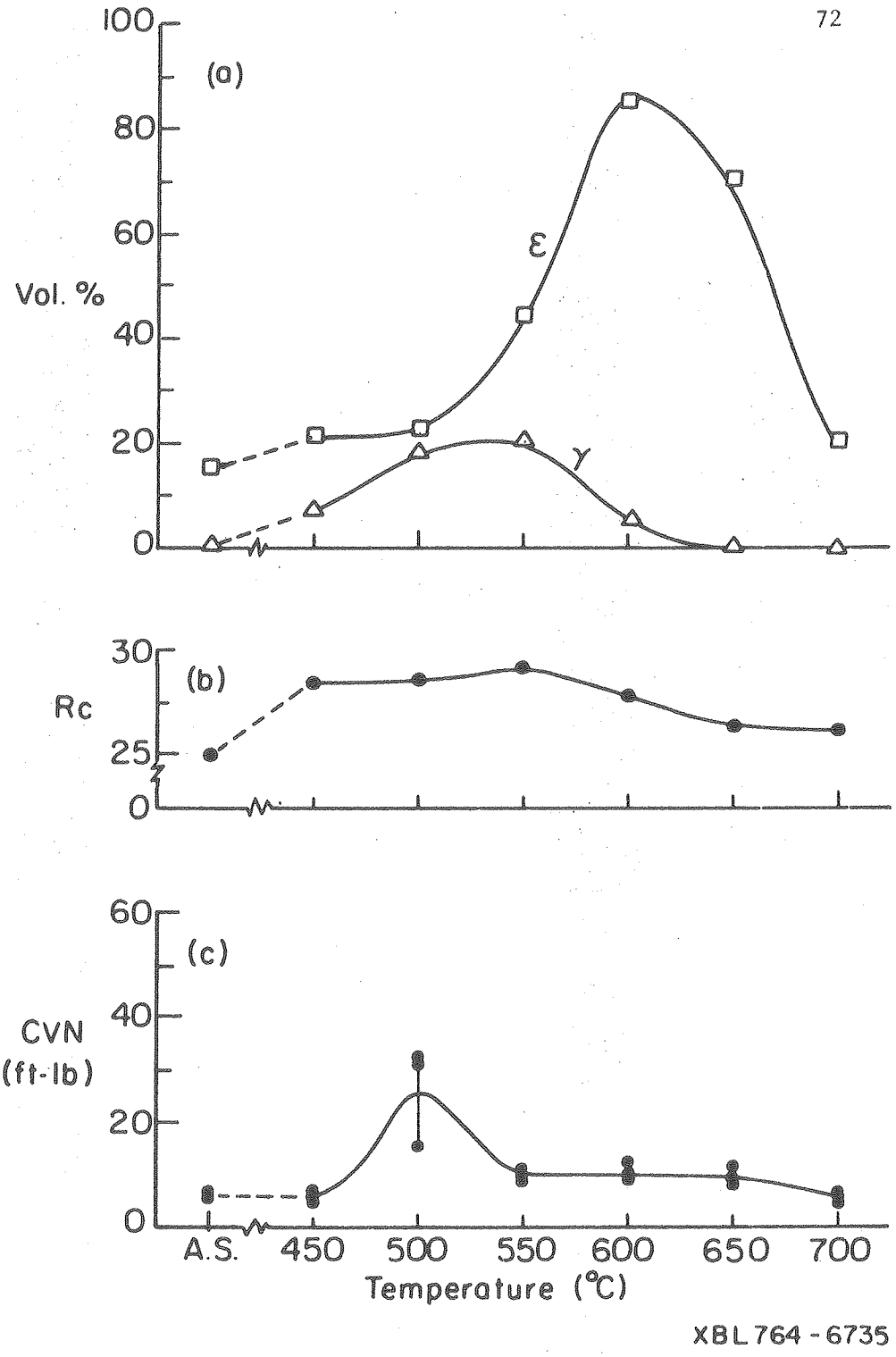
100
80
60
40
20
0
Vol. %
(a)
ε
γ
30
25
0
Rc
(b)
60
40
20
0
CVN
(ft-lb)
(c)
A.S.
450
500
550
600
650
700
Temperature (°C)
XBL764-6735

Fig. 15.

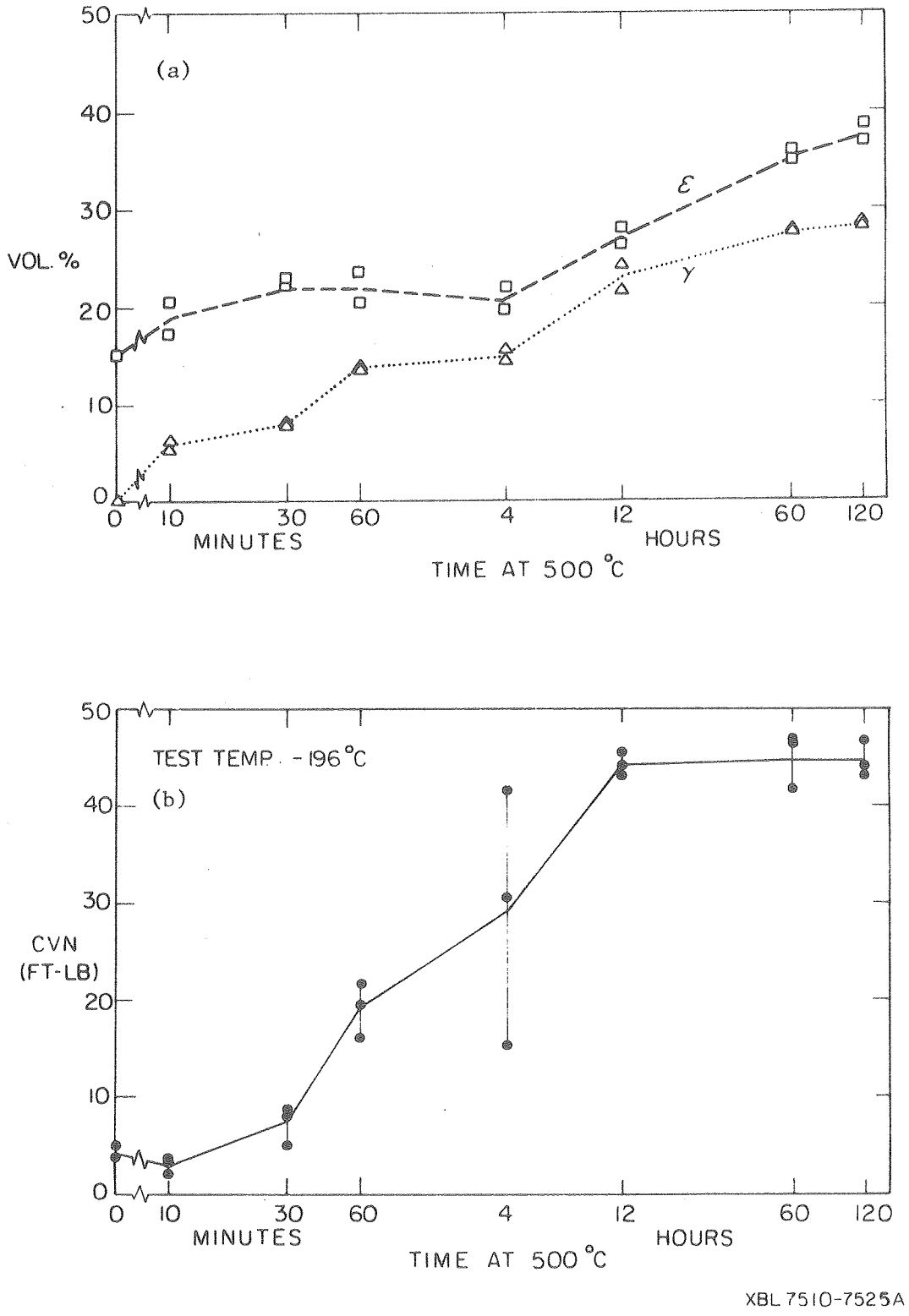

Fig. 16.

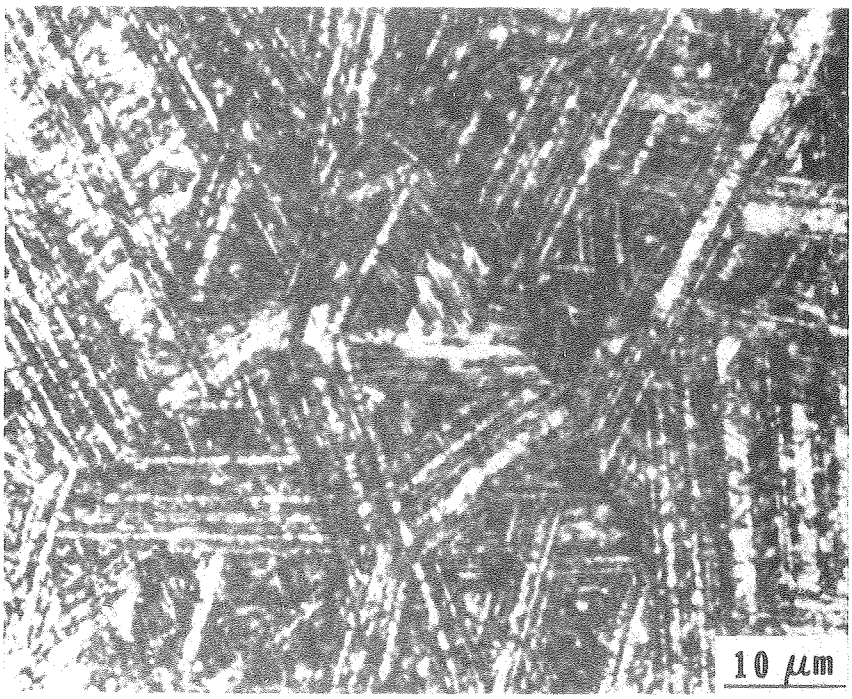

(a)

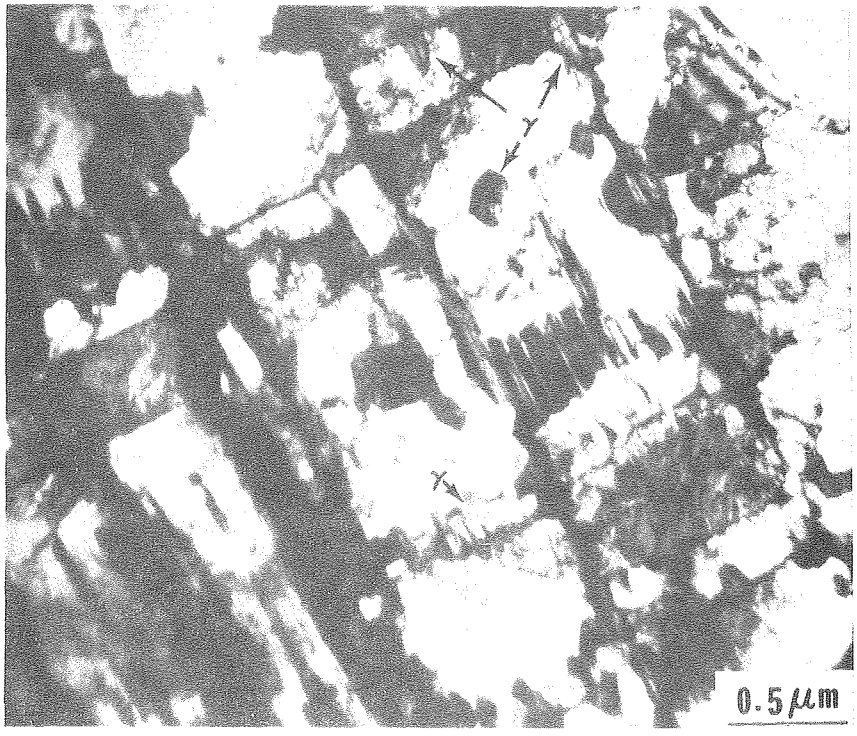

(b)

Fig. 17.

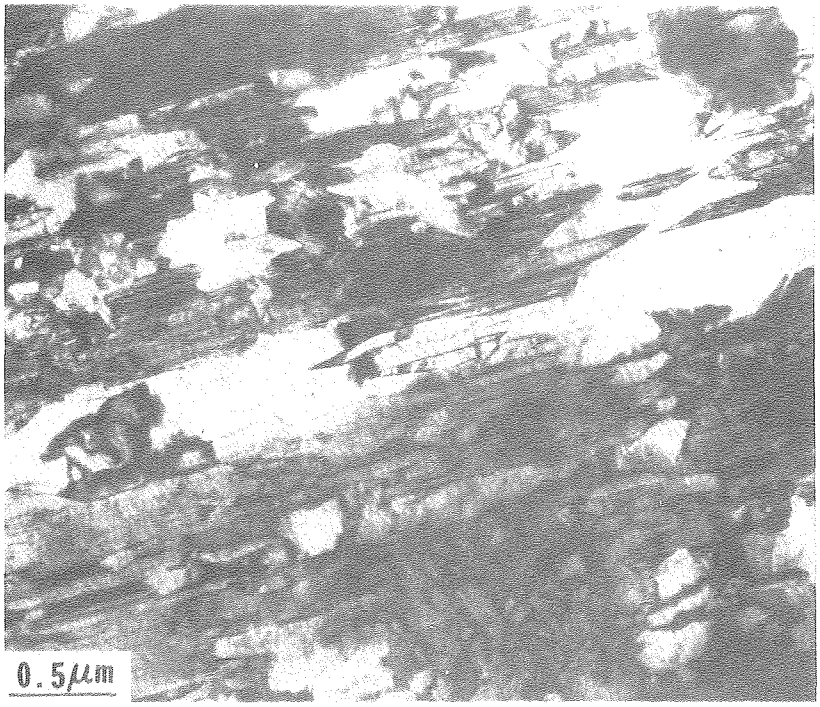

(a)

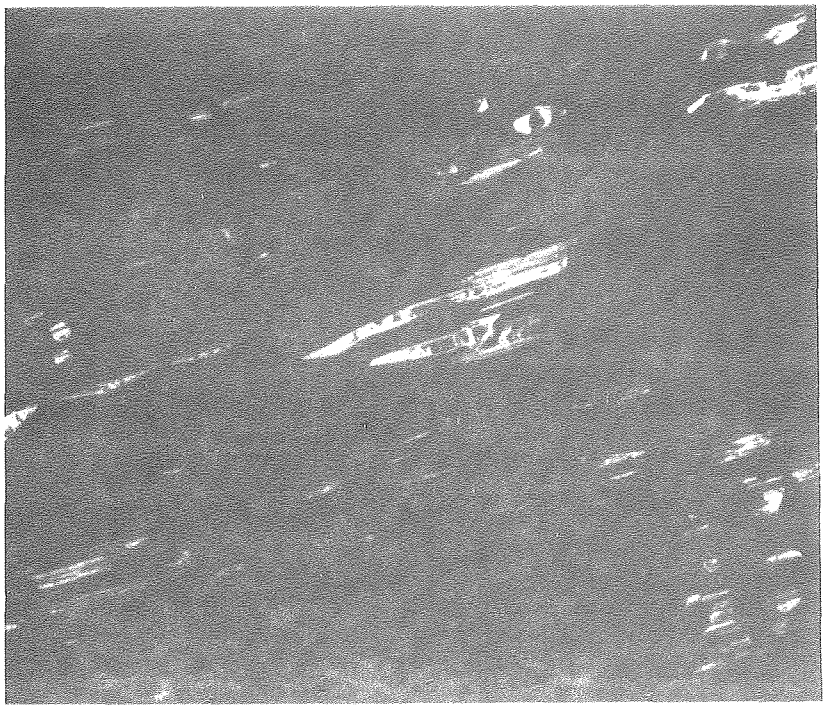

(b)

Fig. 18.

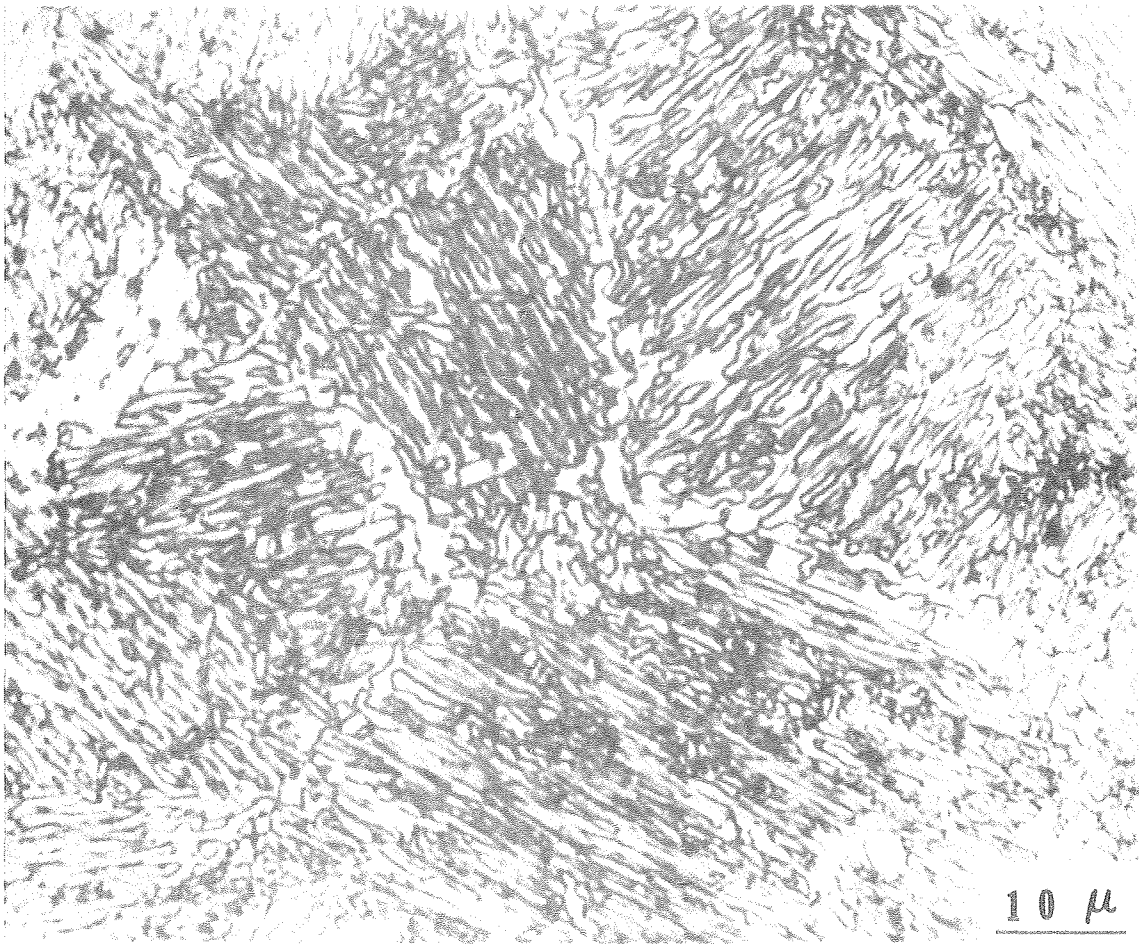

Fig. 19.

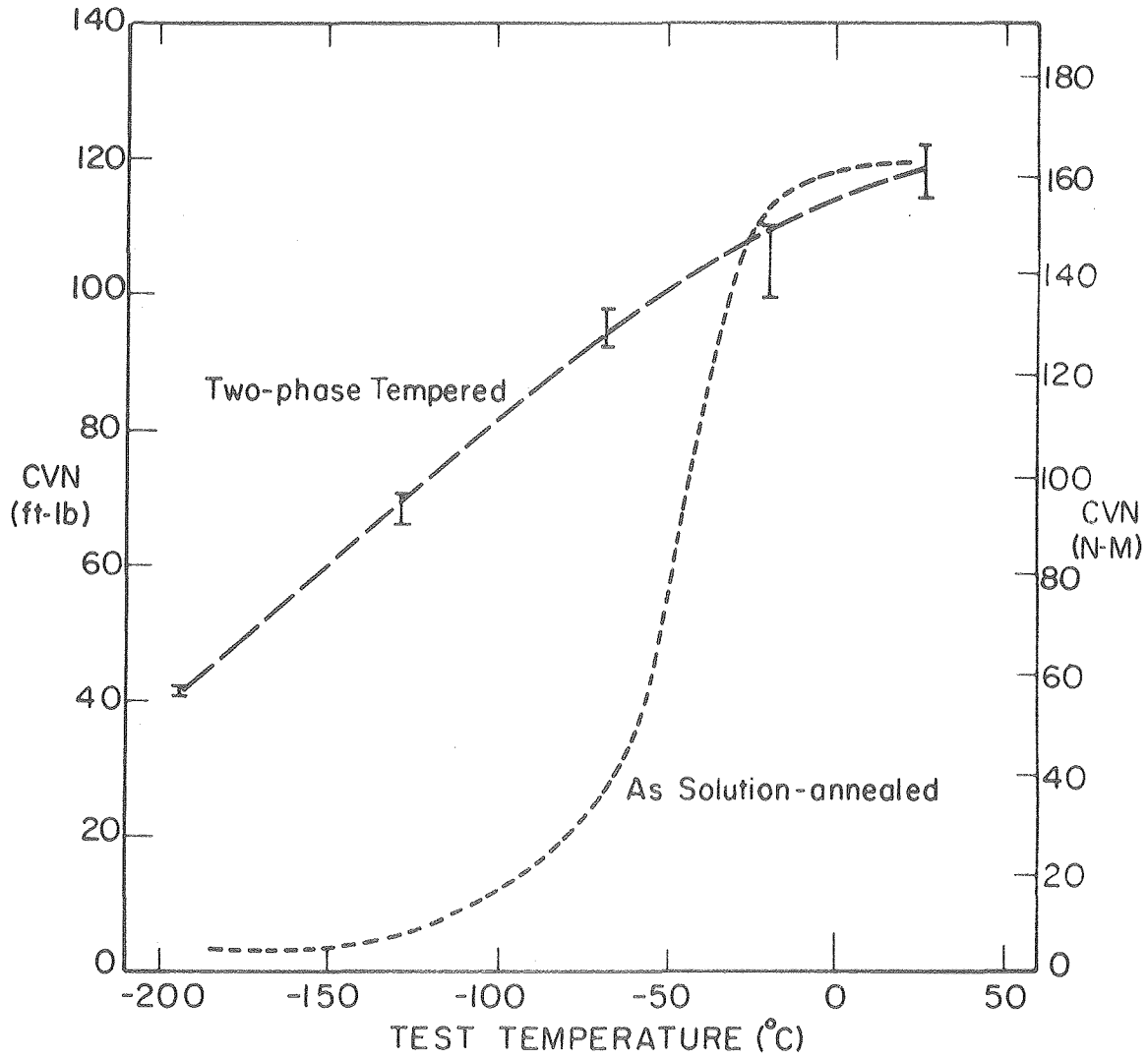

Fig. 20.

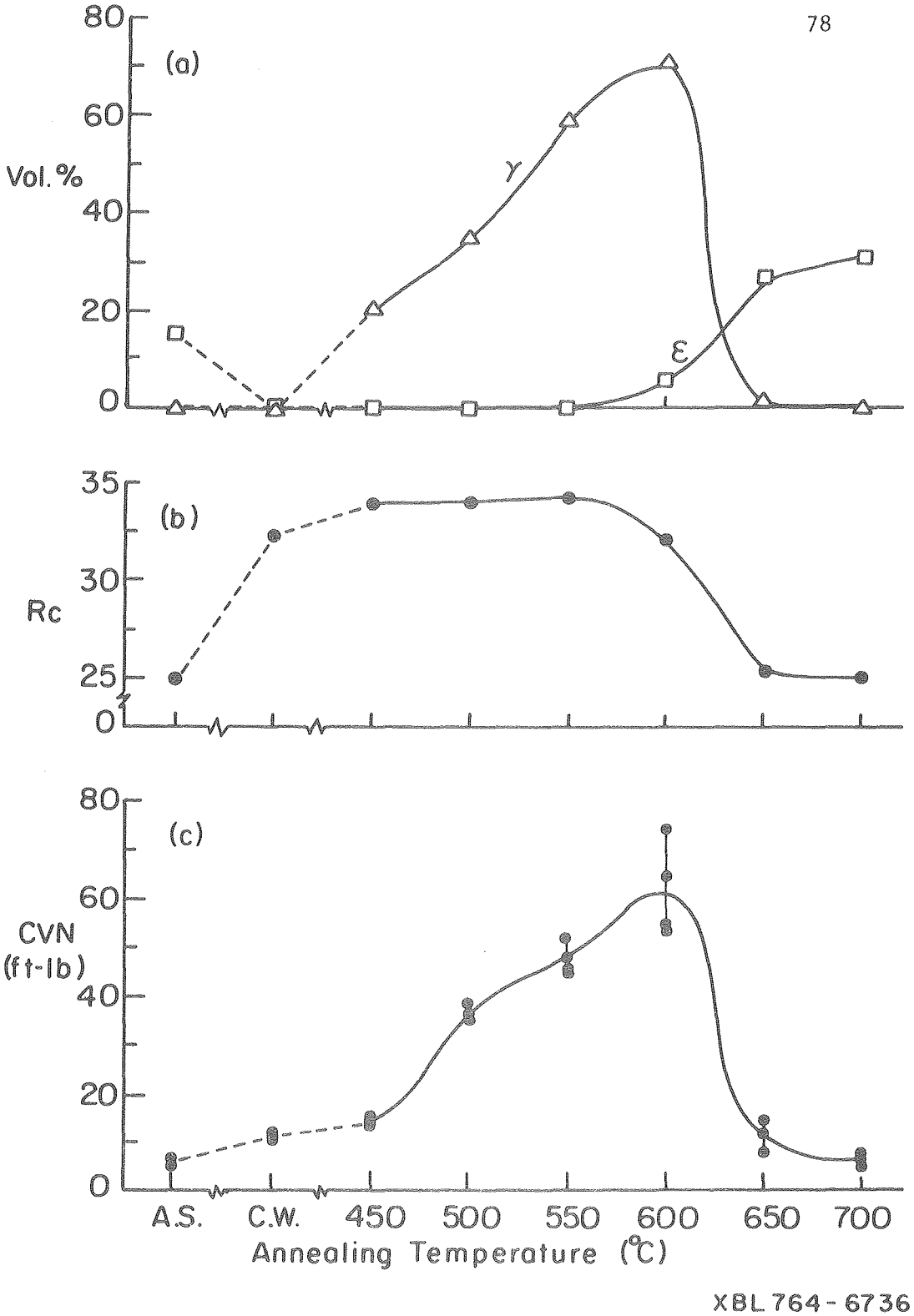
80
(a)
60
Vol.%
40
γ
20
ε
0
35
(b)
Rc
30
25
0
80
(c)
60
CVN
(ft-lb)
40
20
0
A.S.
C.W.
450
500
550
600
650
700
Annealing Temperature (°C)
XBL 764-6736

Fig. 21.

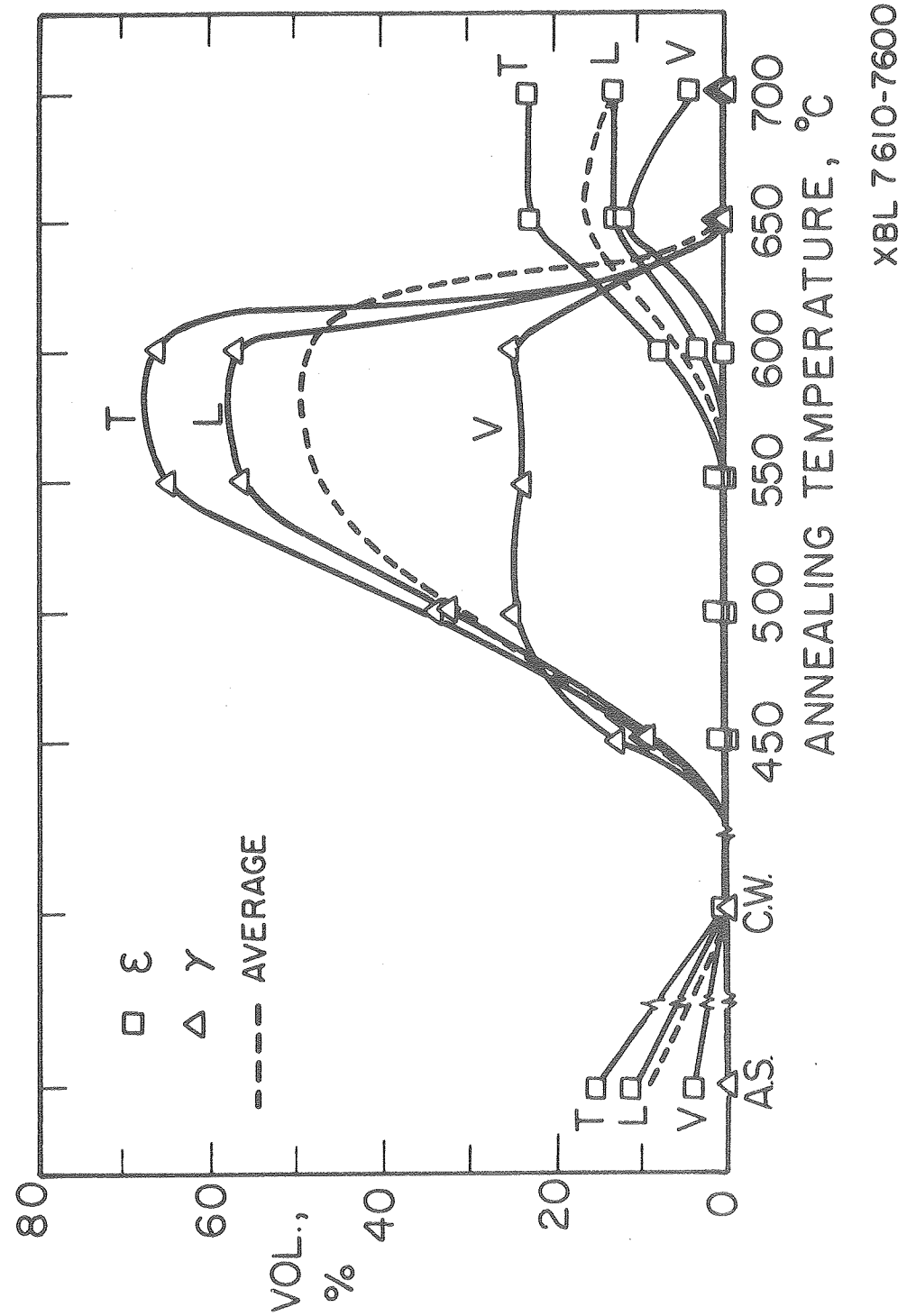
80
60
40
20
0
VOL., %
ε
γ
AVERAGE
A.S.
C.W.
T
L
V
450
500
550
600
650
700
ANNEALING TEMPERATURE, °C
XBL 7610-7600

Fig. 22.

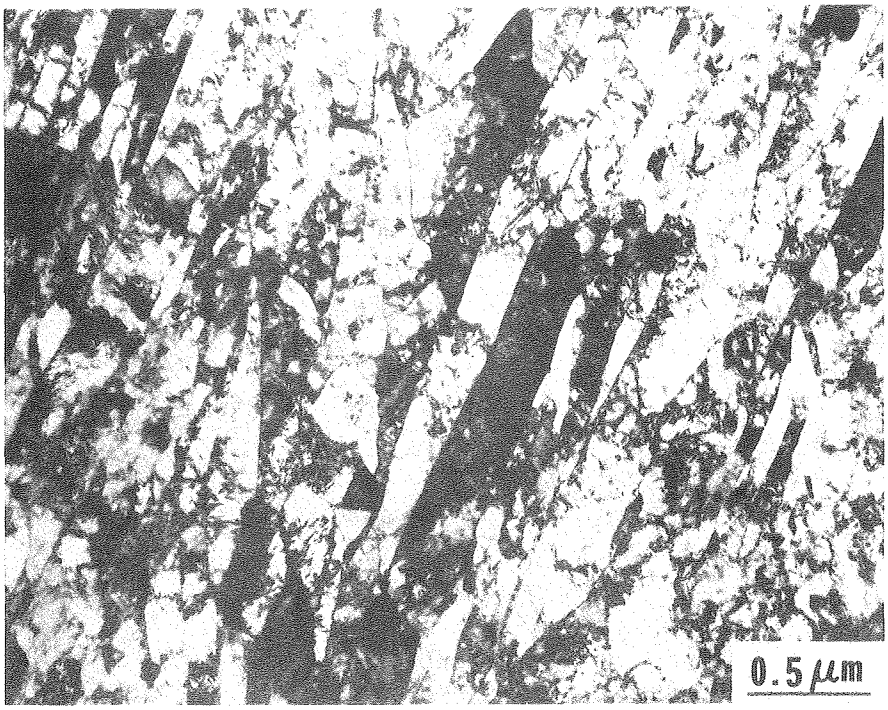

(a)

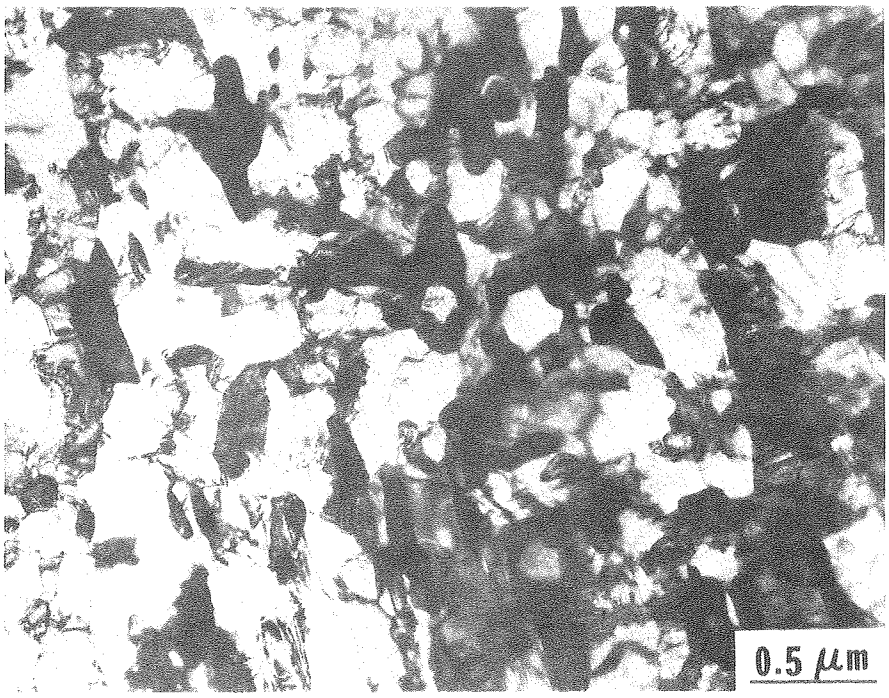

(b)

Fig. 23.

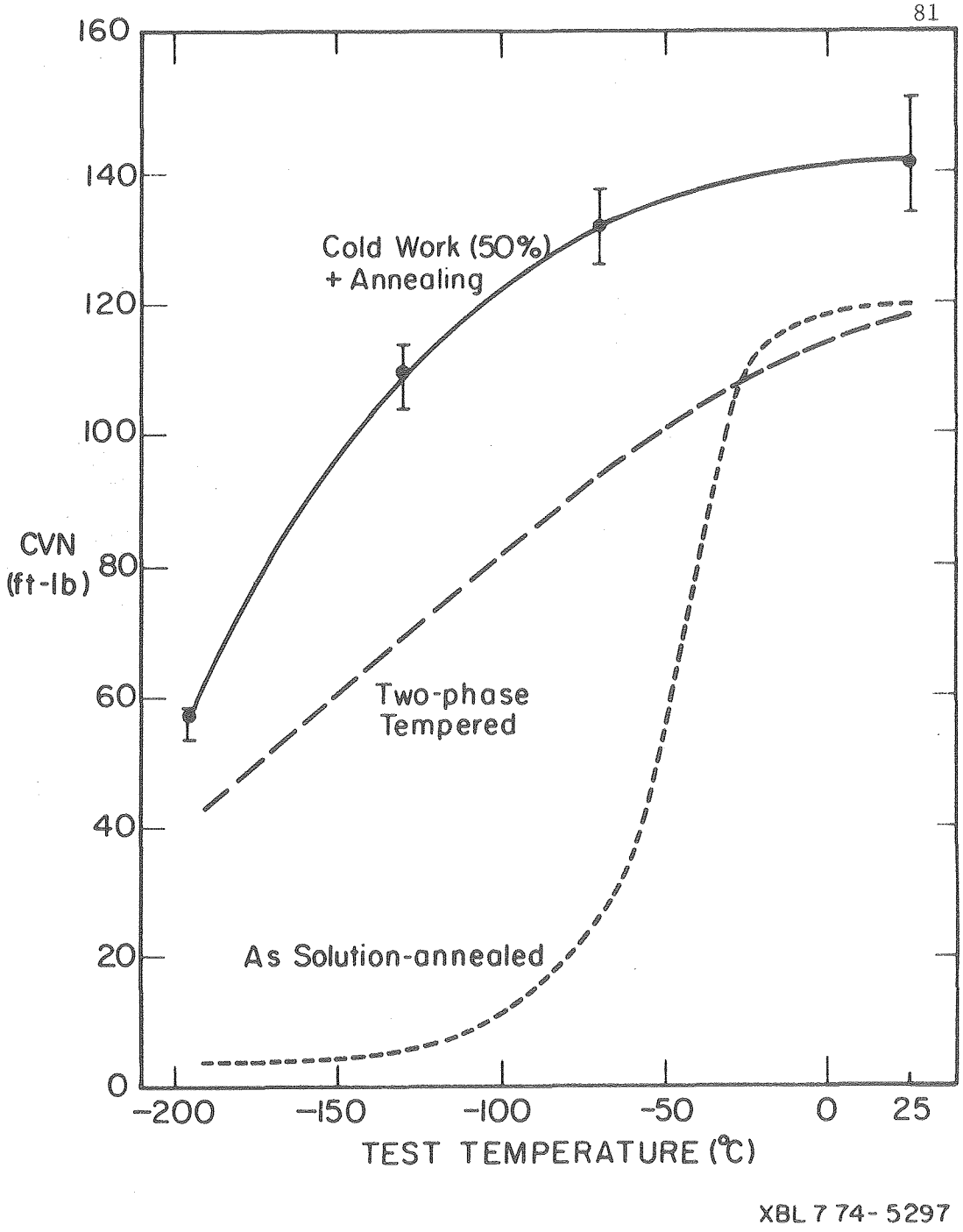
160
140
120
100
80
60
40
20
0
CVN
(ft-lb)
Cold Work (50%)
+ Annealing
Two-phase
Tempered
As Solution-annealed
-200
-150
-100
-50
0
25
TEST TEMPERATURE (°C)
XBL 774-5297

Fig. 24.

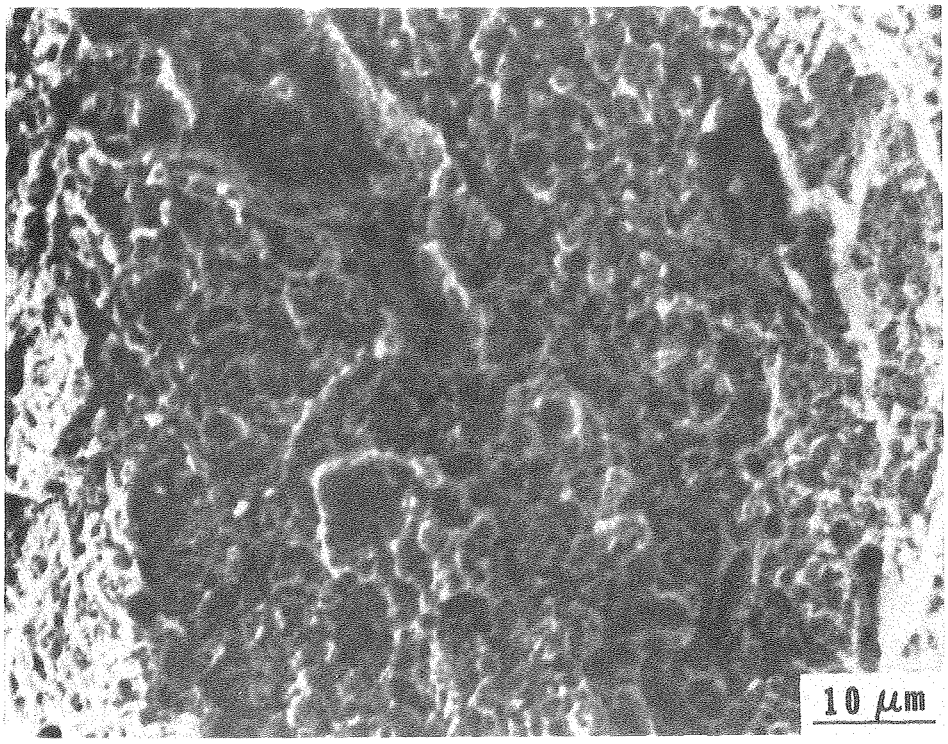

(a)

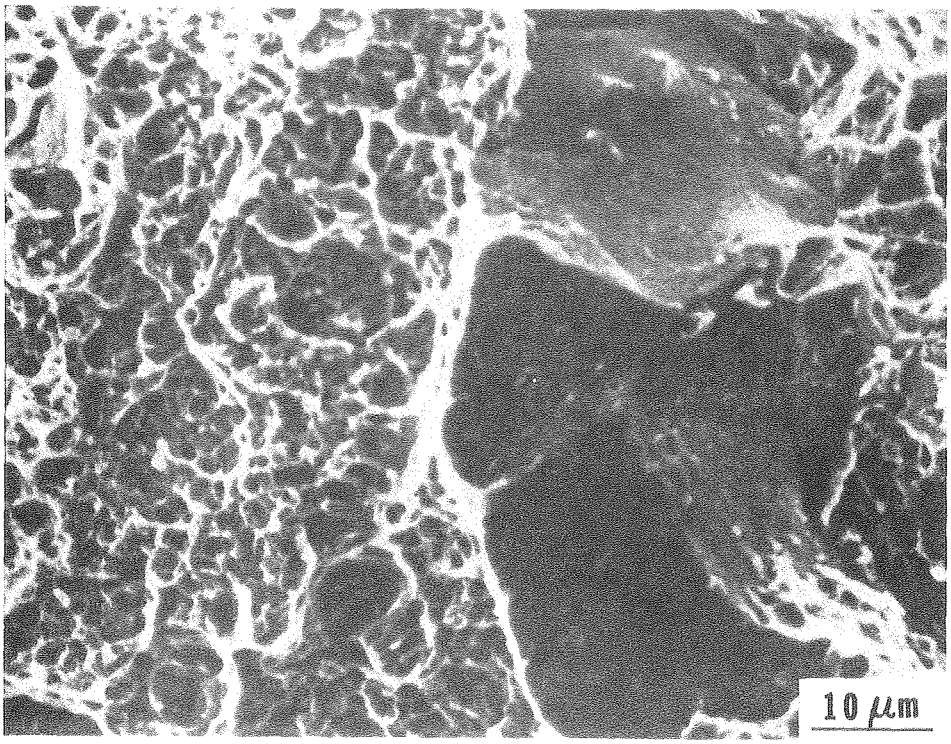

(b)

Fig. 25.

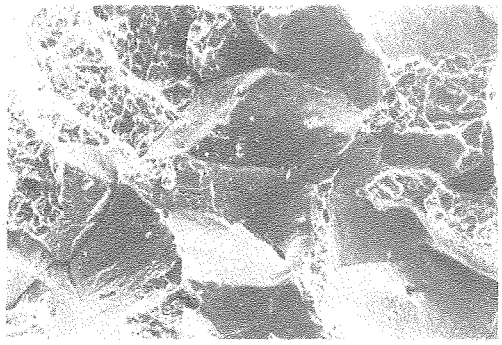

a

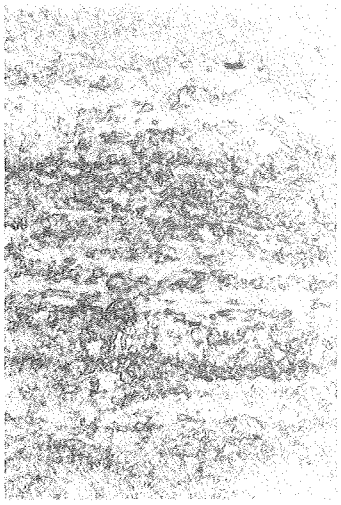

b

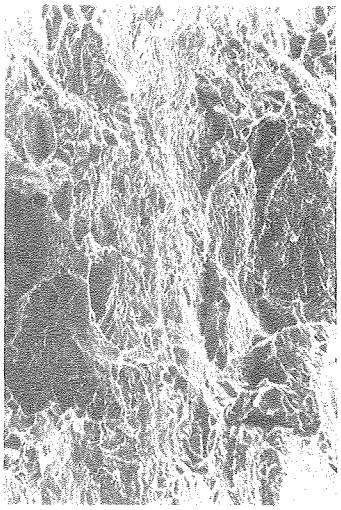

c

d

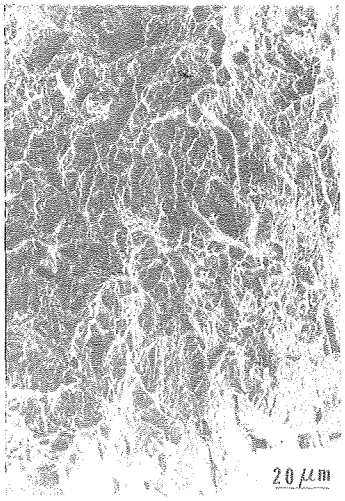

e

Fig. 26.

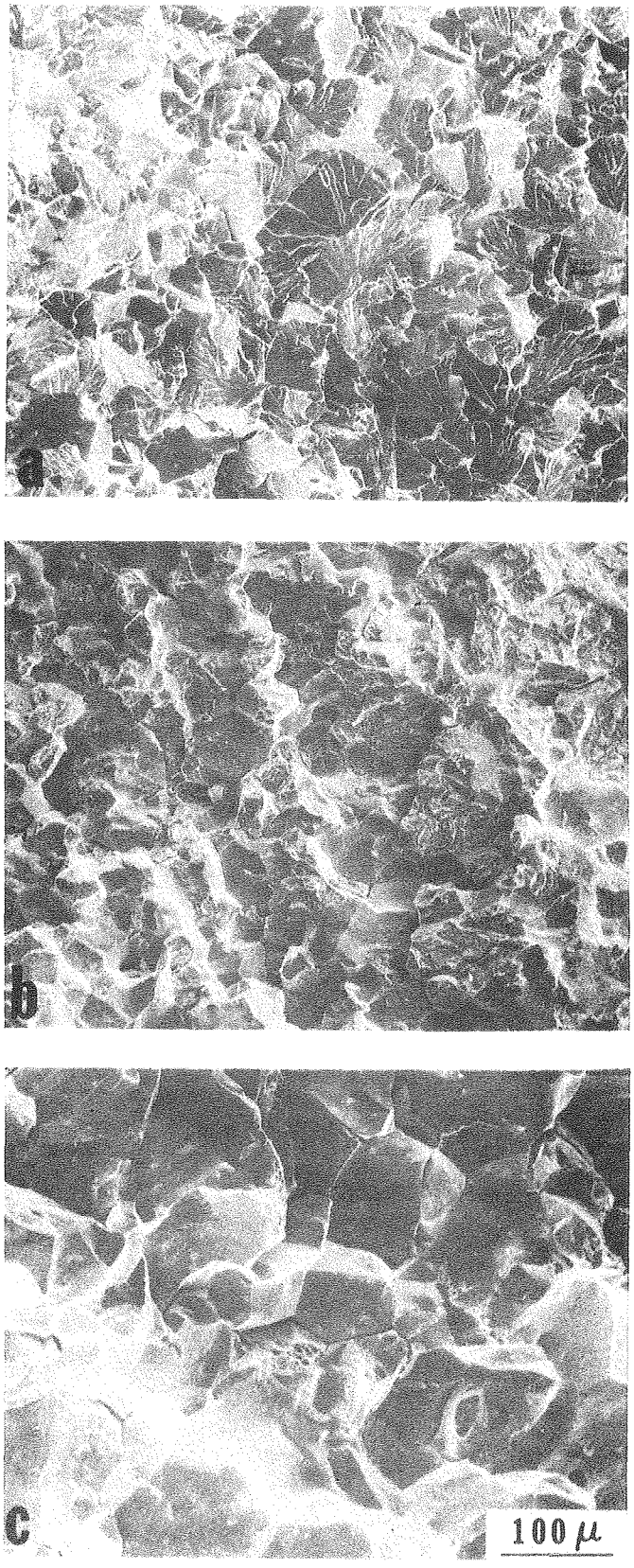

Fig. 27.

Fig. 28.

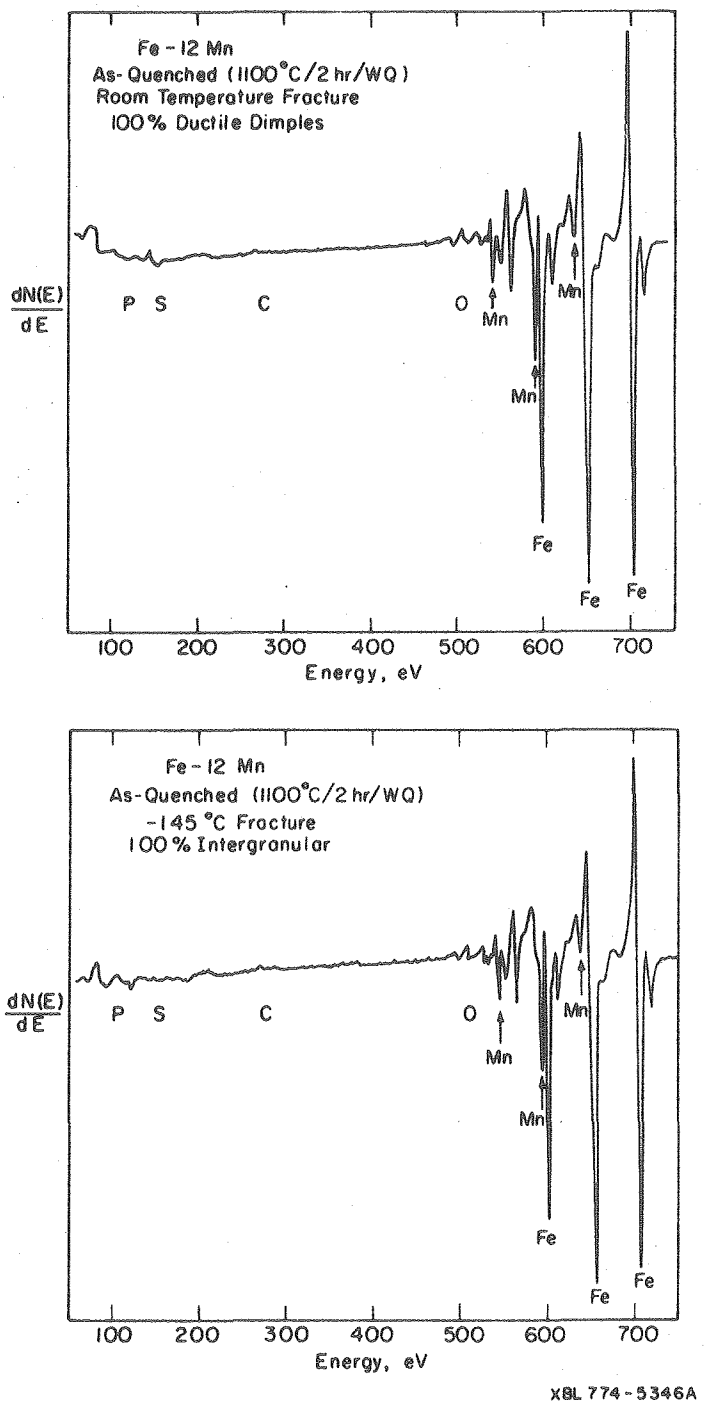
Fe - 12 Mn
As-Quenched (1100°C/2 hr/WQ)
Room Temperature Fracture
100% Ductile Dimples
dN(E)/dE
P S C O Mn Mn Mn Fe Fe Fe
100 200 300 400 500 600 700
Energy, eV
Fe - 12 Mn
As-Quenched (1100°C/2 hr/WQ)
-145 °C Fracture
100% Intergranular
dN(E)/dE
P S C O Mn Mn Mn Fe Fe Fe
100 200 300 400 500 600 700
Energy, eV
XBL 774-5346A

Fig. 29.

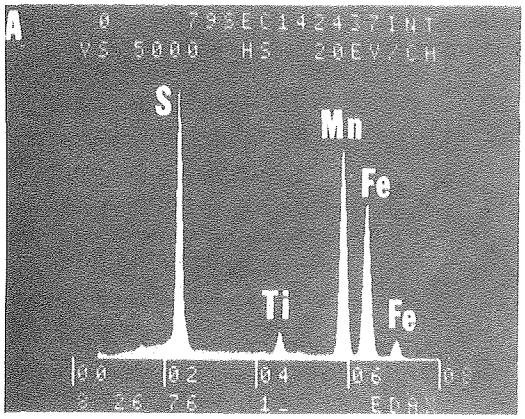

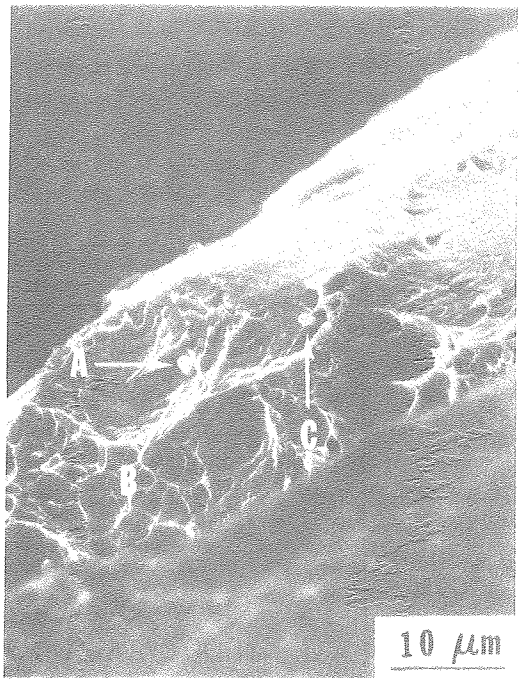

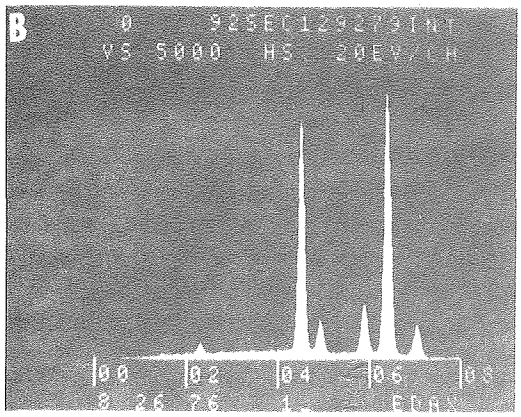

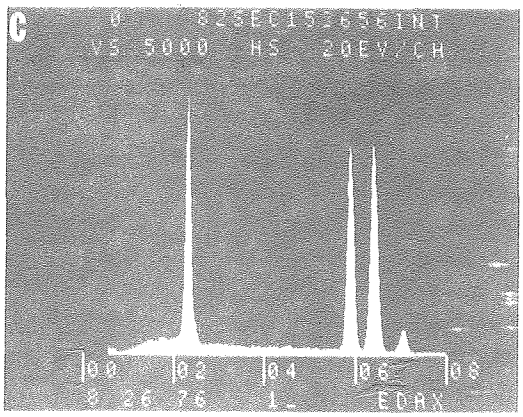

Fig. 30.

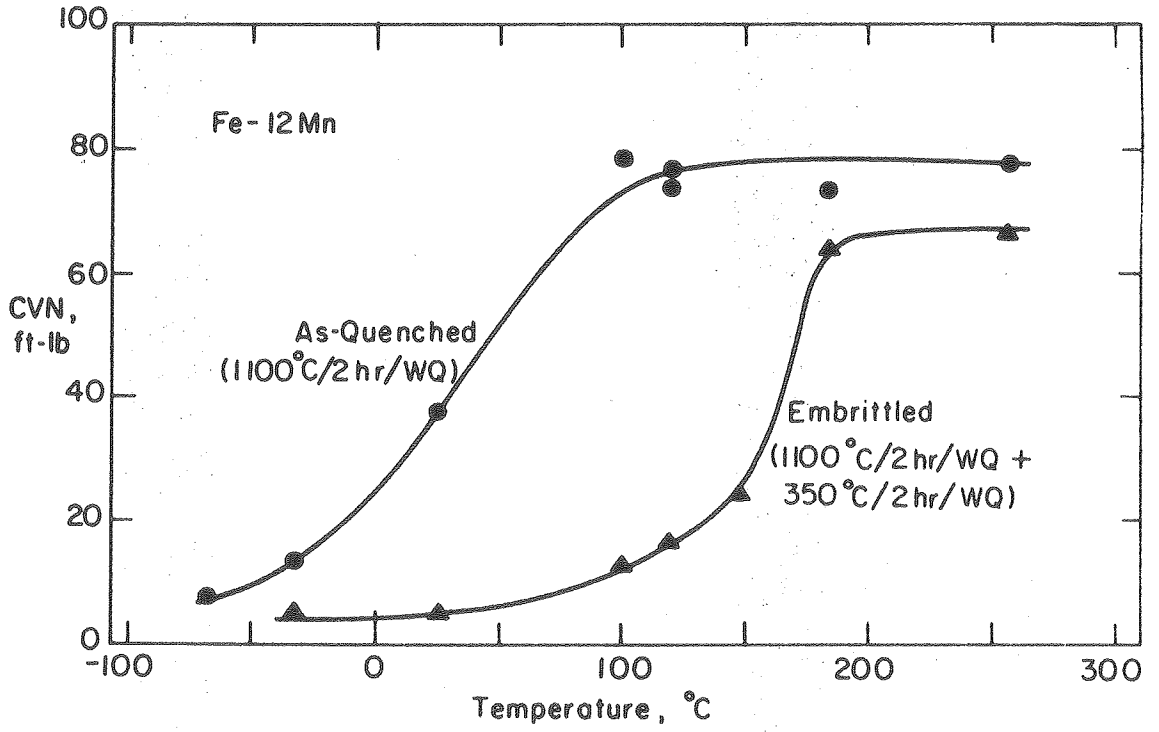
Fe-12Mn
As-Quenched
(1100°C/2hr/WQ)
Embrittled
(1100°C/2hr/WQ +
350°C/2hr/WQ)
CVN,
ft-lb
Temperature, °C
100
80
60
40
20
0
-100
0
100
200
300
XBL774-5344

Fig. 31.

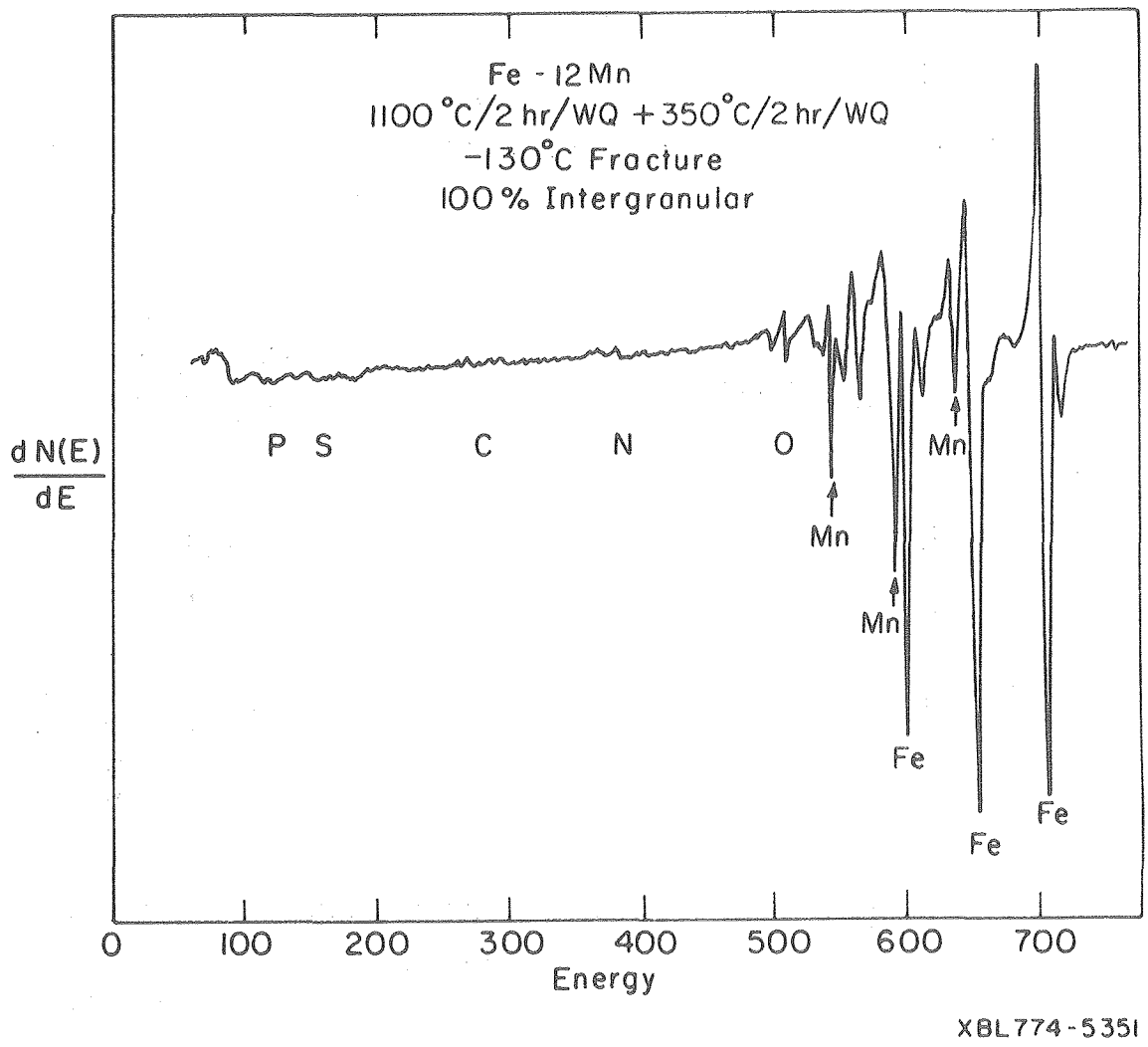

Fig. 32.

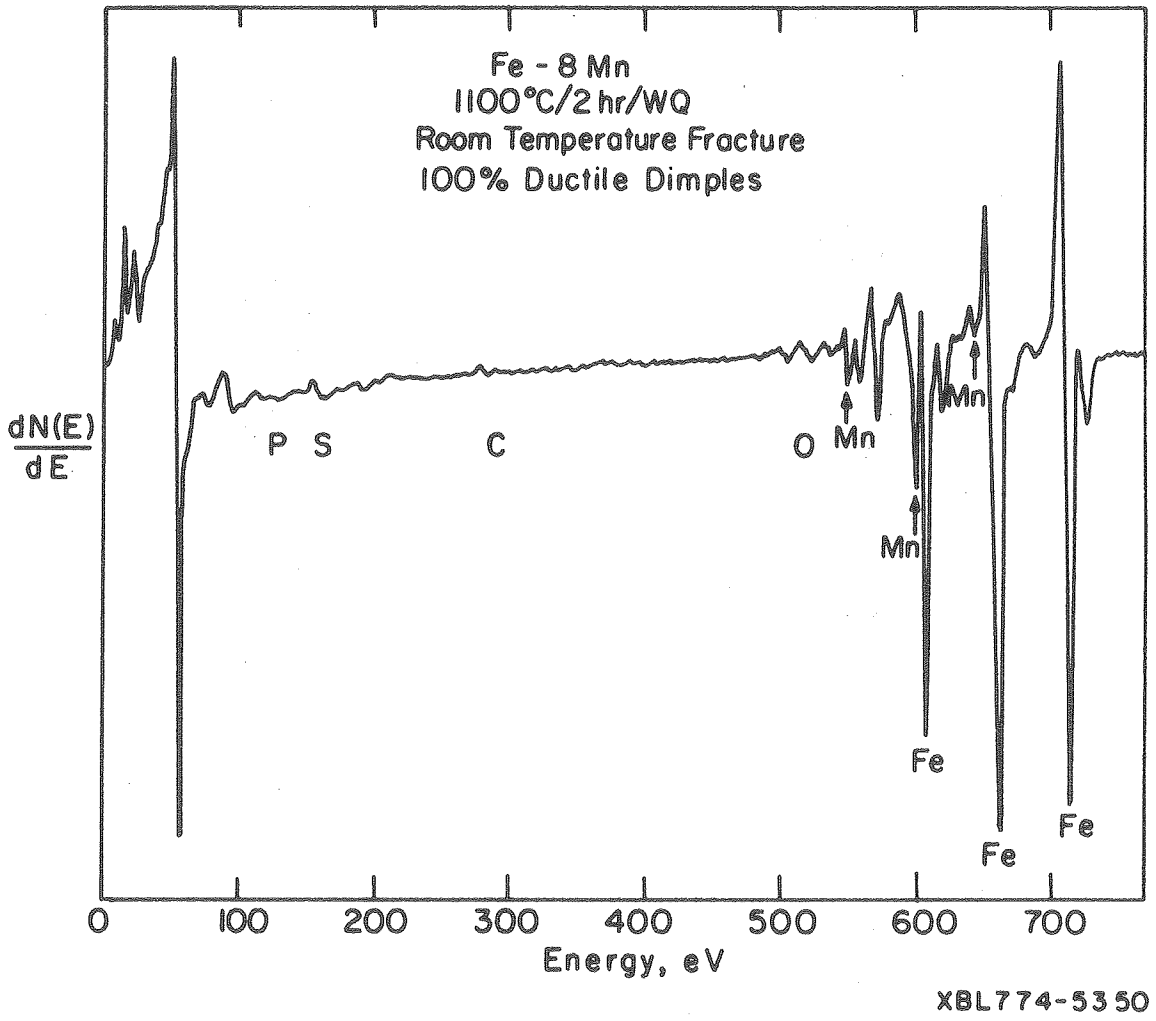
Fe - 8 Mn
1100°C/2 hr/WQ
Room Temperature Fracture
100% Ductile Dimples
dN(E)/dE
P
S
C
O
Mn
Mn
Mn
Fe
Fe
Fe
0
100
200
300
400
500
600
700
Energy, eV
XBL774-5350

Fig. 33.

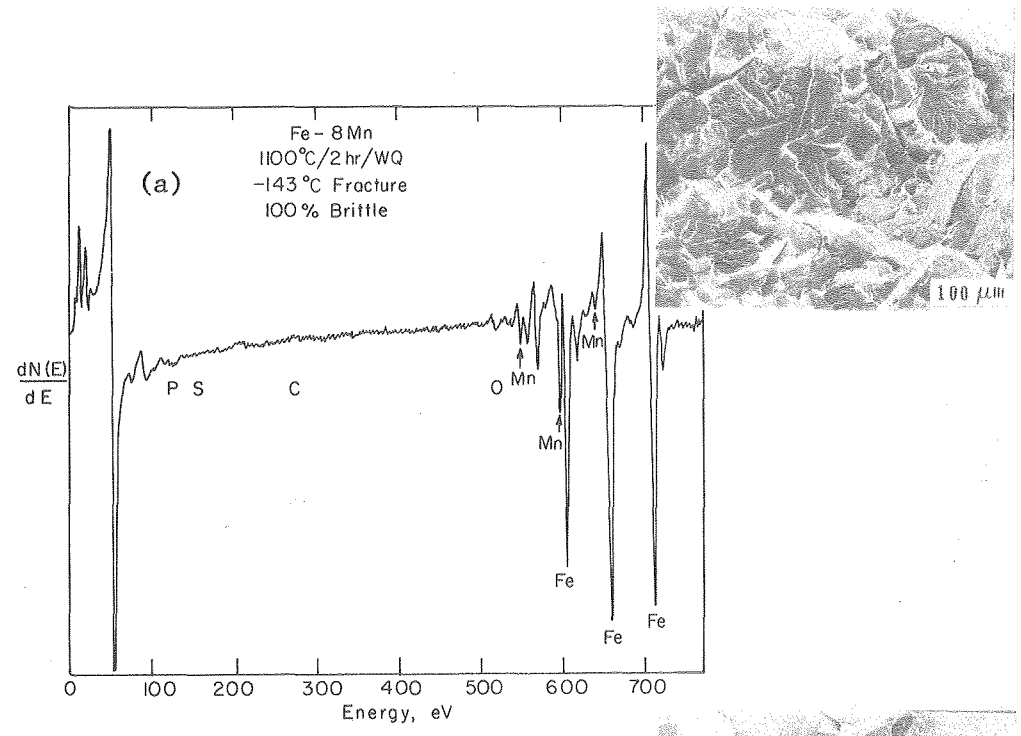
Fe - 8 Mn
1100°C/2 hr/WQ
-143 °C Fracture
100 % Brittle
(a)
100 μm
dN(E)/dE
P S
C
O
Mn
Mn
Mn
Fe
Fe
Fe
0
100
200
300
400
500
600
700
Energy, eV

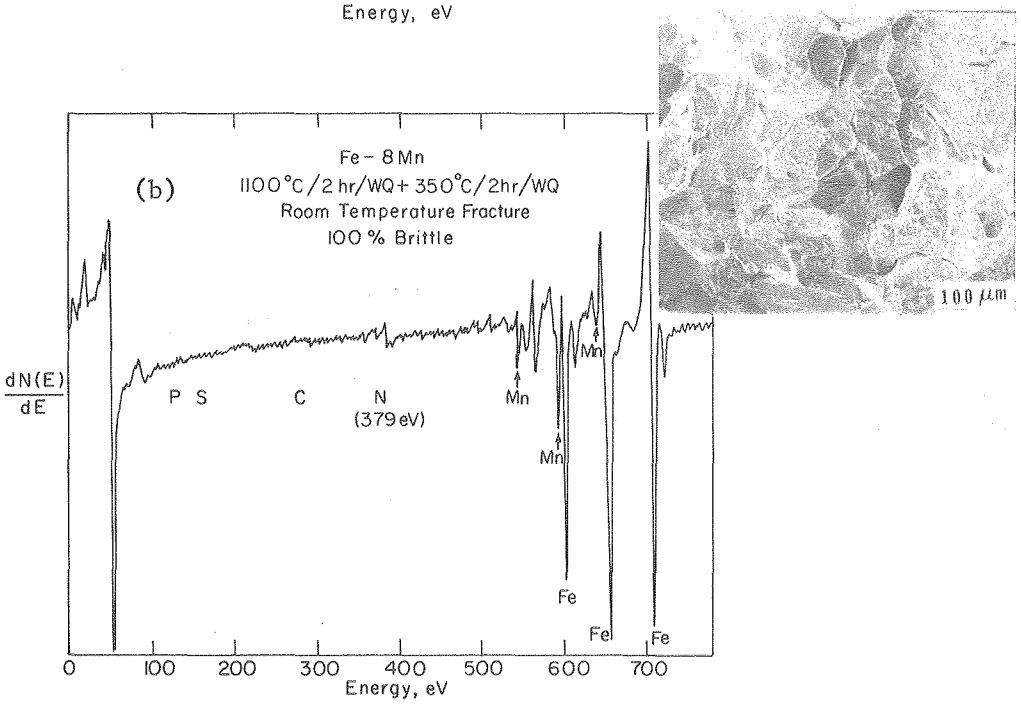
Fe - 8 Mn
1100°C/2 hr/WQ + 350°C/2hr/WQ
Room Temperature Fracture
100 % Brittle
(b)
100 μm
dN(E)/dE
P S
C
N
(379 eV)
Mn
Mn
Mn
Fe
Fe
Fe
0
100
200
300
400
500
600
700
Energy, eV

Fig. 34.

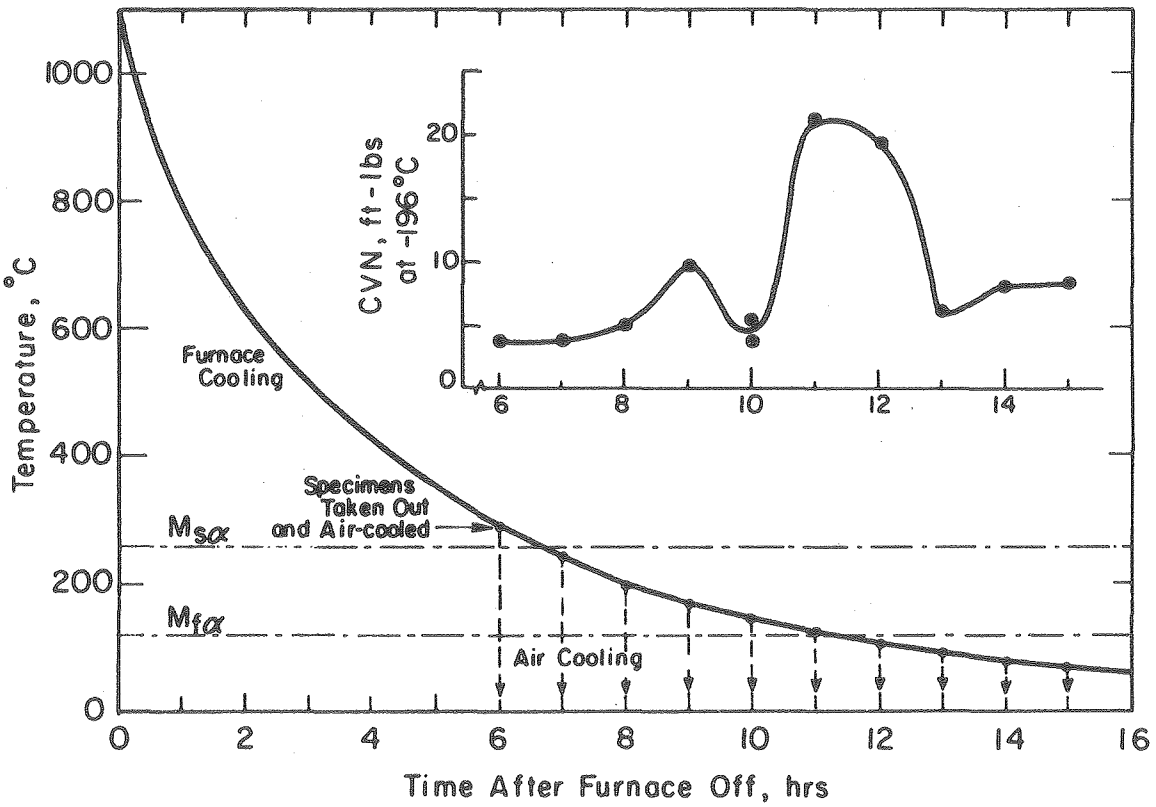
Temperature, °C
1000
800
600
400
200
0
Furnace Cooling
Specimens Taken Out and Air-cooled
$M_{s\alpha}$
$M_{f\alpha}$
Air Cooling
0
2
4
6
8
10
12
14
16
Time After Furnace Off, hrs
CVN, ft-lbs at -196°C
20
10
0
6
8
10
12
14
XBL774-5345

Fig. 35.

a

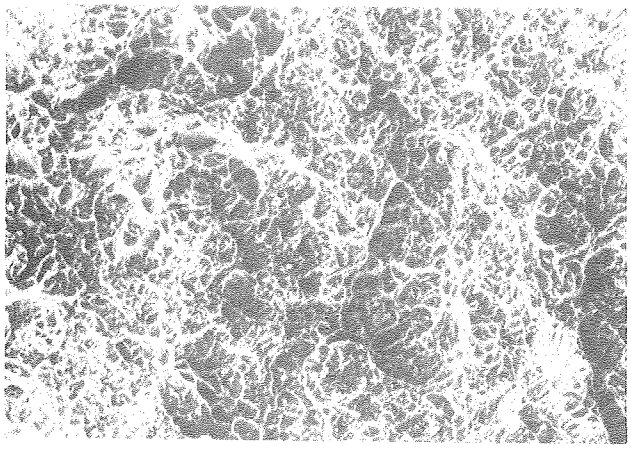

b

c

Fig. 36.

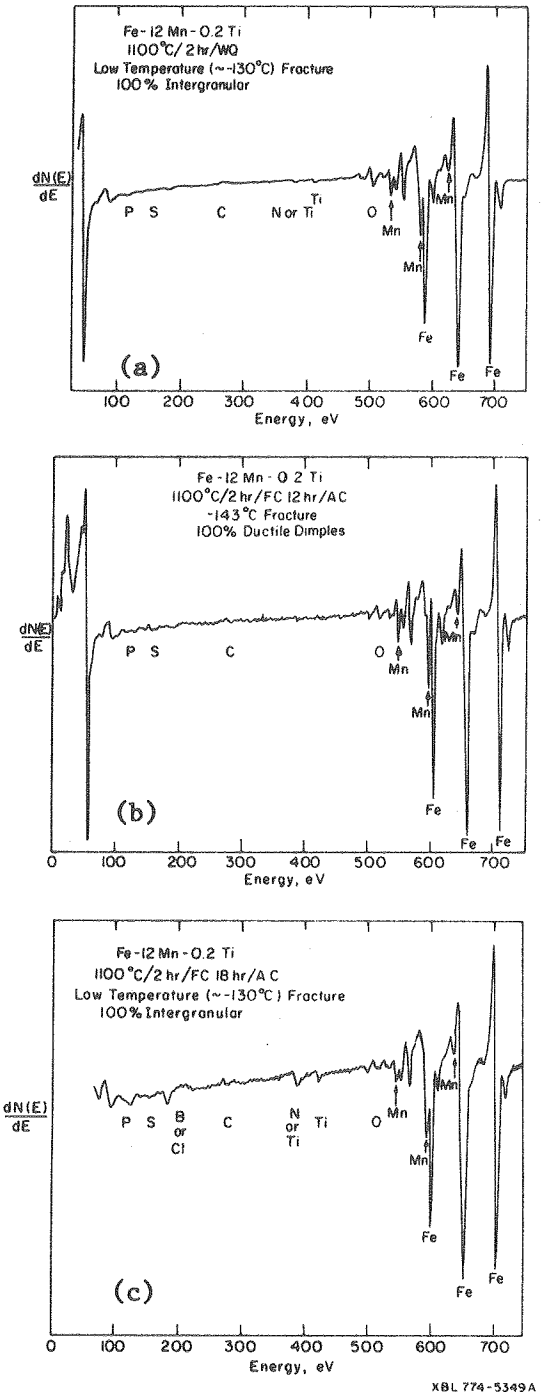
Fe-12 Mn-0.2 Ti
1100°C/2 hr/WQ
Low Temperature (~-130°C) Fracture
100% Intergranular
dN(E)/dE
P S C N or Ti Ti O Mn Mn Mn Fe Fe Fe
(a)
100 200 300 400 500 600 700
Energy, eV
Fe-12 Mn-0.2 Ti
1100°C/2 hr/FC 12 hr/AC
-143°C Fracture
100% Ductile Dimples
dN(E)/dE
P S C O Mn Mn Mn Fe Fe Fe
(b)
0 100 200 300 400 500 600 700
Energy, eV
Fe-12 Mn-0.2 Ti
1100°C/2 hr/FC 18 hr/AC
Low Temperature (~-130°C) Fracture
100% Intergranular
dN(E)/dE
P S B or Cl C N or Ti Ti O Mn Mn Mn Fe Fe Fe
(c)
0 100 200 300 400 500 600 700
Energy, eV
XBL 774-5349A

Fig. 37.

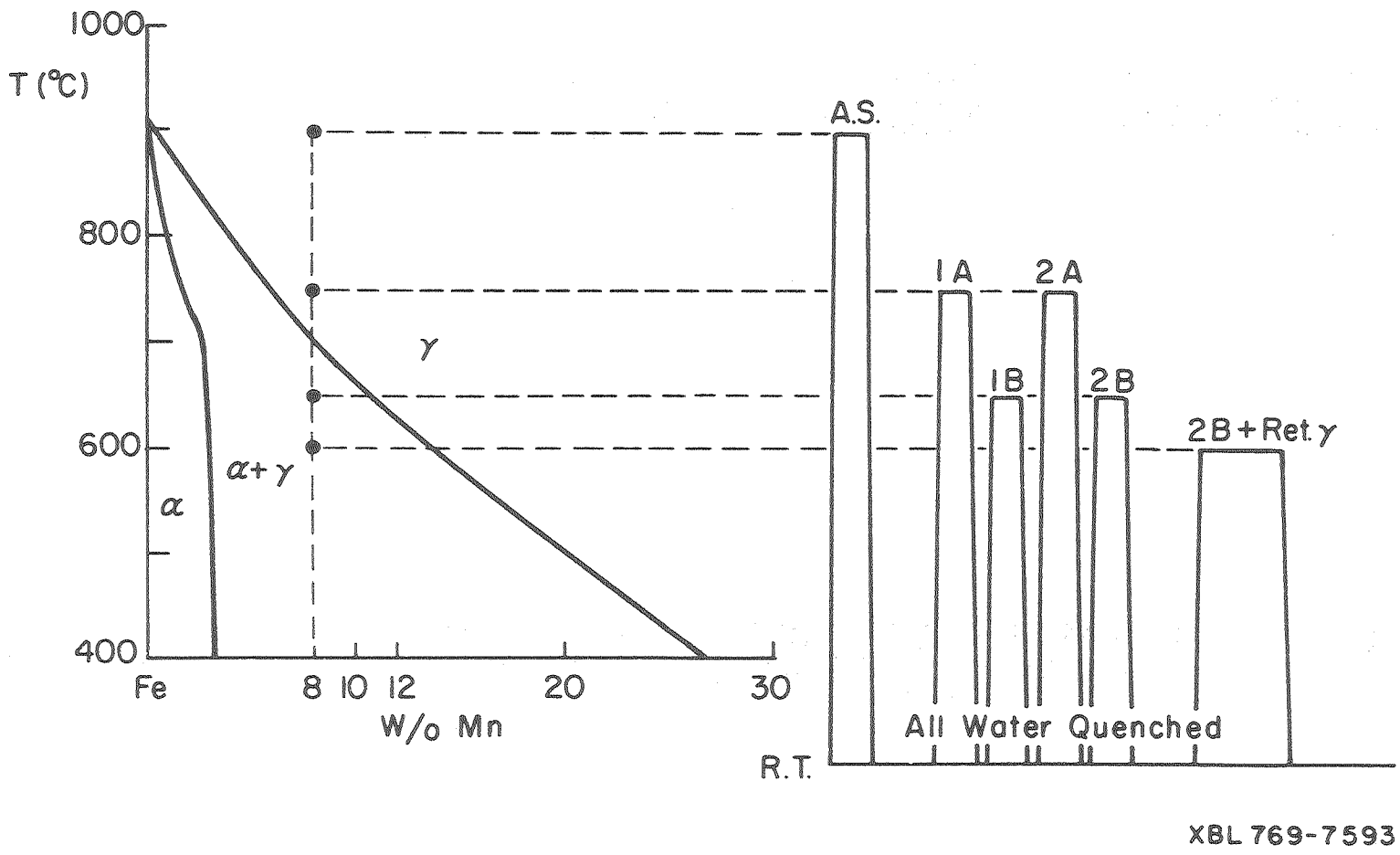
1000
T (°C)
800
600
400
Fe
8 10 12
20
30
W/o Mn
γ
α+γ
α
A.S.
1A
2A
1B
2B
2B+Ret.γ
All Water Quenched
R.T.
XBL 769-7593

Fig. 38.

Fe - 8 Mn

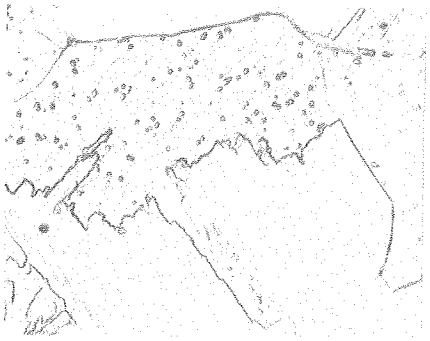

A.S.

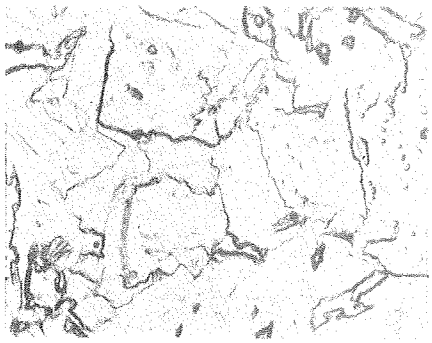

1 A

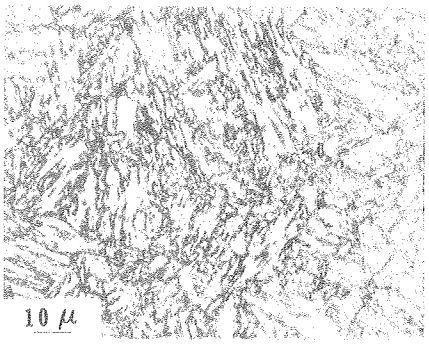

1 B

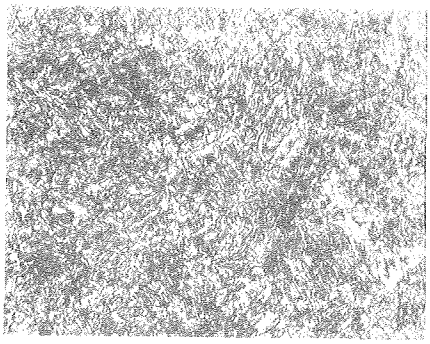

2 B

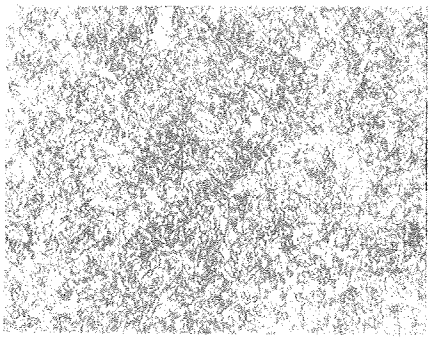

4 B

Fig. 39.

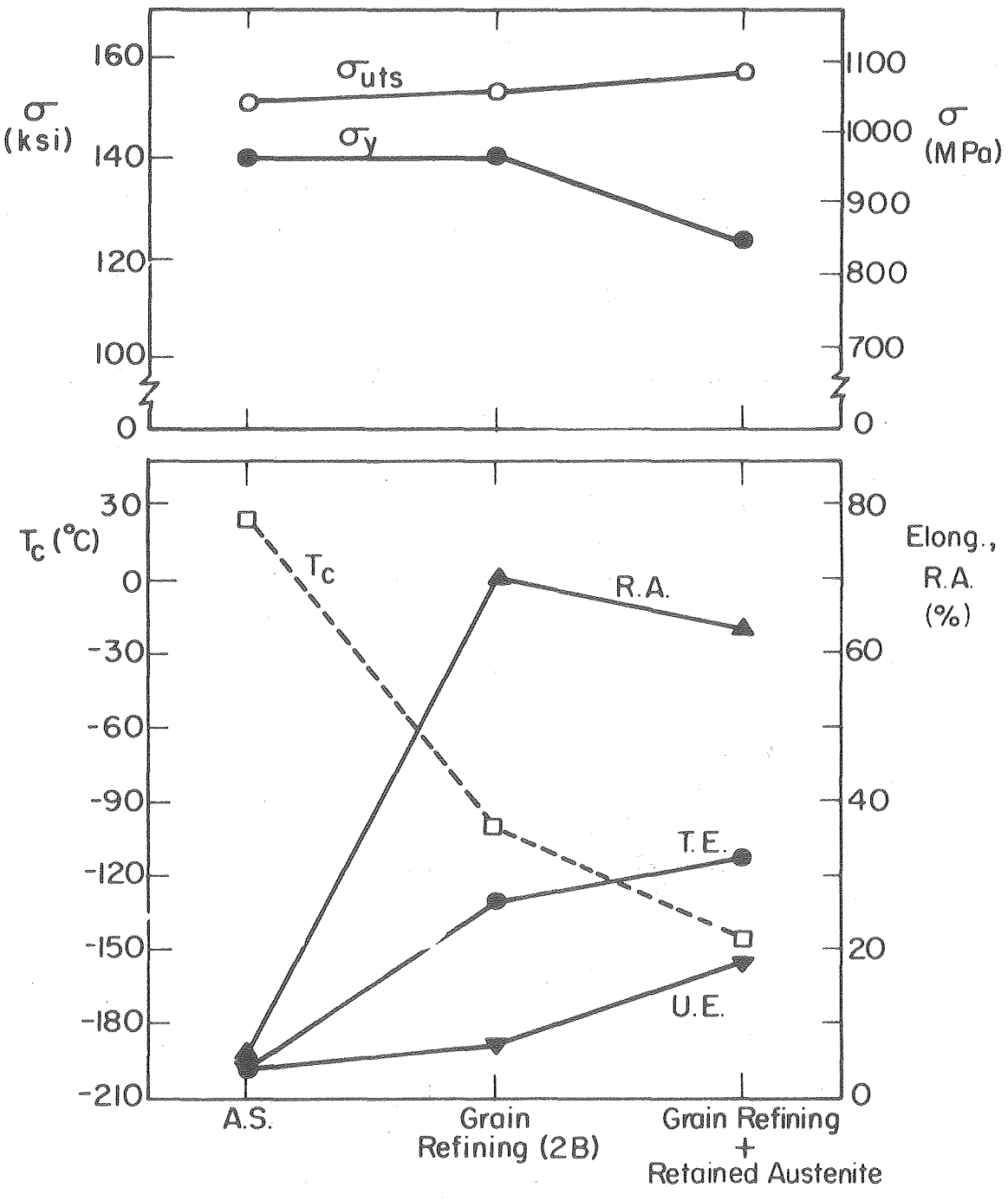

Fig. 40.

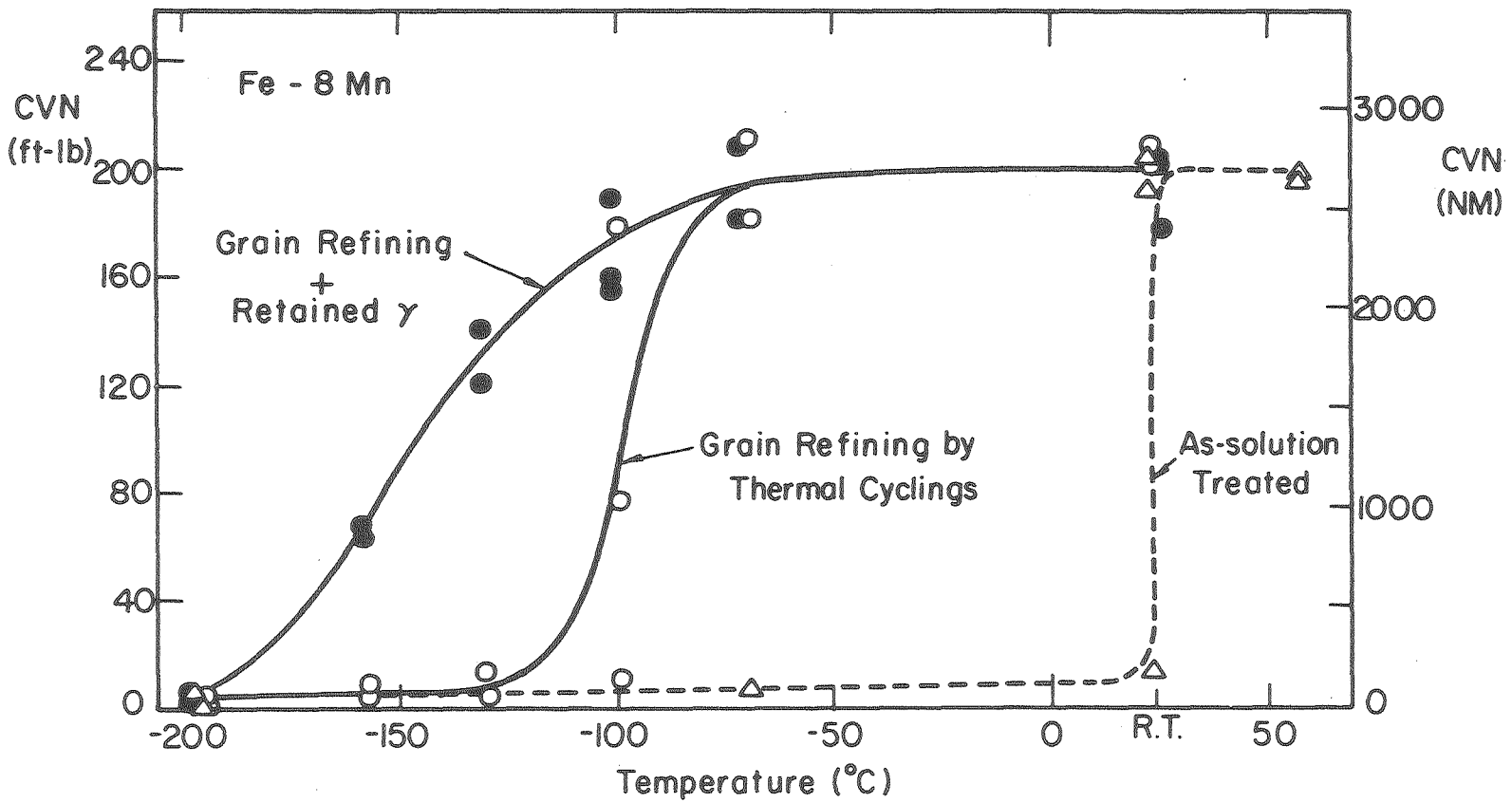
Fe - 8 Mn
CVN (ft-lb)
CVN (NM)
240
200
160
120
80
40
0
3000
2000
1000
0
Grain Refining + Retained γ
Grain Refining by Thermal Cyclings
As-solution Treated
-200
-150
-100
-50
0
R.T.
50
Temperature (°C)
XBL769-7595

Fig. 41.

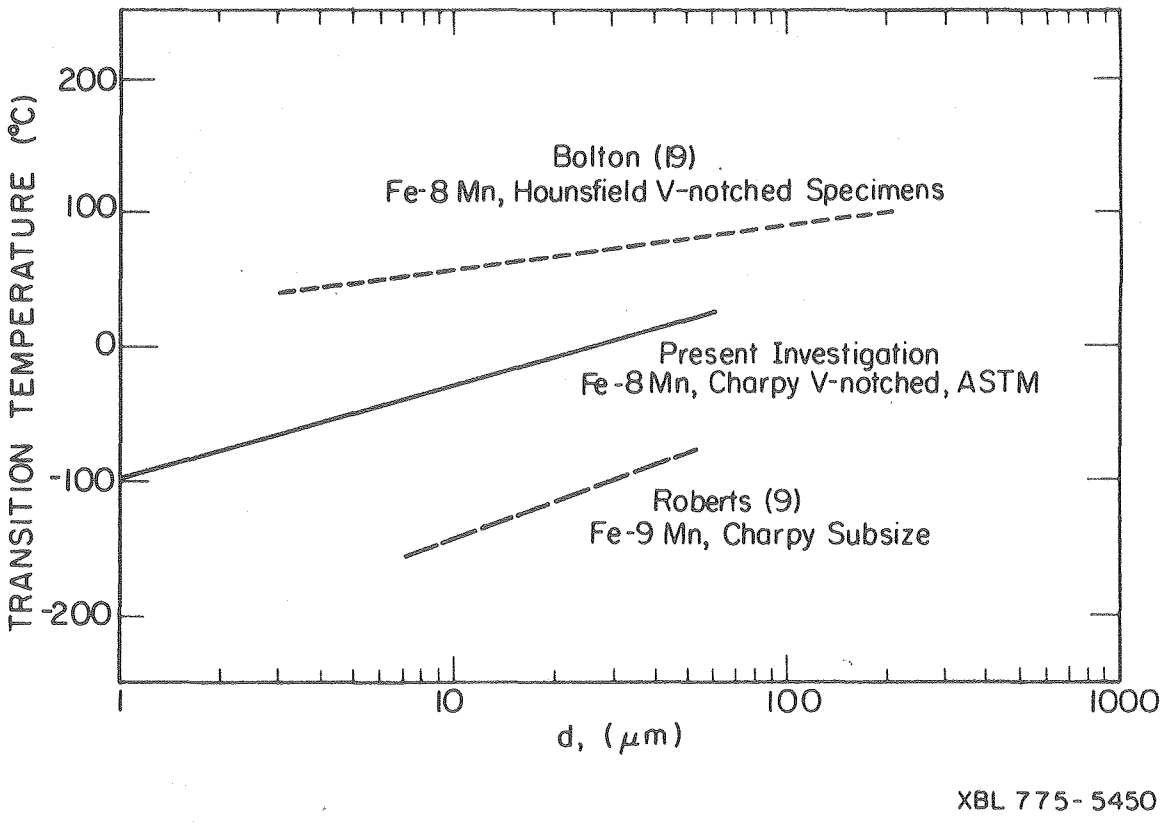

Fig. 42

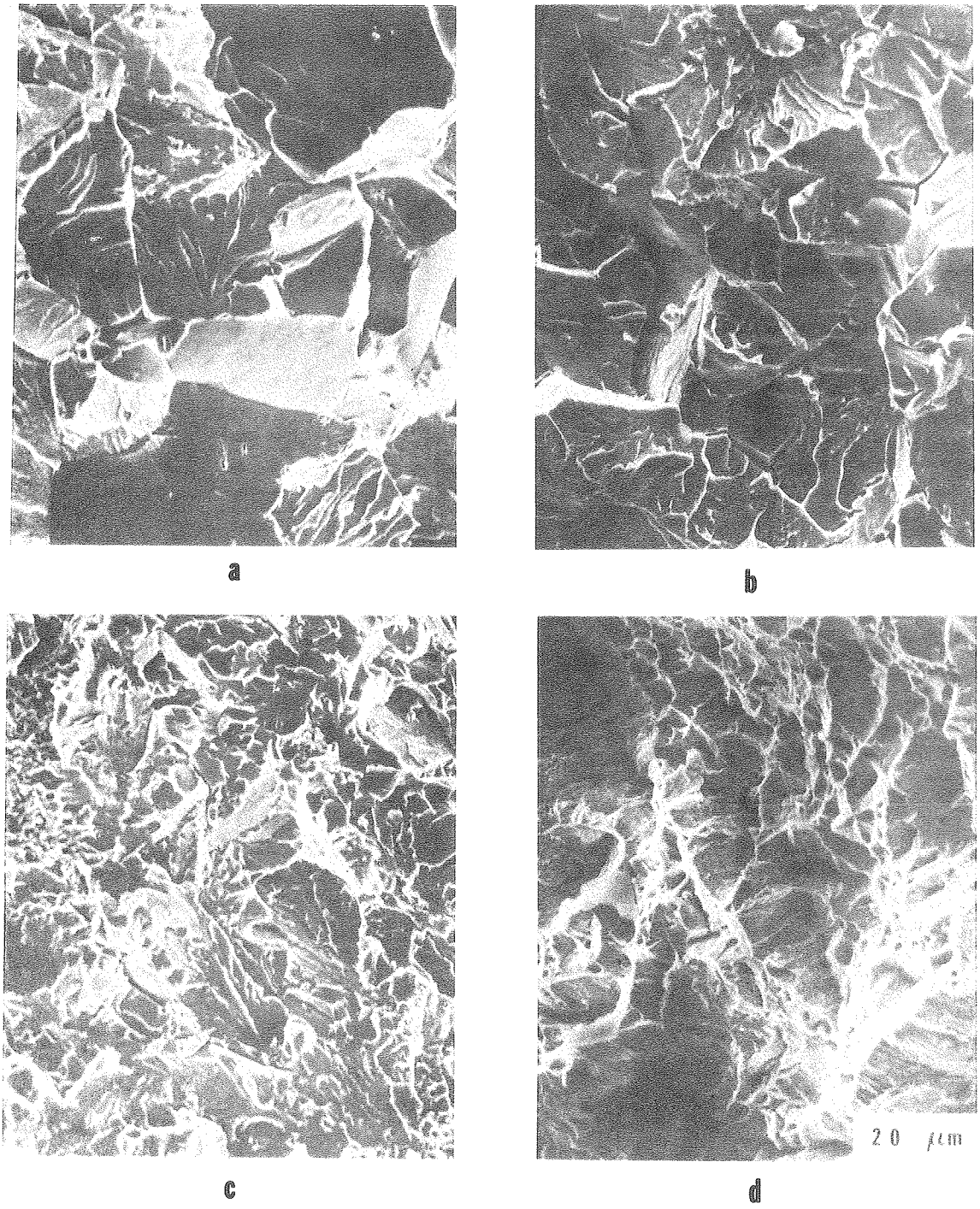

Fig. 43.

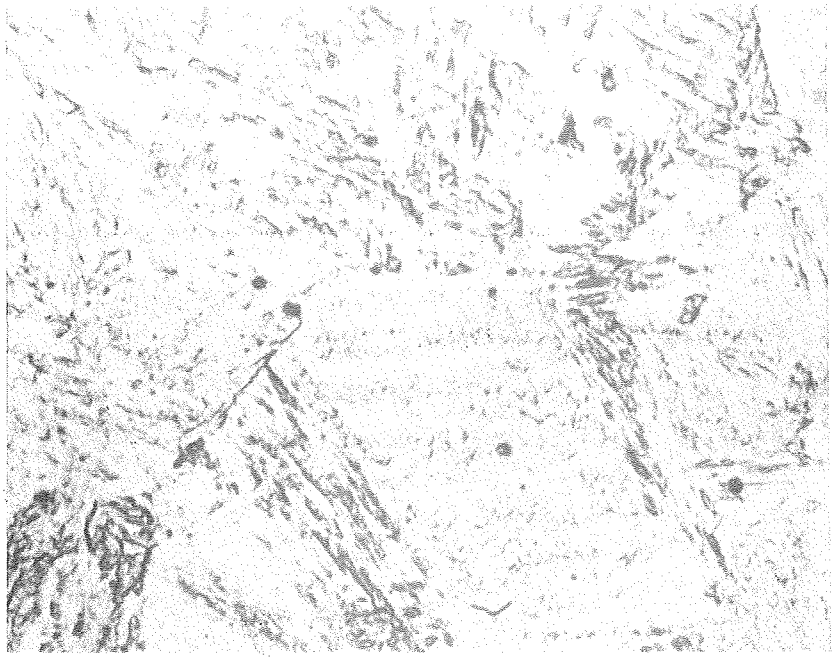

a

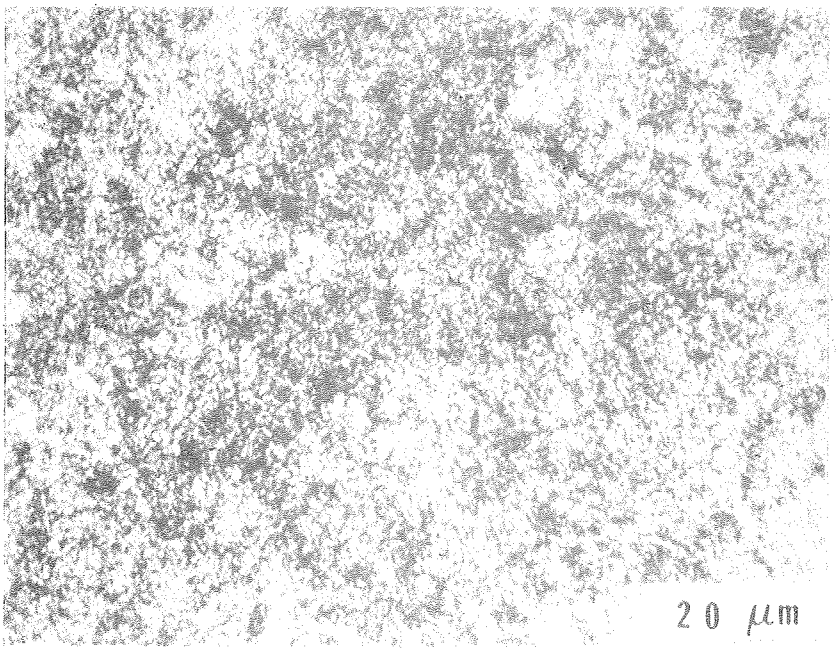

b

Fig. 44.

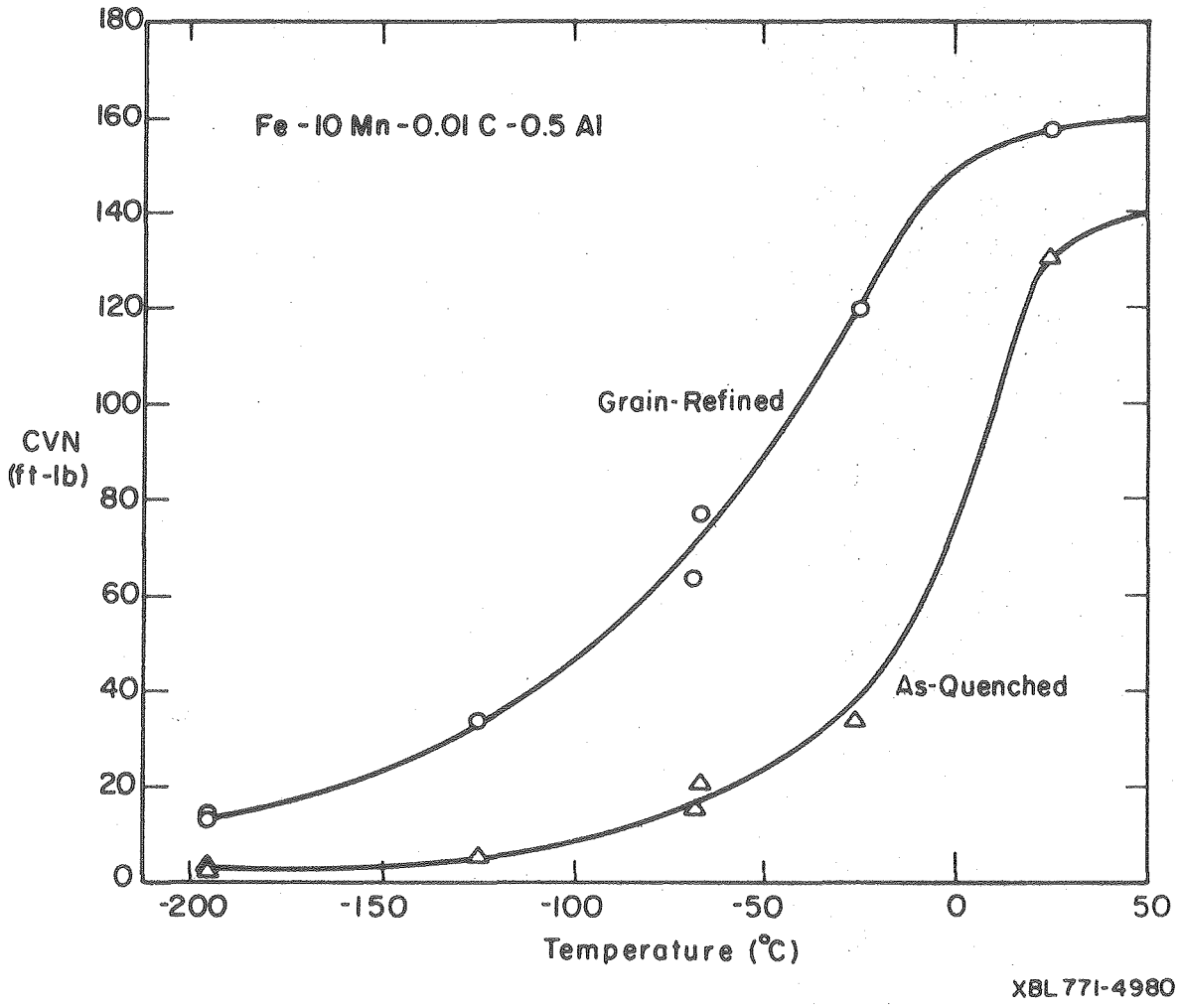
Fe - 10 Mn - 0.01 C - 0.5 Al
Grain-Refined
As-Quenched
CVN
(ft-lb)
180
160
140
120
100
80
60
40
20
0
-200
-150
-100
-50
0
50
Temperature (°C)
XBL 771-4980

Fig. 45.

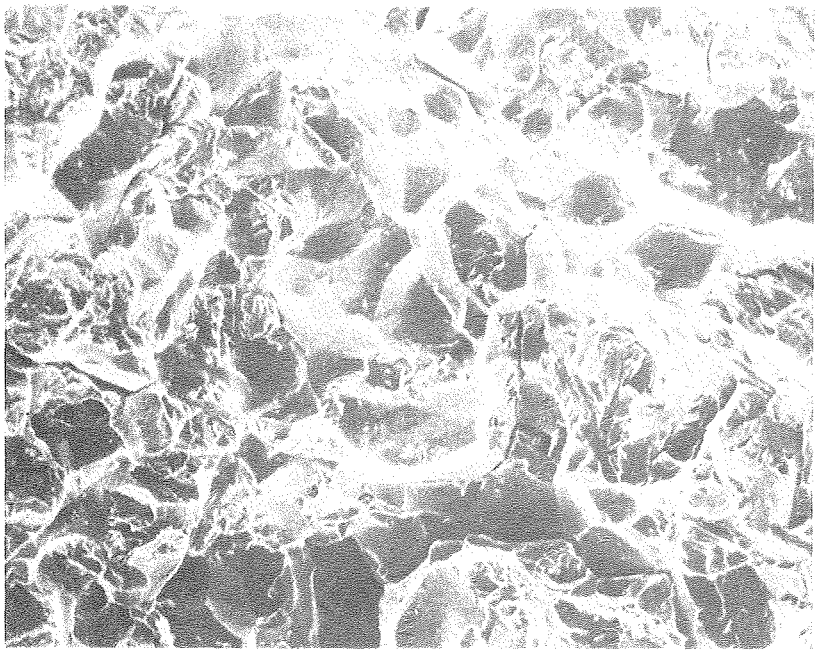

a

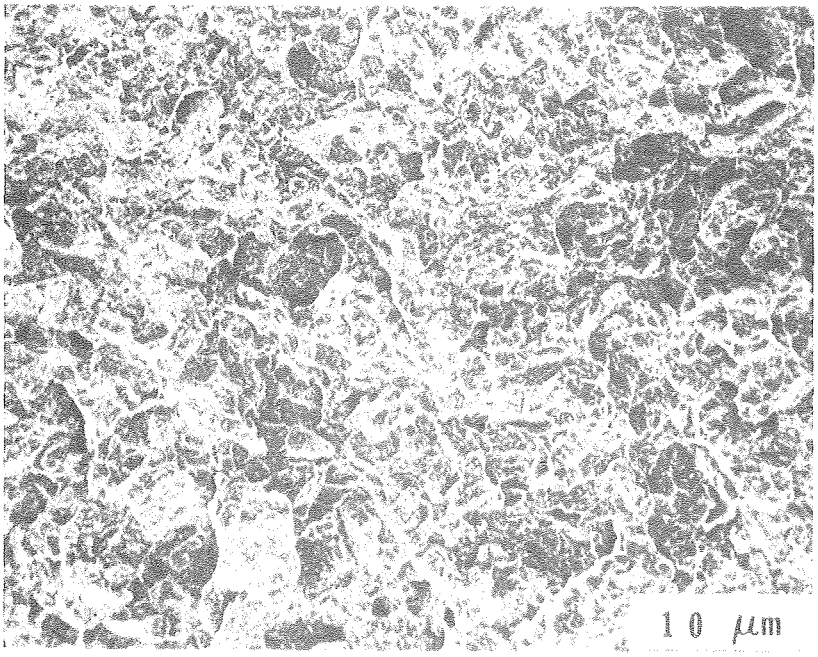

b

Fig. 46.

This report was done with support from the United States Energy Research and Development Administration. Any conclusions or opinions expressed in this report represent solely those of the author(s) and not necessarily those of The Regents of the University of California, the Lawrence Berkeley Laboratory or the United States Energy Research and Development Administration.